ECMWF COPERNICUS REPORT

Copernicus Atmosphere Monitoring Service

Evaluation of the CAMS 2010 reanalysis test run experiment gls8

Issued by: KNMI

Date: 23/01/2016

Ref: CAMS84_2015SC2_WP84.7_2010_test_reanalysis_v1

Evaluation of the CAMS 2010 reanalysis test run experiment gls8

AUTHORS:
T. ANTONAKAKI (AA), S. BASART (BSC), A. BENEDICTOW (METNO), A.-M. BLECHSCHMIDT (IUP-UB), S. CHABRILLAT (BIRA-IASB), Y. CHRISTOPHE (BIRA-IASB), H. CLARK (CNRS-LA), E. CUEVAS (AEMET), H. ESKES (KNMI), K. M. HANSEN (AU), U. IM (AU), J. KAPSOMENAKIS (AA), B. LANGEROCK (BIRA-IASB), M. RAMONET (CEA-LSCE), A. RICHTER (IUP-UB), M. SCHULZ (METNO), N. SUDARCHIKOVA (MPG), A. WAGNER (MPG), T. WARNEKE (UBC), C. ZEREFOS (AA)

REPORT OF THE COPERNICUS ATMOSPHERE MONITORING SERVICE, VALIDATION SUBPROJECT

STATUS:
VERSION 1

DATE:
23/01/2017

Summary

The Copernicus Atmosphere Monitoring Service (CAMS, http://atmosphere.copernicus.eu) is a component of the European Earth Observation programme Copernicus. The CAMS global near-real time (NRT) service provides daily analyses and forecasts of reactive trace gases, greenhouse gases and aerosol concentrations. A reanalysis for the period 2003-2017 will be produced during the years 2017-18. The CAMS system was developed by a series of MACC research projects (MACC I-II-III) until July 2015.

CAMS has a sub-project dedicated to the validation of the service products. The validation results for the CAMS global NRT service (the o-suite) products and high-resolution greenhouse gas simulations can be found in Huijnen et al. (2016) and Eskes et al. (2015). The observational datasets used for this validation, with a focus on real-time observations, are described in Eskes et al. (2016). These validation reports and the verification websites can be found here: http://atmosphere.copernicus.eu/user-support/validation/verification-global-services.

To prepare for the CAMS reanalysis, a test reanalysis run has been produced by ECMWF for the year 2010. The data from this run (experiment gls8) will not become available publicly, but is meant to evaluate and optimise the model and assimilation components. This document contains an evaluation of this 2010 dataset, validating the aerosol, greenhouse gas and reactive trace gas analyses with available observations. The main results are summarised below for the key constituents.

Global Aerosol

The test experiment for the CAMS reanalysis has been compared consistently against the MACC reanalysis and the MACC o-suite experiment having all covered the year 2010. Results are displayed on a subsection of the AeroCom/CAMS website. Taking the old MACC reanalysis (Experiment FBOV) as reference, the following changes wrt to aerosol optical depth (AOD) can be found in the GLS8 reanalysis: AOD reductions (-26%) are seen both in Northern hemisphere pollution regions, sea salt and dust regions. Quite a big change in composition is found like a +90% increase in organic aerosol compensated by a -36% decrease in sulphate. The sum of sulphate and organic AOD is increased by 5% in gls8, but the decrease in sea salt (-42%) and dust (-68%) is contributing to the overall reduction in AOD in the gls8 reanalysis.

The RMS error against daily Aeronet in 2010 went down both due to better spatial and temporal representation of the AOD field. Statistics show a temporal-spatial RMS error reduction from 0.167 (FBOV) to 0.143 (gls8), consistent with a reduction of MNMB going from 31% to 7%, respectively. An overall positive bias in the previous analysis FBOV has become a smaller positive bias in the gls8 analysis. The spatial distribution of AOD bias has become more evenly distributed with few spots sticking out. The dust AOD may be too small, showing up in a high bias of the Angstrom coefficient in cases of low Angstrom coefficient. However, 86% of the Angstrom coefficient values are within a factor of two.

The quality of the IFS gls8 reanalysis, despite or because of the significant shift in the aerosol composition is better as in the previous MACC reanalysis or o-suite. No major issues have been found. See section 2.1.1 for more details.

Dust

The seasonal AOD and DOD fields from CAMS reanalysis (gsl8) show a distinct seasonal pattern linked to the spatial distribution of dust emissions and transport throughout the year, in good qualitatively agreement with the MODIS and MISR AOD observations (Figure 2.1.6). The Bodéle as well as desert dust sources in Maghreb is systematically underestimated along the year. Although, this new experiment tends to underestimate AOD results in comparison with MODIS and MISR particularly over the subtropical and tropical North Atlantic transport (see Dakar in Figure 2.1.7). However, the most striking and strange results is finding such a big difference between AOD and DOD from CAMS precisely in desert areas where clearly dominates the mineral dust aerosol unambiguously. The differences between AOD and DOD are high over the Sahara and the Middle East (see Banizoumbou, Saada and Kuwait in Figure 2.1.7). The extremely low DOD values provided by CAMS are clearly underestimated. The comparison with AERONET quality-assured AOD observations (on 3-hourly basis) show that the reanalysis can reproduce the annual evolution (see Figure 2.1.7 and Figure 2.1.8) with a better than acceptable annual correlation coefficient of 0.75 in average for all the AERONET sites (with maximum of 0.89 in Tropical North Atlantic and minimum of 0.71 in the Middle East). However, CAMS tends to underestimate AOD observations with an MB of -0.1 and RMSE of 0.26 and FGE of 1.30 in average for all the AERONET sites.

A Saharan dust event over Germany was analysed using Ceilometer observations. Qualitatively this dust plume was reproduced by the reanalysis (Fig. 2.1.11).

Aerosol validation over the Mediterranean

Over the Mediterranean, CAMS reanalysis can reproduce the AOD variability of AERONET observations (see Figure 2.1.9) with a correlation coefficient of 0.75 in average for all the AERONET available sites. The highest AOD peaks are associated with desert dust intrusions (see Figure 2.1.8). The model tends to underestimate the AOD observations (see Figure 2.1.9). The south-to-north gradient observed in the FGE is associated to the decreasing AOD values towards northern latitudes. On surface levels (see Figure 2.1.10), the model tends to underestimate the Airbase observations with largest differences in PM2.5 than PM10 (annual MB of -5.12 µg/m3 for PM10 and -10.17 µg/m3 for PM2.5 in average for all the sites).

Tropospheric ozone (O_3)

For the free troposphere, between 750 and 350 hPa (750 and 200 in tropics), the evaluation with ozone sondes (Fig. 2.2.1) shows that ozone mixing ratios are underestimated over the Arctic and the Northern Midlatitudes by up to -15%. Over Antarctica, MNMBs are positive for the Antarctic summer season (up to 20%) and negative for the winter season (up to -7%). This is similar to the southern midlatitudes , however, winter MNMBs are larger here (up to -20%). Over the tropics, MNMBs are mostly positive (up to 20%). In the UTLS (Fig. 2.2.2) for all latitude regions positive MNMBs appear for the whole period. MNMBs are mostly within 20%. MNMBS over the Arctic are smallest and remain within 10%.

Surface ozone in 2010 is globally mostly overestimated by the reanalysis compared to GAW station observations, Fig. 2.2.3 to 2.2.7. For most stations in Europe (KPU, MCI, NGW, PAY, PIC, RIG, SCH, SBL, SFH, ZIN) however, small negative MNMBs are shown (with exception to RIG, which is located in complex terrain). The time series plots show positive offsets for tropical stations, same as for the previous o-suites. Correlation coefficients are 0.65 on average. RMSEs are 9.8 ppb on average.

Predicted ozone mixing ratios are compared to Arctic measurements from 4 surface stations in Alaska, Canada and Greenland (Fig. 2.2.13). Surface ozone is overestimated at most sites (MNMB = 14% - 21%) except for Summit where the bias is negative (MNMB = -10%). The correlation is between 0.3 and 0.72. For the free troposphere, ozone mixing ratios are underestimated over the Arctic by up to -15% when comparing to ozone sonde data. Overall the reanalysis performs well with respect to surface ozone and CO as well as for the ozone sondes within the Arctic with comparable statistical parameters as for the present o-suite.

The gls8 reanalysis experiment was compared to surface EMEP ozone observations and the MACC reanalysis on a seasonal basis for the latitudinal zones of 30N-40N, 40N-50N and 50N-70N, see Fig. 2.2.8. As can be seen from Fig. 2.2.8 and 2.2.9, over Southern Europe, the gls8 Reanalysis systematically overestimates ozone mixing ratios with the highest positive biases being observed during the period April-August (up to 7 ppbv). Over Central Europe, the model overestimates ozone mixing ratios during the period May-December (up to 7 ppbv), while a negative bias is observed during winter. Lastly, over Northern Europe, the model underestimates O_3 mixing ratios for the first 4 months of the year (MNMBs down to 5 ppbv) and overestimates O_3 during May to November (up to 10 ppbv during August). It should be noted that new Reanalysis gls8 is significantly better than the MACC reanalysis in terms of biases during all season particularly over Central and Southern Europe. The gls8 reanalysis experiment reproduces well enough the surface ozone variability during all seasons over Europe ($0.3<r<0.9$ with very few exceptions), see figure 2.2.10. It is also evident that the new reanalysis in general shows better correlations that the MACC reanalysis particularly over Central Europe.

IAGOS aircraft profiles, Fig. 2.2.11, of ozone at Frankfurt show that the reanalysis and the control are very similar. The differences are greatest in the free troposphere where the reanalysis underestimates ozone and the control run overestimates ozone, examples are shown for February and October. In figure 2.2.12 we show three examples where the reanalysis shows a slight improvement over the control in the sensitive UTLS.

Tropospheric Carbon Monoxide (CO)

Surface CO for European and Asian GAW stations is mostly underestimated (around -10%) by the reanalysis. For stations in the US and Canada the model shows an overestimation (between 2-20%) of surface mixing ratios. This seems to go back to CO peaks in the model (fires?). Correlation coefficients are 0.68. Average RMSE is 42 ppb. See Fig. 2.3.1 to 2.3.5. Comparison with lower tropospheric FTIR CO observations (Fig. 2.3.7, table 2.3.1) show a negative bias of about 8% in northern midlatitudes and good agreement in the southern hemisphere. The TCCON sites show a good agreement of the seasonality and shorter time scale variability at all sites, and some strong events are well captured (Fig. 2.3.8 - 12). An overestimate of > 10% is found over the Antarctic, and an underestimation during local spring in the Arctic. In the Arctic we also compared with CO mixing ratios available for seven months of 2010 from Alert, Canada. There is a low negative bias (MNMB = -7%) and a high correlation (r = 0.9) for this site.

The IAGOS aircraft profiles of carbon monoxide at Frankfurt during December and November 2010 show that the reanalysis and the control are very similar. Both runs lie within the standard deviation of the measurements throughout the profiles but CO is underestimated throughout the surface layer and free troposphere over Frankfurt.

Regional comparisons were made for the CAMS reanalysis 2010 (gls8) with MOPITT V5 and V6 and IASI CO data. CO total column seasonality in different regions is reproduced well by the model. CO total column is slightly underestimated over Europe, US, Alaskan and Siberian fire regions (up to 10 %). Overall monthly averaged MNMBs in selected regions are not exceeded 10% (Fig. 2.3.8).

Tropospheric Nitrogen dioxide (NO_2)

Tropospheric NO_2 in the CAMS 2010 test reanalysis has the known problems also observed in the operational forecasts: too large values for biomass burning in boreal forests, too high shipping signals. Apart from that it is comparable to MACC reanalysis (Fig. 2.4.1). Tropospheric NO_2 shows unusually low values in some areas of the tropics over the continents (Central Africa, Northern South America), lower than in MACC reanalysis and lower than in SCIAMACHY (Fig. 2.4.2). The MAX-DOAS in Xianghe, China indicates that the analysis is improving the bias compared to the forecast (Fig. 2.4.3).

Formaldehyde (HCHO)

Tropospheric HCHO appears generally too high, in particular in September, October, and November over Africa and Australia (Fig.2.5.1). This agreement with the satellite data was much better in the MACC reanalysis.

Stratospheric ozone

For the evaluation of stratospheric ozone in the reanalysis gls8, we use ozone sounds, NDACC observations, satellite observations of ozone profiles from AURA MLS Offline version 4.2, ACEFTS v3.5/v3.6 and Odin OSIRIS v5. The MACC reanalysis serves as a reference system.

In the stratosphere, for all regions except the Arctic, MNMBs against ozone sondes (averaged between 90 and 10 hPa, and between 60 and 10 hPa in the Tropics) are positive but remain within 10%, for Antarctica within 20% (Figure 2.6.1). In the Arctic MNMBs are close to zero.

Agreement with AURA-MLS v4 Offline observations time series (Fig. 2.6.2) is generally much better than in the MACC reanalysis for ozone in polar regions and in tropical region for higher stratosphere (03-10hPa), middle stratosphere (30-70hPa) and lower stratosphere (70-120hPa). For the considered period, the MACC reanalysis assimilated AURA MLS V02 NRT, while gls8 assimilates a more recent version of AURA MLS, which explains this behaviour. A quick look time-series (Fig. 2.6.3) of the bias wrt ACEFTS in the polar regions of the lower stratosphere show clearly an improvement.

As shown by ACEFTS, OSIRIS and MLS, the shape of the profiles (in volume mixing ratio) has improved (Fig. 2.6.4, 2.6.5, 2.6.6, 2.6.7, 2.6.8) in comparison with the MACC reanalysis, where a positive bias was clearly visible between 30km and 40km. However there seems to be an anomaly in gls8 in the higher stratosphere above 55km where a positive bias develops at the end of the polar summer. Because of the assimilation of AURA MLS, the shape of the gls8 profiles are much closer to the MLS observations; the deviations which were visible in the lower part of the profiles (in partial pressure) of the MACC reanalysis have been corrected in gls8. A closer look at the MNMB against ACEFTS shows that the gls8 profiles are more regularly close to ACEFTS observations up to 40km. Between 40km and 50km approximately, the 0-day forecasts (0h to 24h) of gls8 present a slight negative bias wrt the analysis, especially at the polar regions. A closer look at the MNMB against AURA MLS shows that the gls8 profiles are more regularly close to AURA MLS observations up to 3hPa. Between 4hPa and 1hPa approximately, the 0-day forecasts (0h to 24h) of gls8 present a slight negative bias wrt the analysis, especially at the Polar Regions. As an independent source of observations, the MNMB wrt OSIRIS confirms that the bias is always negative between 35km and 55 km approximately, while under 25km the profile of the MNMB is more irregular, depend on the season and varies according to the source of satellite observation used.

NDACC observations of stratospheric ozone confirm the good quality of the reanalysis ozone profiles, see Fig. 2.6.9 and 2.6.10, and the comparison is within the microwave and lidar uncertainty ranges of about 7% between 20 and 40 km.

Stratospheric Nitrogen dioxide (NO_2)

Large biases are observed against FTIR observations (Fig. 2.7.1) which is as expected, because the C-IFS configuration does not include a description of stratospheric chemistry.

Greenhouse gases (CO_2 and CH_4)

In Europe, the CAMS reanalysis 2010 (gls8) can reproduces the phasing of the anthropogenic events observed at the surface with correlation coefficient of about 0.8 for CH_4 all over the year and for CO_2 in winter (Fig. 2.8.1-4). The model generates too high short-term variations of CO_2 total columns at all latitudes (Fig. 2.8.5-9). In the North Hemisphere the model overestimates the amplitude of the seasonal cycles of CO_2 and CH_4 (Fig. 2.8.10-14). For CO_2 the bias (±1%) is consistent at the surface and over the total column: concentrations are overestimated in late spring, and underestimated in autumn. For CH_4 similar seasonal bias (±2%) is observed at the surface, but a systematic negative bias of 1.5 to 2.5% is observed at all total column measurement stations.

Table of Contents

1. Description of the C-IFS reanalysis system setup

The CAMS Reanalysis test production run (experiment **gls8**) was started on 2016-10-20 for the analysis cycle 20100101 based on C-IFS (Flemming et al., 2015). This aim of this run is to test and validate the proposed reanalysis set-up before starting with the year 2003. Main features are:

- IFS cycle 42R1
- branch: std_CY42R1_REAN_20161017_prog_o3
- TM5 CB05 chemical scheme
- Aerosol bin scheme
- Coupled CHTESSEL CO2 flux scheme
- model resolution T255L60
- 48h long forecast at 00UTC
- Blacklist: ec:/std/blacklist/black_42r1_cams_rean, and ec:/std/blacklist/external_bl_mon_monit.CAMS_REAN
- analysis resolution T159/T95, using 12h 4D-Var and VarBC
- time period 20100101 - 20101231
- Available species on model levels: total aerosol, dust 1, dust 2, dust 3, sea salt 1, sea salt 2, sea salt 3, organic matter 1, organic matter 2, black carbon 1, black carbon 2, sulphates, precursor SO2, aldehydes, c2h4, c2h5oh, c2h6, c3h8, c5h8, ch3coch3, ch3oh, ch3ooh, ch4, co, co2, go3, h2o2, hcho, hcooh, hno3, no, no2, oh, olefins, organic nitrates, pan, so2

The assimilated observations of atmospheric composition (Inness et al., 2015) are provided in the table below:

Instrument and Parameter	**Satellite**
MODIS-AOD	TERRA, AQUA
AATSR AOD	Envisat
SBUV/2 O3	NOAA-17
SBUV/2 O3	NOAA-16
SBUV/2 O3	NOAA-18
SBUV/2 O3	NOAA-19
SCIAMACHY O3	Envisat
GOME O3	ERS-2

GOME-2 O3	METOP-A
MIPAS O3	Envisat
MLS O3	AURA
OMI O3	AURA
MOPITT CO	TERRA
SCIAMACHY NO2	Envisat
OMI NO2	AURA
IASI CO2	METOP-A
TANSO CO2	GOSAT
IASI CH4	METOP-A
TANSO CH4	GOSAT
SCIAMACHY CH4	Envisat

An overview of the data usage over time (period up to May 2010):

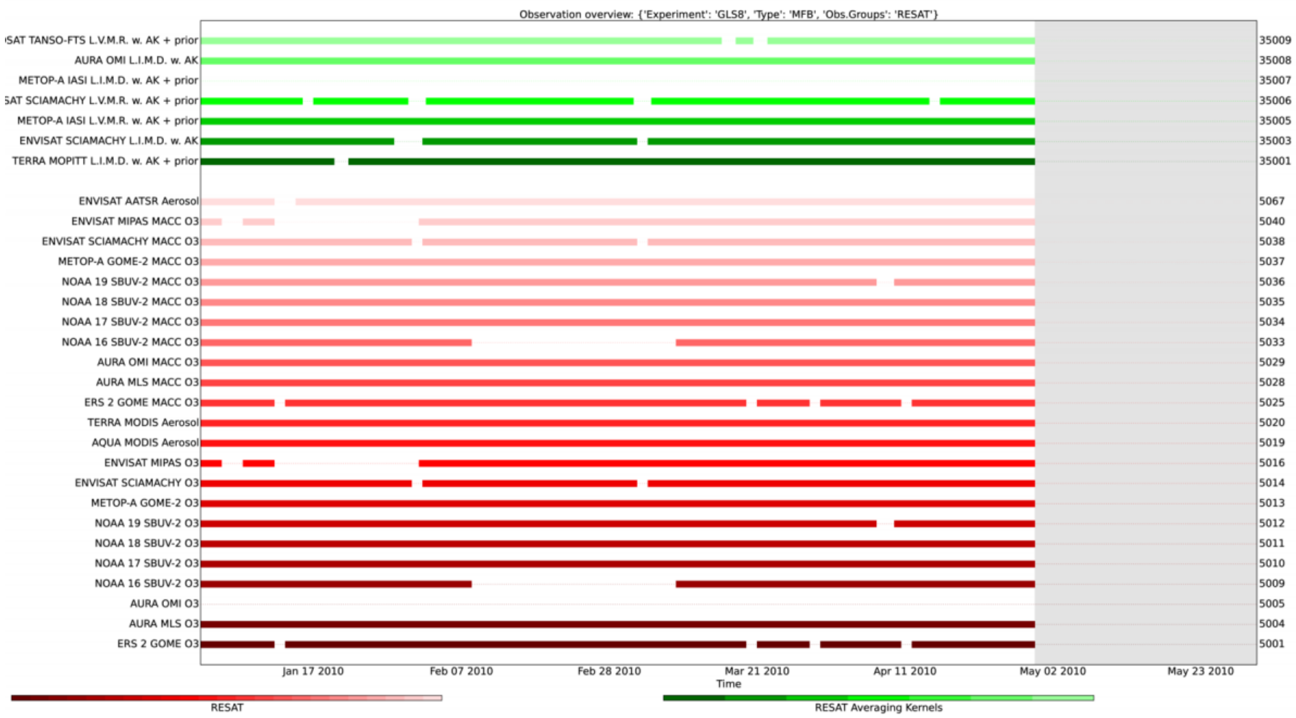

2. Evaluation results for the 2010 reanalysis run

2.1 Aerosol evaluation

2.1.1 Global aerosol distribution

Results can be found on the AeroCom/CAMS website (http://aerocom.met.no/cgi-bin/aerocom/surfobs_annualrs.pl?PROJECT=CAMS&MODELLIST=CAMS-reanalysis&FULL=2abbrev)

Table 2.1.1: Mean annual, global total and speciated aerosol optical depth (AOD) in the IFS experiment GLS8 (new CAMS reanalysis), in the MACC o-suite produced at the time and MACC reanalysis experiment FBOV for the year 2010.

	GLS8	O-SUITE	FBOV
AOD@550	0.143	0.158	0.192
BC-OD@550	0.006	0.008	0.007
Dust-OD@550	0.019	0.029	0.045
OA-OD@550	0.048	0.029	0.025
SO4-OD@550	0.034	0.039	0.053
SS-OD@550	0.036	0.053	0.062

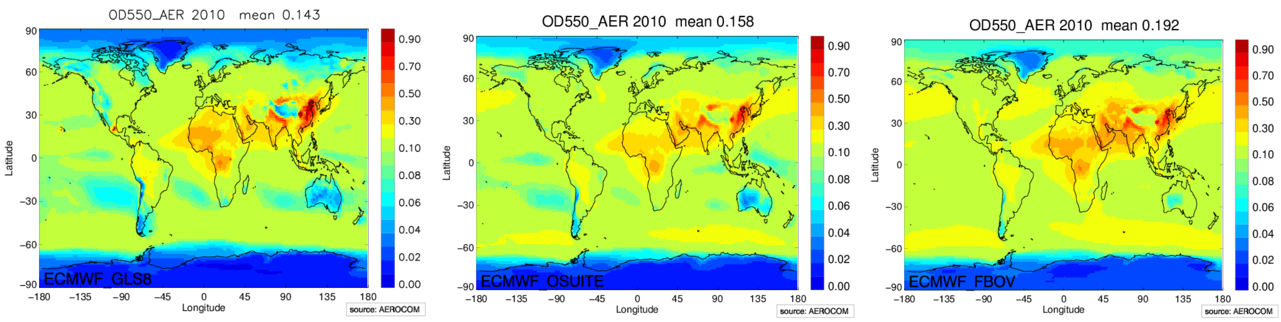

Figure 2.1.1: Averaged aerosol optical depth (AOD) from IFS experiments CAMS GLS8 (left), MACC o-suite (middle) and MACC FBOV (right) for the year 2010. Mean AOD in GLS8 is at 0.143, which is 34% less than what was in the earlier MACC reanalysis FBOV. Reductions are seen both in Northern hemisphere pollution regions and dust regions.

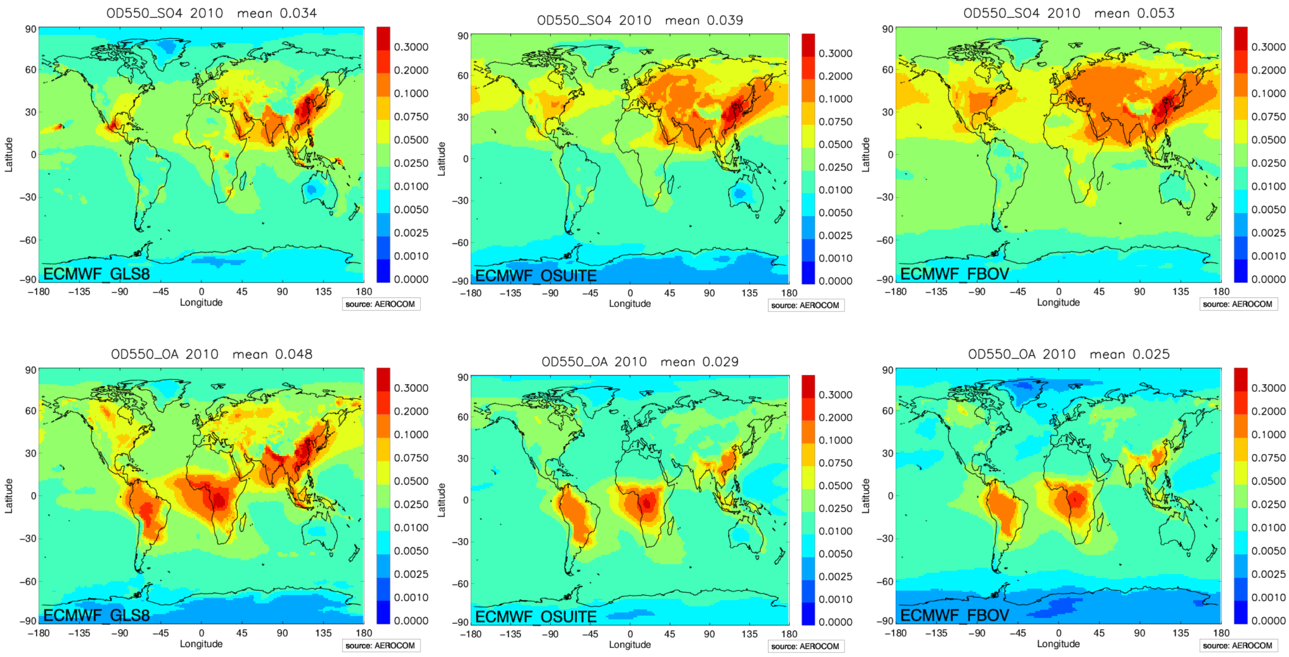

Figure 2.1.2: Averaged sulfate optical depth in upper row (GLS8 (left), o-suite (middle) and FBOV (right)) and organic aerosol optical depth lower row, for the year 2010. While sulphate AOD was dominating over organic aerosol AOD in the FBOV reanalysis, mean AODs of the two components are opposite in the GLS8 reanalysis (sulphate AOD: 0.034, organic AOD: 0.048). An important shift in aerosol composition appears when comparing GLS8 and FBOV. The sum of sulphate and organic AOD has increased by 10% in GLS8, but a larger decrease in dust and sea salt is finally contributing to the overall decrease in AOD.

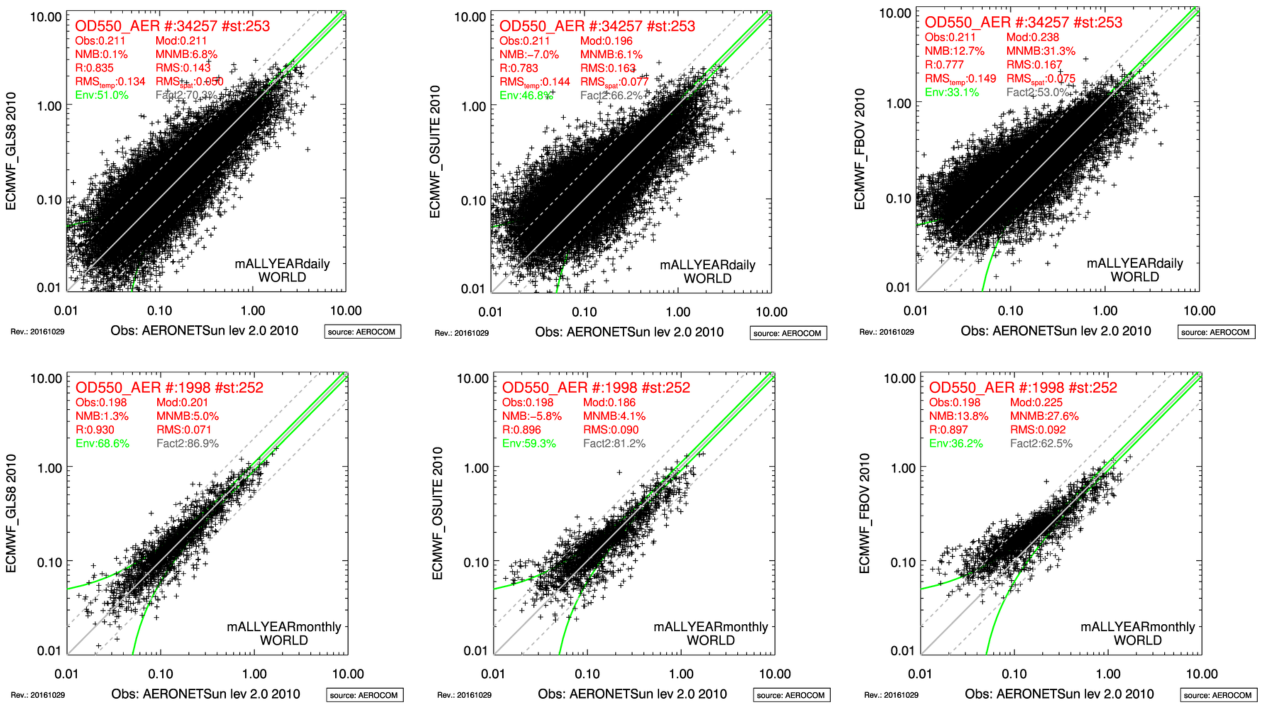

Figure 2.1.3: Evaluation of simulated daily (upper row) and monthly (lower row) AOD against Aeronet level 2.0 sun photometer measurements in GLS8 (left), o-suite (middle) and FBOV (right) for the year 2010. Statistics shown in the figure show a temporal-spatial RMS error reduction from 0.167 in FBOV to 0.143 in GLS8, consistent with a reduction of MNMB from 31% in FBOV to 7% in GLS8. An overall positive bias in FBOV has become a small positive bias in the GLS8 experiment. The quality of the IFS GLS8 experiment, despite or because of the significant shift in the aerosol composition is better or as good as the o-suite.

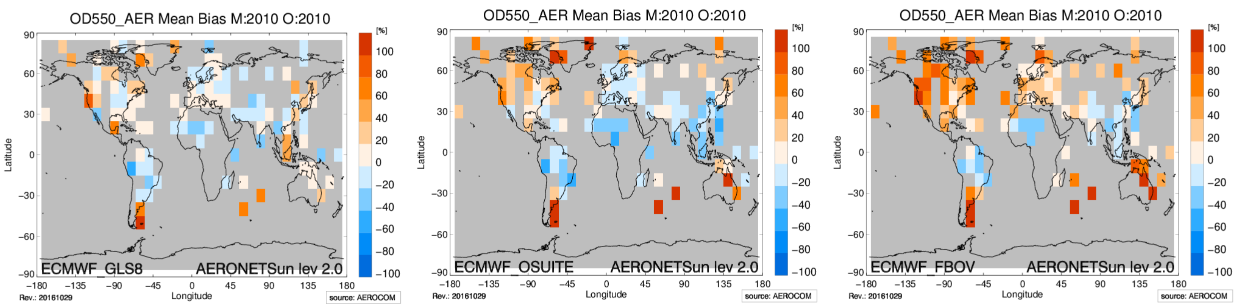

Figure 2.1.4: Regional relative mean bias of simulated daily AOD against Aeronet sun level 2.0 sun photometer measurements in GLS8 (left), o-suite (middle) and FBOV (right) for the year 2010. The regions with positive bias are considerable reduced in the o-suite and GLS8 experiment. More regions exhibit a bias of only +-20%, supporting that the GLS8 experiment, despite or because of the significant shift in the aerosol composition is better or as good as the o-suite was.

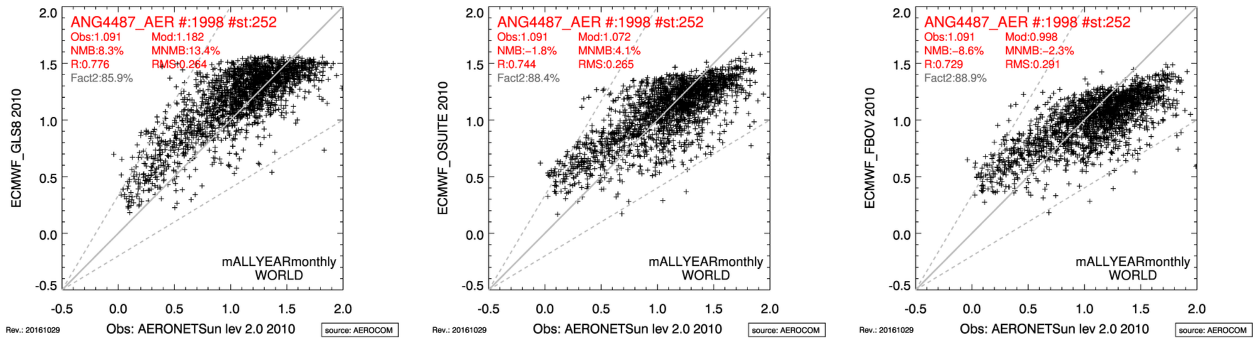

Figure 2.1.5: Evaluation of simulated daily Angstroem Coefficient against Aeronet sun level 2.0 photometer measurements in GLS8 (left), o-suite (middle) and FBOV (right) for the year 2010. Statistics shown in the figure show a temporal-spatial RMS error reduction from 0.29 in FBOV to 0.26 in GLS8. The MNMB-bias increased from -2.3% in FBOV to +13% in GLS8.

2.1.2 Dust

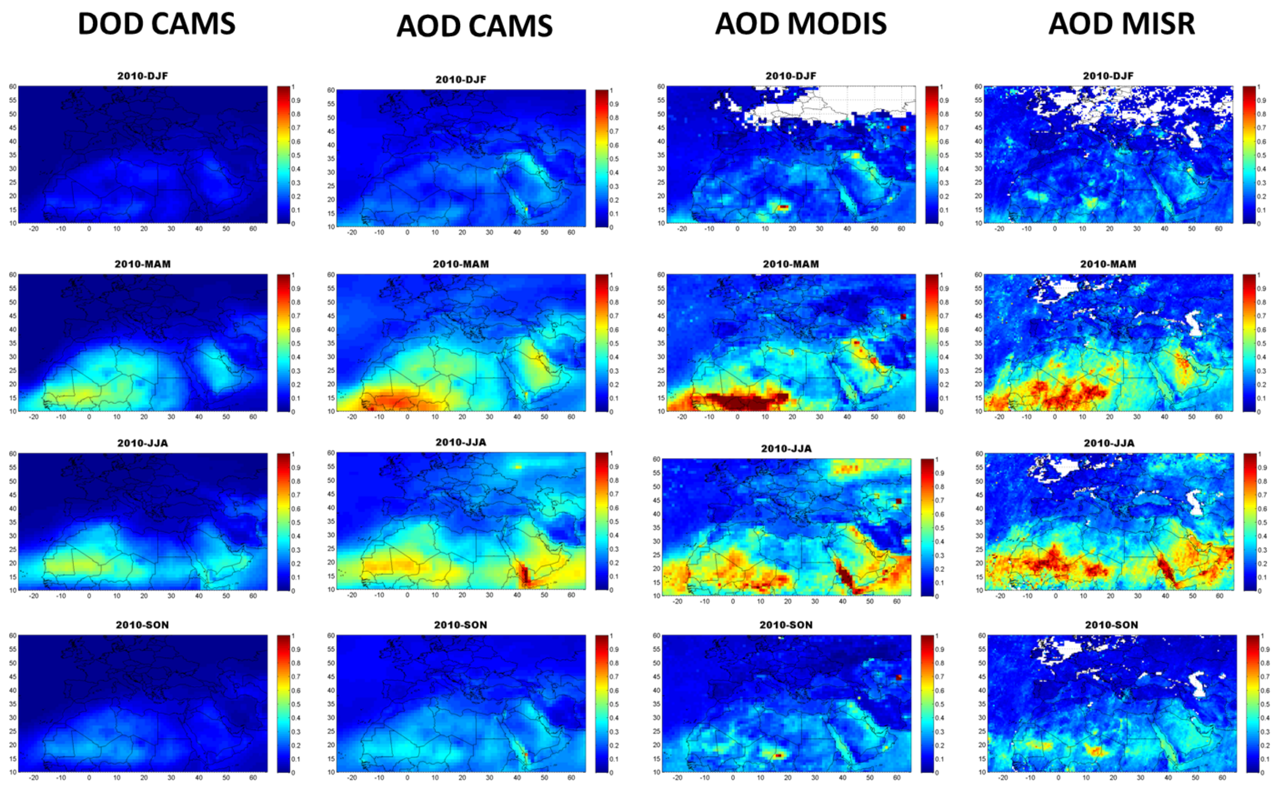

Figure 2.1.6: Seasonal averaged DOD and AOD from CAMS reanalysis (on 3-hourly basis) as well as AOD from Aqua/MODIS combined Dark target and Deep Blue daily global product and MISR daily global AOD product for the year 2010. Winter (DJF), spring (MAM), summer (JJA) and autumn (SON).

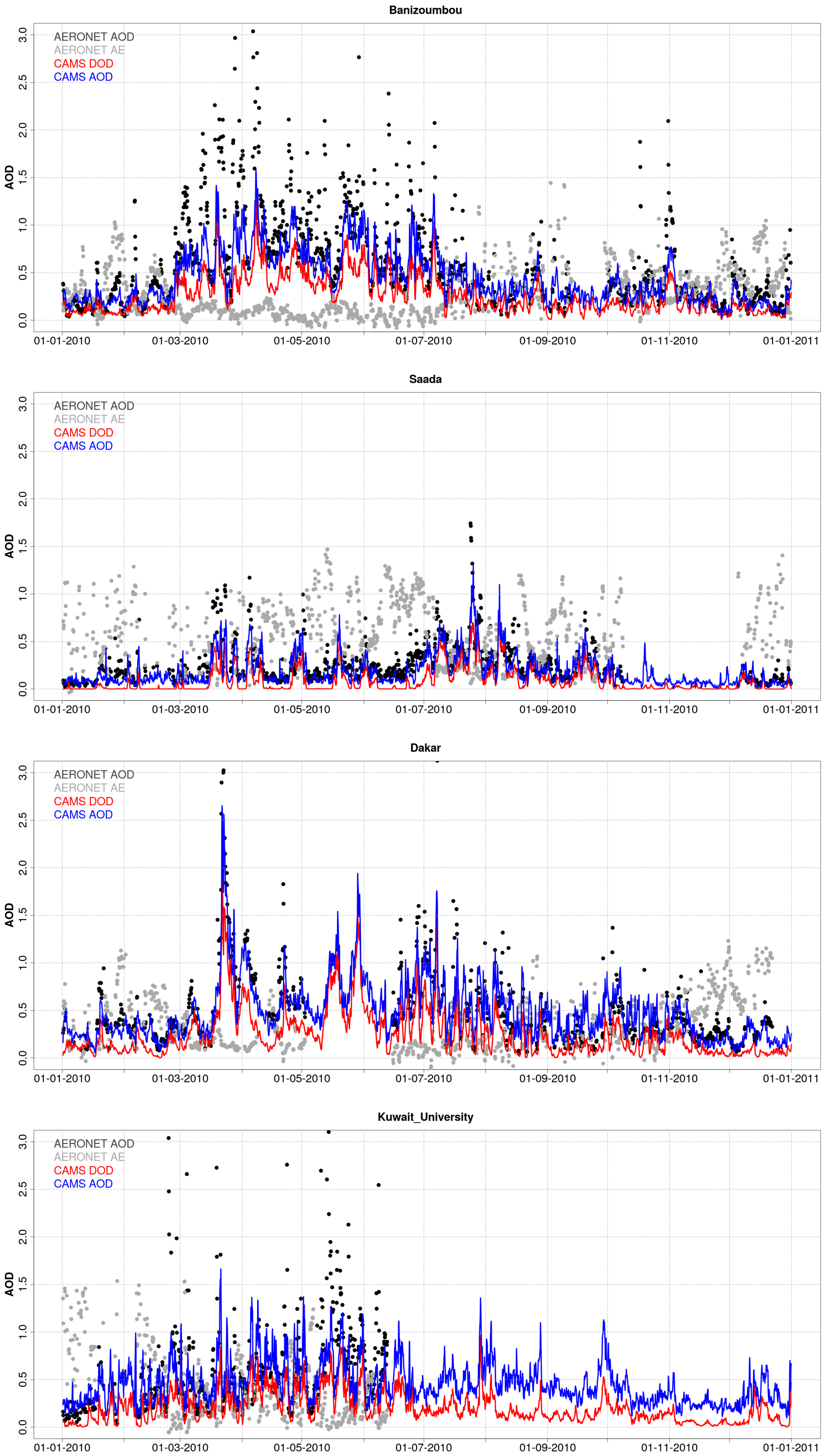

Figure 2.1.7: 3-houly AOD and AE Level 2.0 Direct-Sun AERONET observations (black and grey dots, respectively), as well as CAMS DOD (red line) and CAMS AOD (blue line) over Banizoumbou (Sahel) Saada (NW Maghreb), Dakar (Tropical North Atlantic) and Kuwait University (Middle East). AE < 0.6 indicates desert dust dominant regimes.

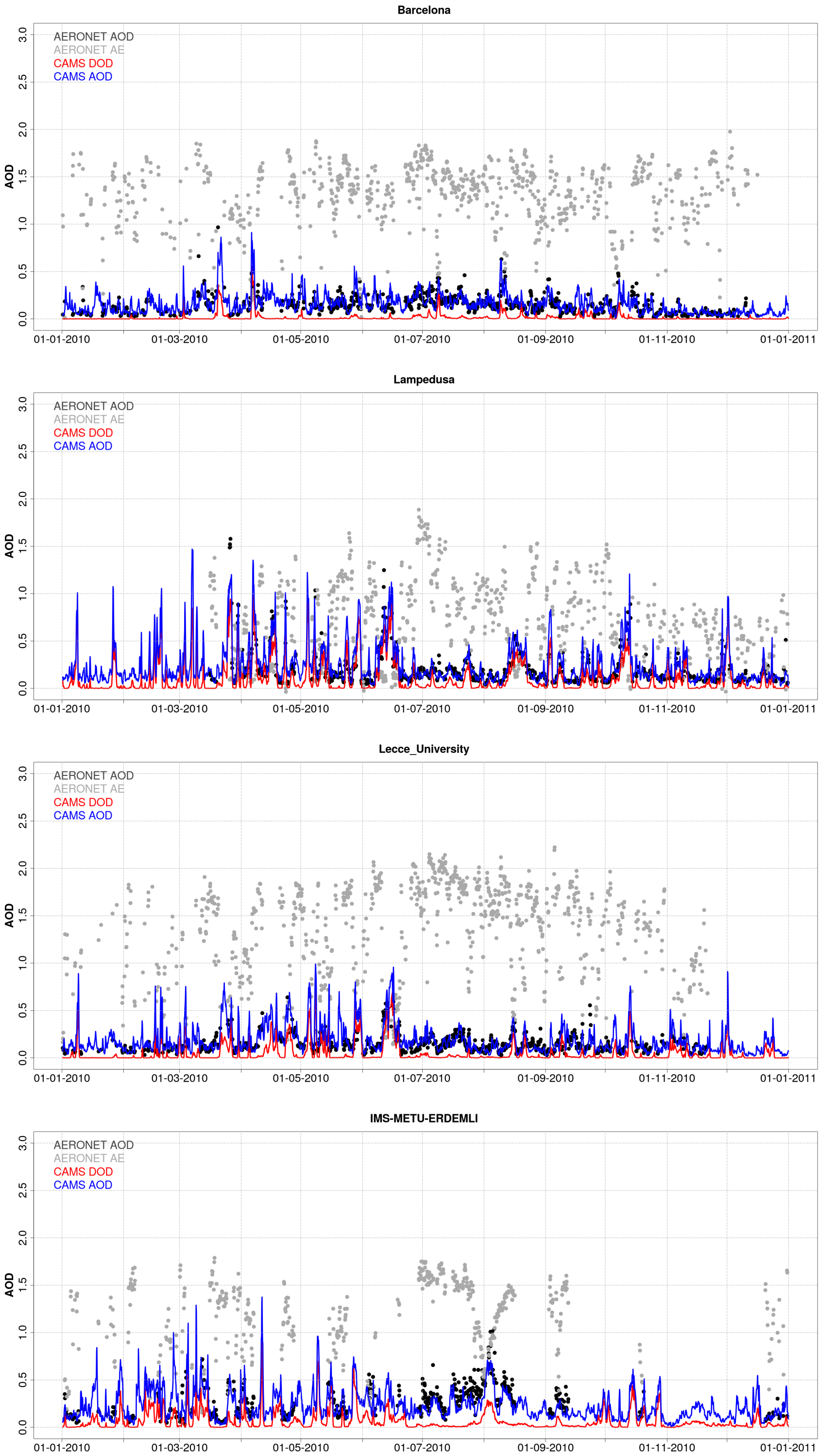

Figure 2.1.8: 3-houly AOD and AE Level 2.0 Direct-Sun AERONET observations (black and grey dots, respectively), as well as CAMS DOD (red line) and CAMS AOD (blue line) over Barcelona (W. Mediterranean), Lampedusa (Central Mediterranean), Lecce University (Central Mediterranean) and IMS-METU-ERDEMLI (E. Med). AE < 0.6 indicates desert dust dominant regimes.

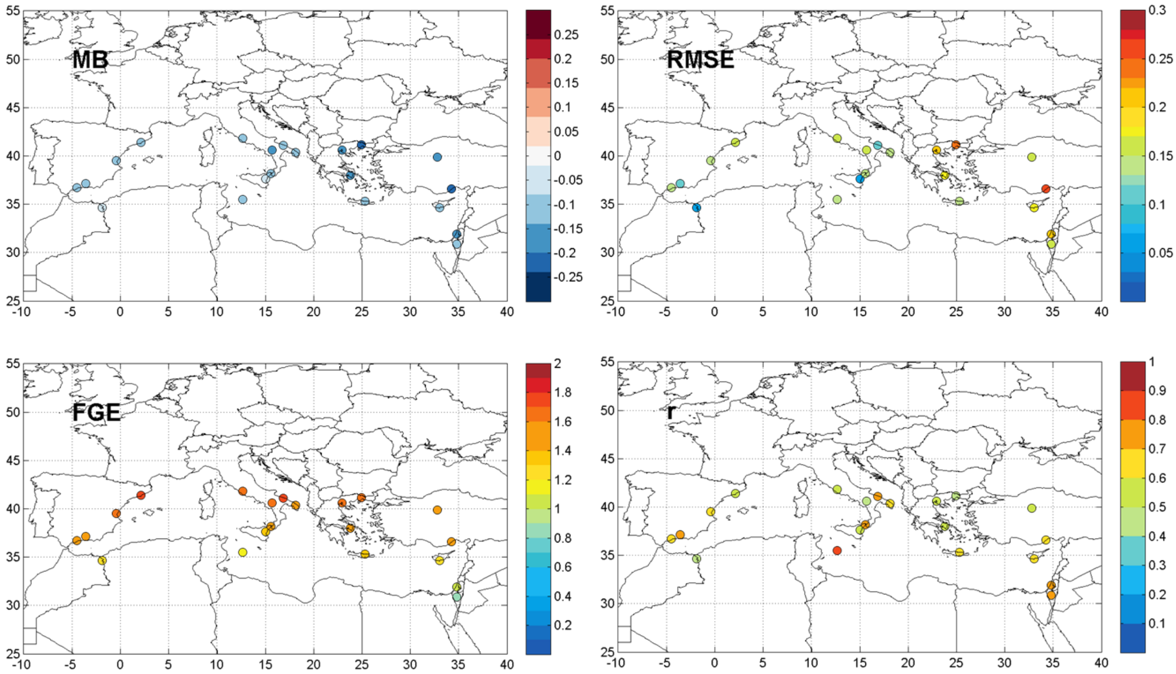

Figure 2.1.9: Skill scores (MB, FGE, RMSE and r) of CAMS reanalysis (on 3-hourly basis) for the year 2010. AOD from AERONET (quality-assured) is the reference (on 3-hourly basis).

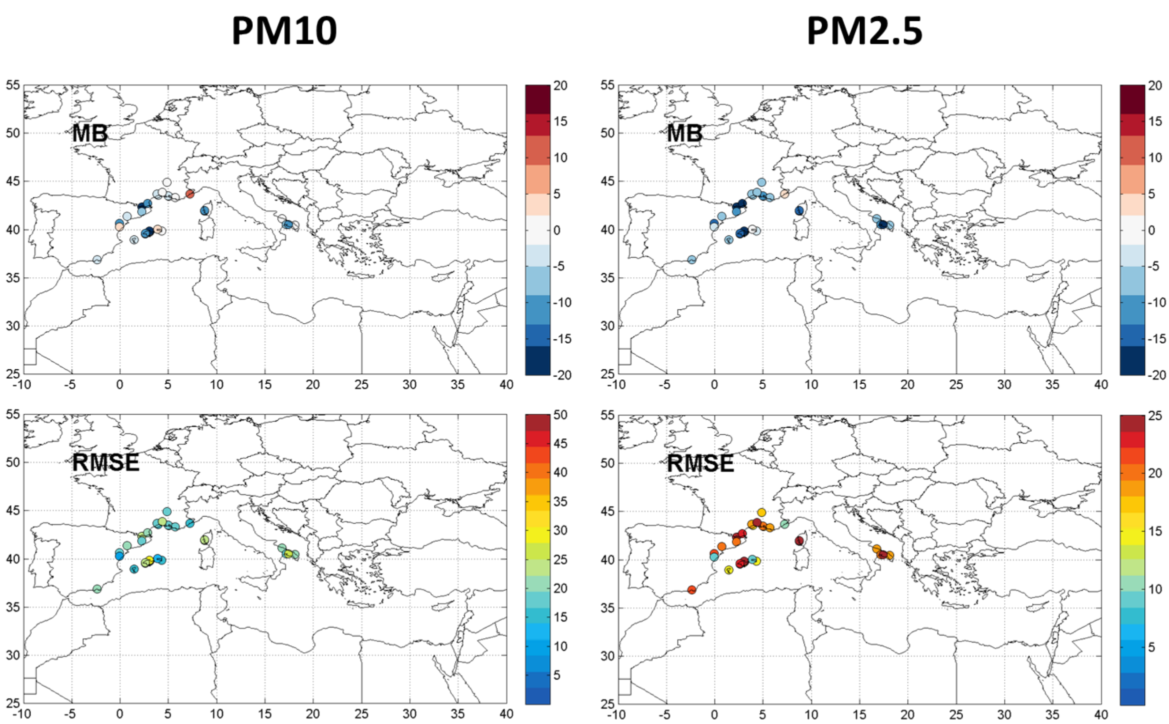

Figure 2.1.10: Skill scores (MB and FGE) of CAMS reanalysis (on 3-hourly basis) for the year 2010. PM10 and PM2.5 from Airbase observations (validated) are the reference. Only background available suburban and rural stations are displayed. In average for all the sites, MB is -5.12 µg/m3 for PM10 while PM2.5 is -10.17 µg/m3 and FGE is 0.70 µg/m3 for PM10 while PM2.5 is 0.80 µg/m3.

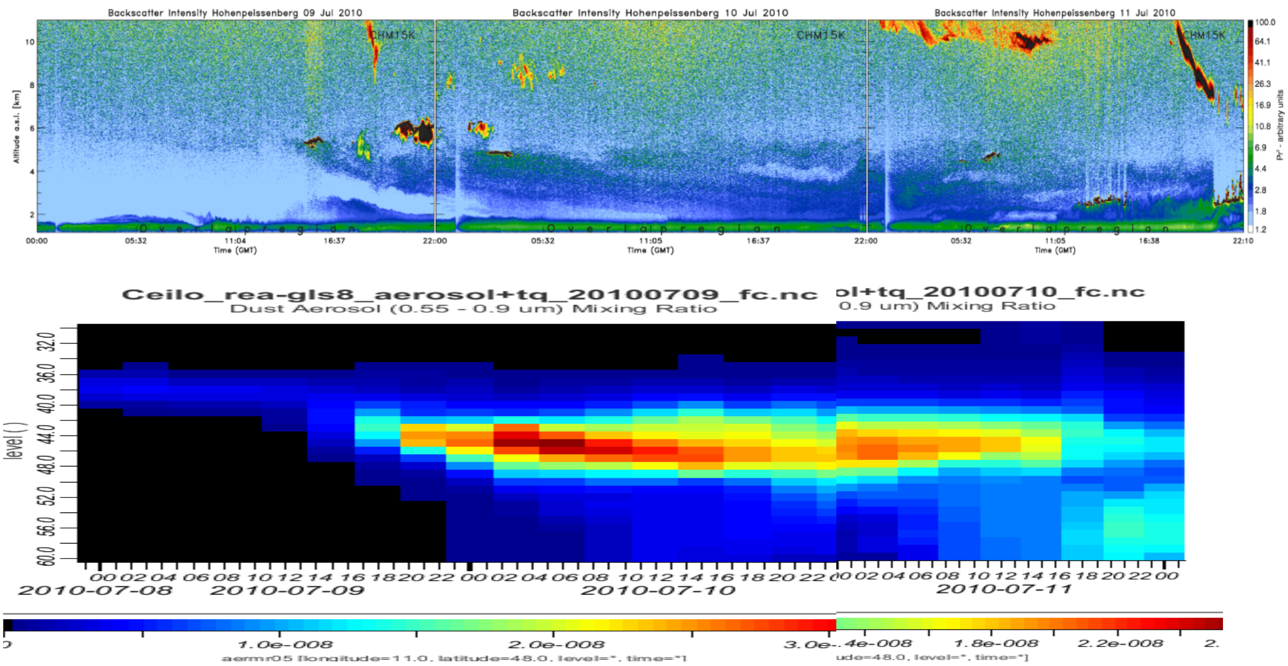

Fig 2.1.11: Saharan Dust Event over Hohenpeissenberg Germany (48°N, 11°E) on 9.-11.July 2010. The qualitative range corrected backscatter time-height section shows the reproduction of the SD plume by the reanalysis run gls8. The center of the layer around lev 44 corresponds to roughly 3 km altitude.

2.2 Verification of tropospheric ozone

2.2.1 Verification with sonde data in the free troposphere

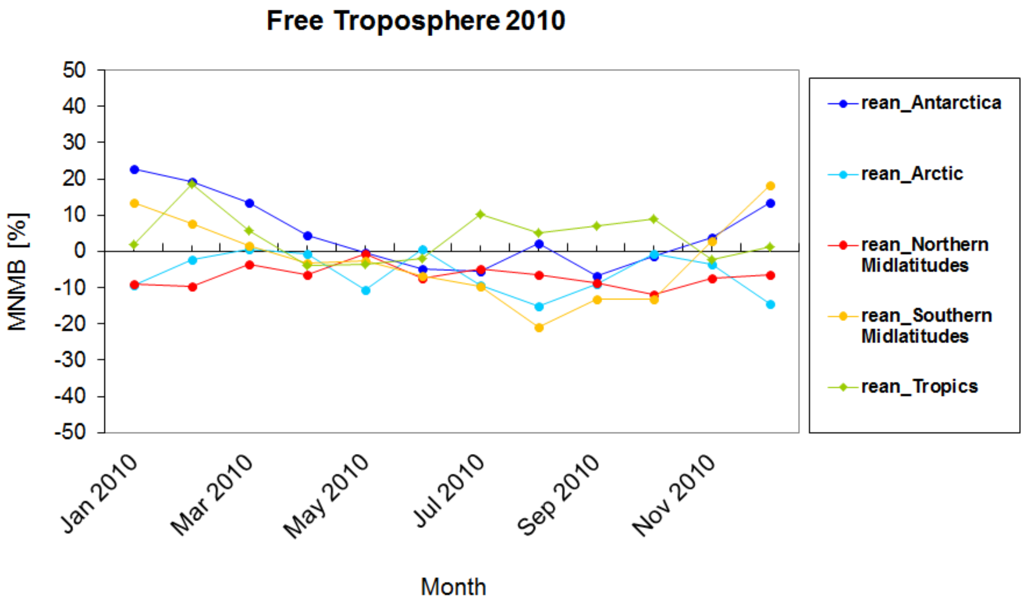

Fig. 2.2.1: MNMBs (gls8 minus ozone sondes) for the 5 latitude regions in the free troposphere (layer between 750 and 350 hPa, and between 750 and 200 in the Tropics).

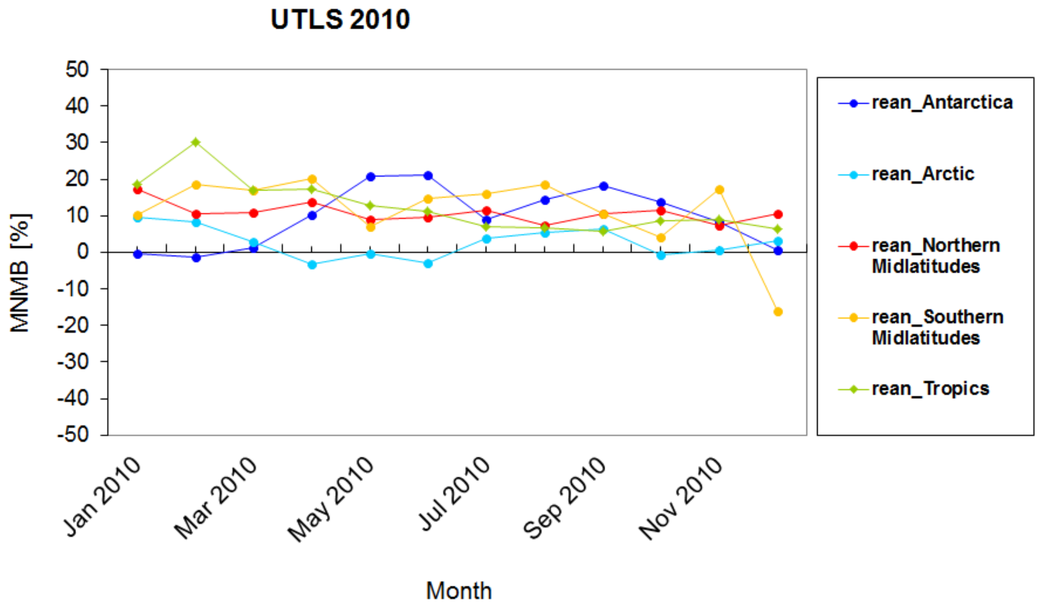

Fig. 2.2.2: MNMBs (gls8 minus ozone sondes) for the 5 latitude regions in the UTLS (layer between 300 and 100 hPa, and between 100 and 60 in the Tropics).

2.2.2 Verification with GAW surface observations

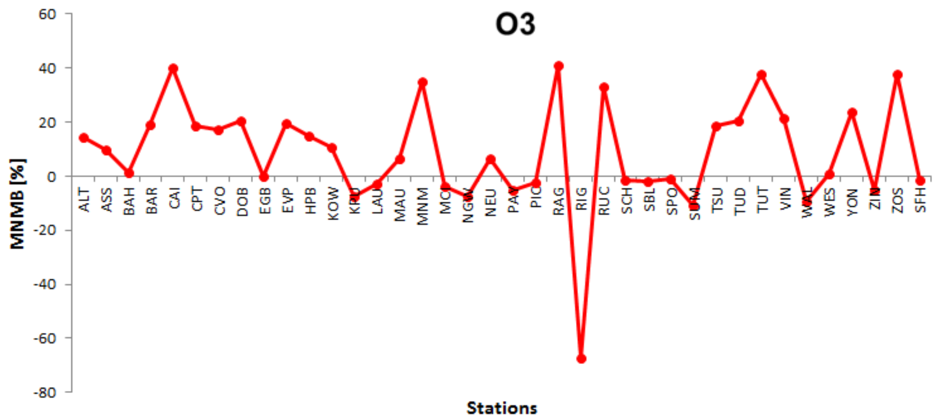

Fig. 2.2.3: MNMBs for reanalysis minus ozone observations from GAW stations.

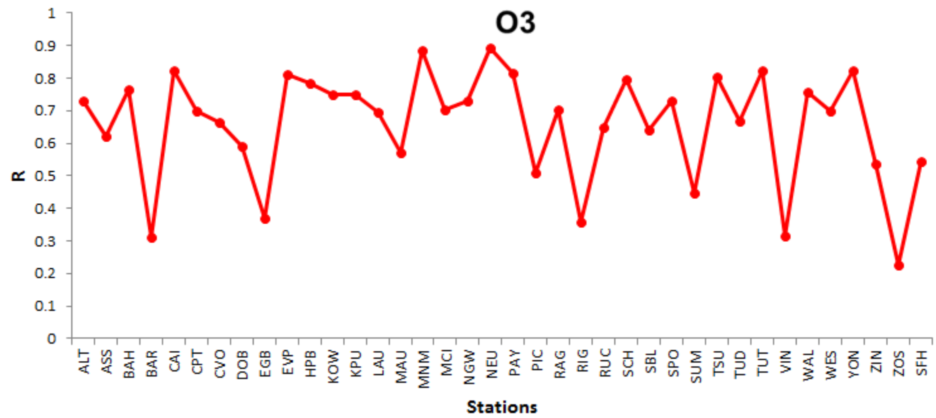

Fig. 2.2.4: Correlation coefficient R for reanalysis minus ozone observations from GAW stations.

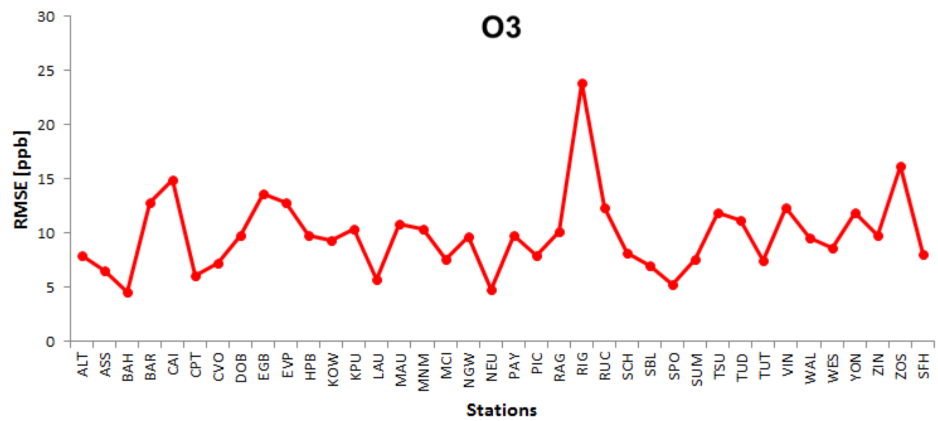

Fig. 2.2.5: RMSEs for reanalysis minus ozone observations from GAW stations.

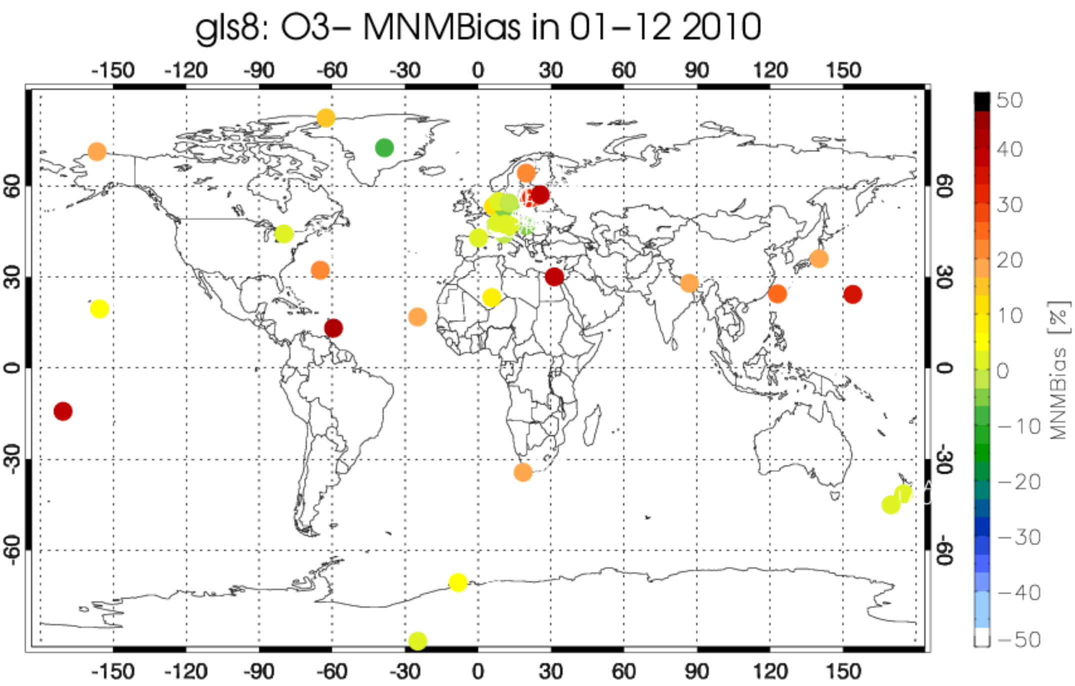

Fig. 2.2.6: Map of MNMBs at the GAW station locations averaged over the time period January-December 2010.

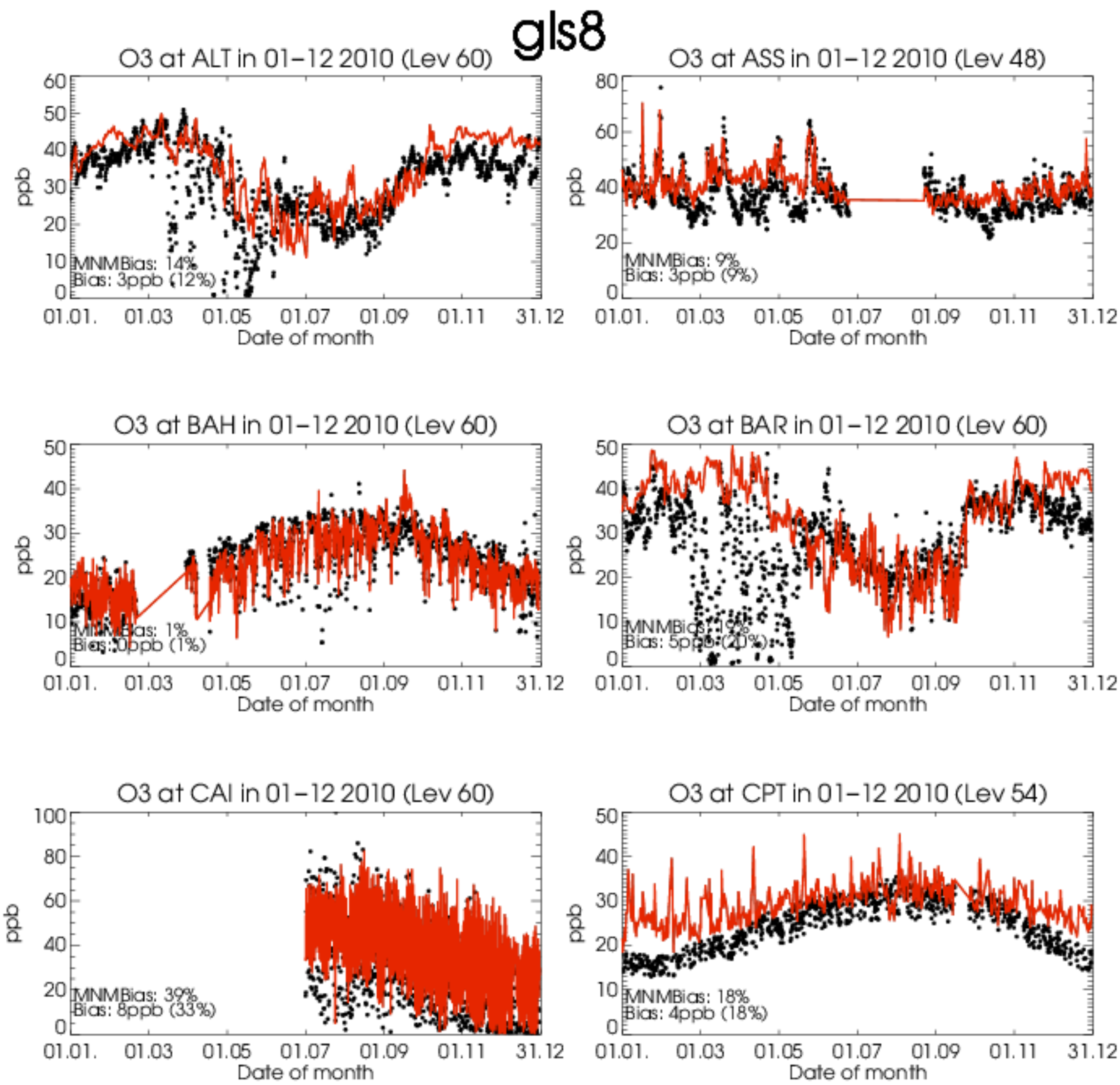
gls8
O3 at ALT in 01–12 2010 (Lev 60)
MNMBias: 14%
Bias: 3ppb (12%)
O3 at ASS in 01–12 2010 (Lev 48)
MNMBias: 9%
Bias: 3ppb (9%)
O3 at BAH in 01–12 2010 (Lev 60)
MNMBias: 1%
Bias: 0ppb (1%)
O3 at BAR in 01–12 2010 (Lev 60)
O3 at CAI in 01–12 2010 (Lev 60)
MNMBias: 39%
Bias: 8ppb (33%)
O3 at CPT in 01–12 2010 (Lev 54)
MNMBias: 18%
Bias: 4ppb (18%)
ppb
Date of month
01.01.
01.03
01.05
01.07
01.09
01.11
31.12

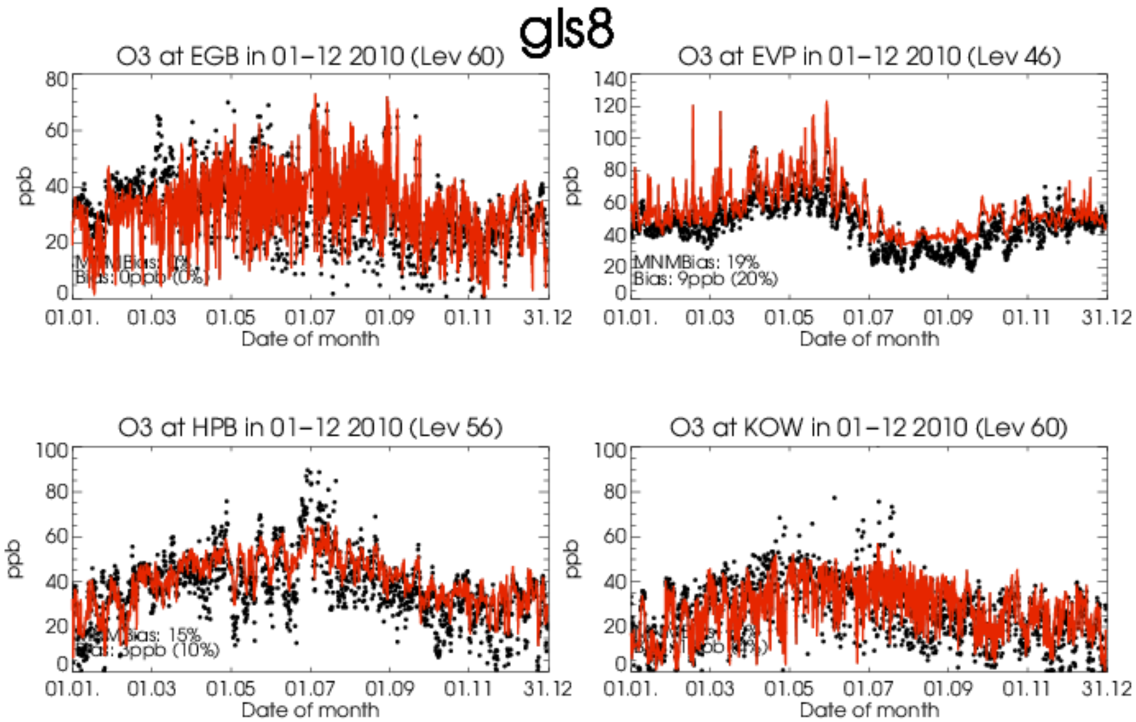
gls8
O3 at EGB in 01–12 2010 (Lev 60)
O3 at EVP in 01–12 2010 (Lev 46)
MNMBias: 19%
Bias: 9ppb (20%)
O3 at HPB in 01–12 2010 (Lev 56)
O3 at KOW in 01–12 2010 (Lev 60)
ppb
Date of month
01.01. 01.03 01.05 01.07 01.09 01.11 31.12

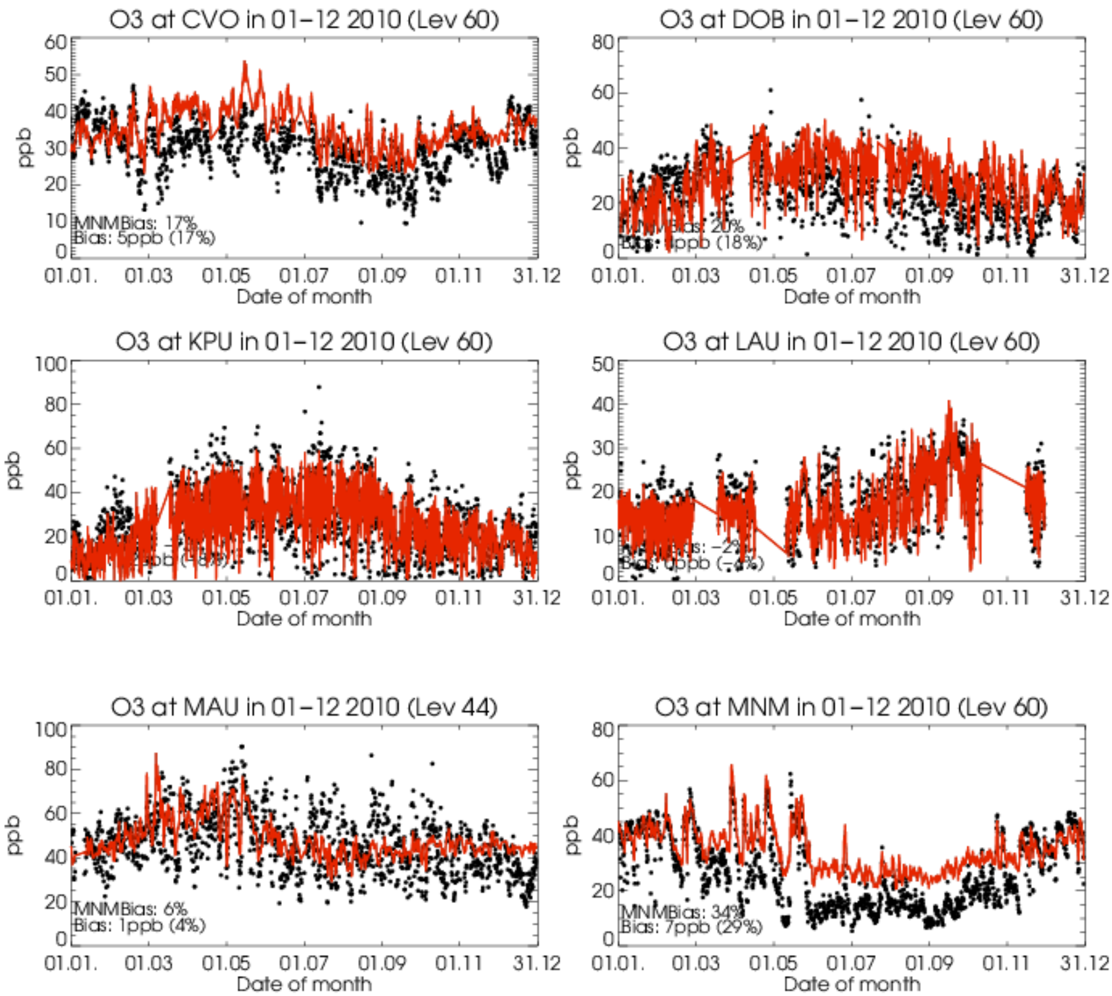
O3 at CVO in 01−12 2010 (Lev 60)
MNMBias: 17%
Bias: 5ppb (17%)
O3 at DOB in 01−12 2010 (Lev 60)
O3 at KPU in 01−12 2010 (Lev 60)
O3 at LAU in 01−12 2010 (Lev 60)
O3 at MAU in 01−12 2010 (Lev 44)
MNMBias: 6%
Bias: 1ppb (4%)
O3 at MNM in 01−12 2010 (Lev 60)
MNMBias: 34%
Bias: 7ppb (29%)
ppb
Date of month
01.01. 01.03 01.05 01.07 01.09 01.11 31.12

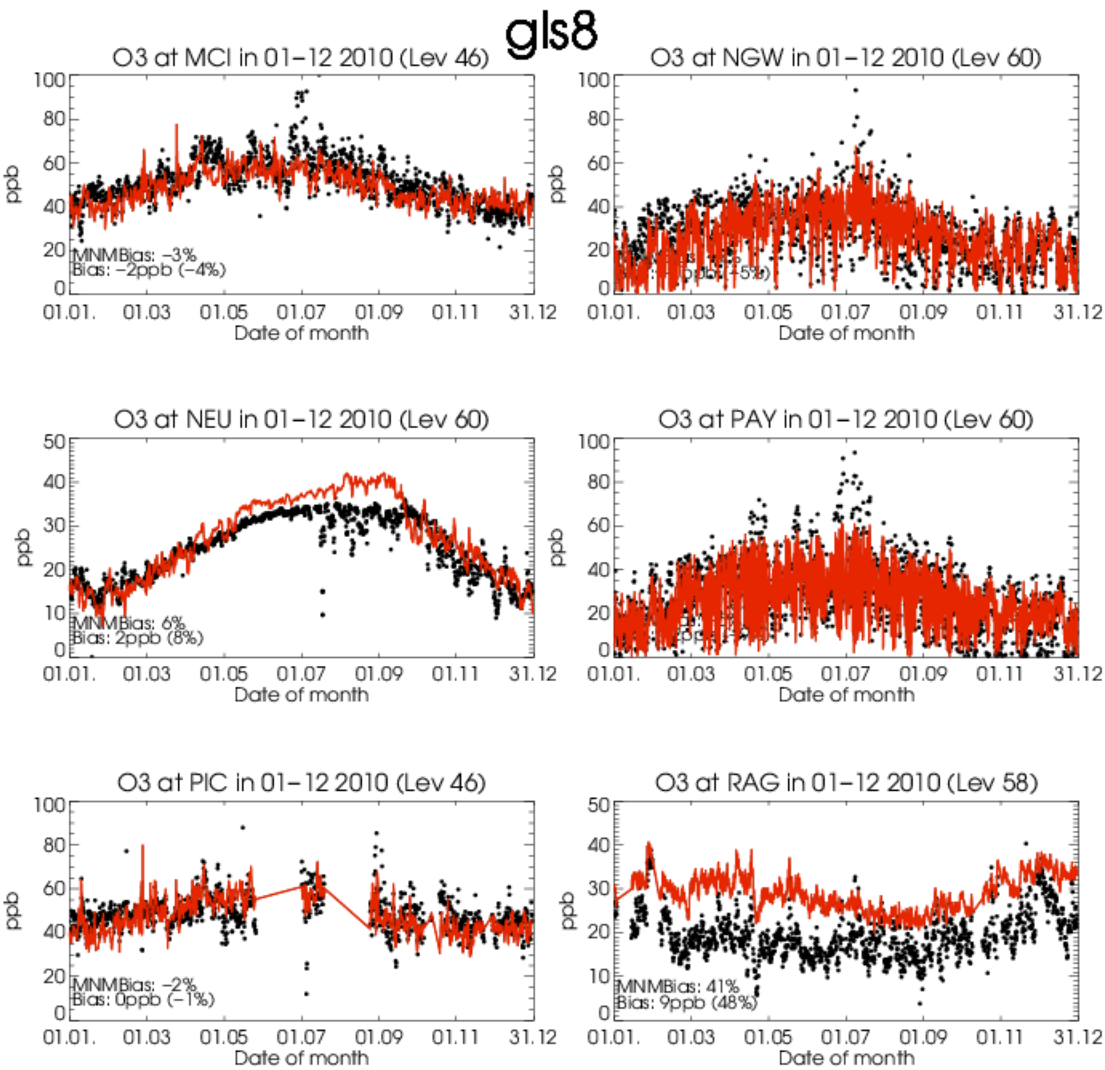
gls8
O3 at MCI in 01–12 2010 (Lev 46)
MNMBias: –3%
Bias: –2ppb (–4%)
O3 at NGW in 01–12 2010 (Lev 60)
O3 at NEU in 01–12 2010 (Lev 60)
MNMBias: 6%
Bias: 2ppb (8%)
O3 at PAY in 01–12 2010 (Lev 60)
O3 at PIC in 01–12 2010 (Lev 46)
MNMBias: –2%
Bias: 0ppb (–1%)
O3 at RAG in 01–12 2010 (Lev 58)
MNMBias: 41%
Bias: 9ppb (48%)
ppb
Date of month
01.01. 01.03 01.05 01.07 01.09 01.11 31.12

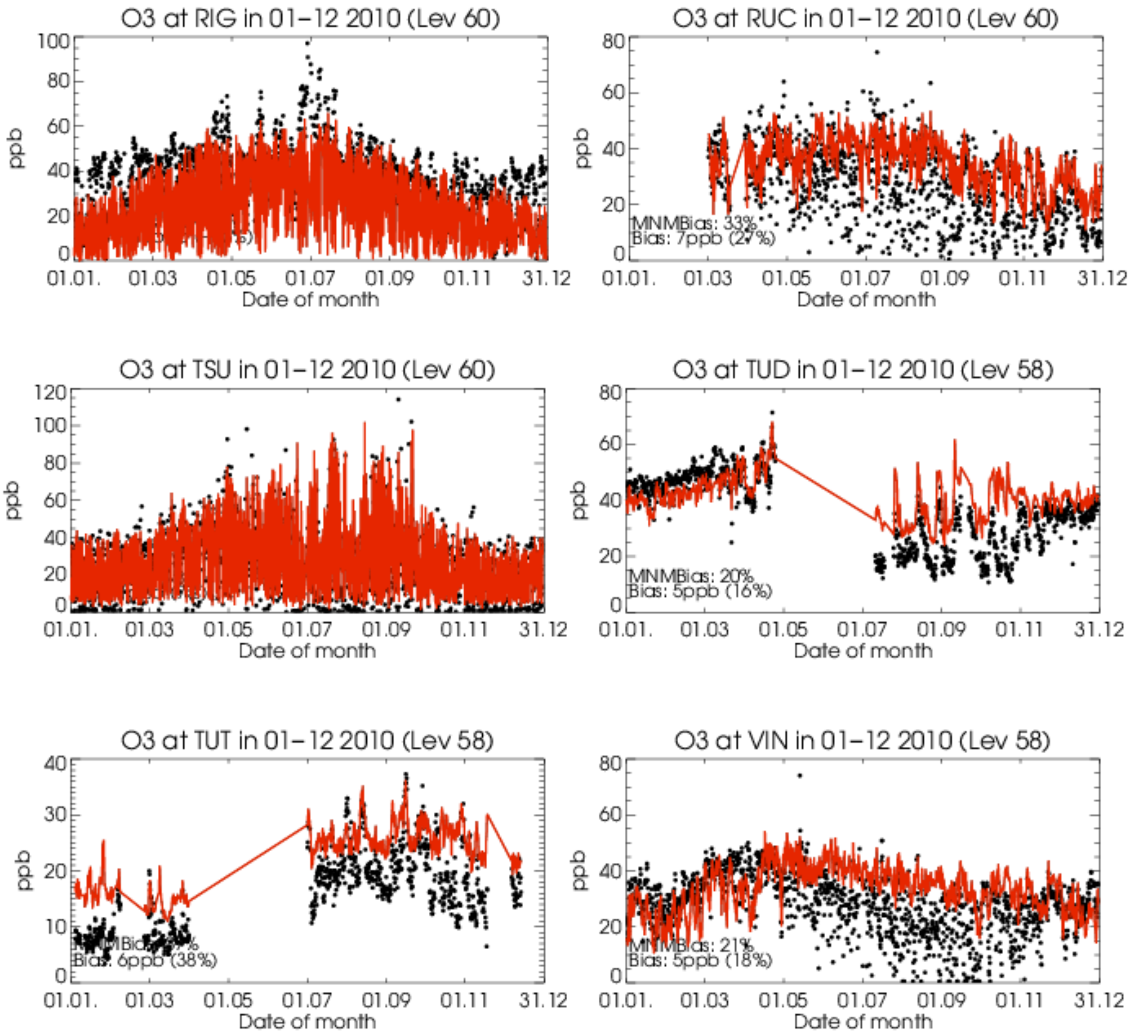

O3 at RIG in 01−12 2010 (Lev 60)
O3 at RUC in 01−12 2010 (Lev 60)
MNMBias: 33%
O3 at TSU in 01−12 2010 (Lev 60)
O3 at TUD in 01−12 2010 (Lev 58)
MNMBias: 20%
Bias: 5ppb (16%)
O3 at TUT in 01−12 2010 (Lev 58)
Bias: 6ppb (38%)
O3 at VIN in 01−12 2010 (Lev 58)
MNMBias: 21%
Bias: 5ppb (18%)
ppb
Date of month
01.01.
01.03
01.05
01.07
01.09
01.11
31.12

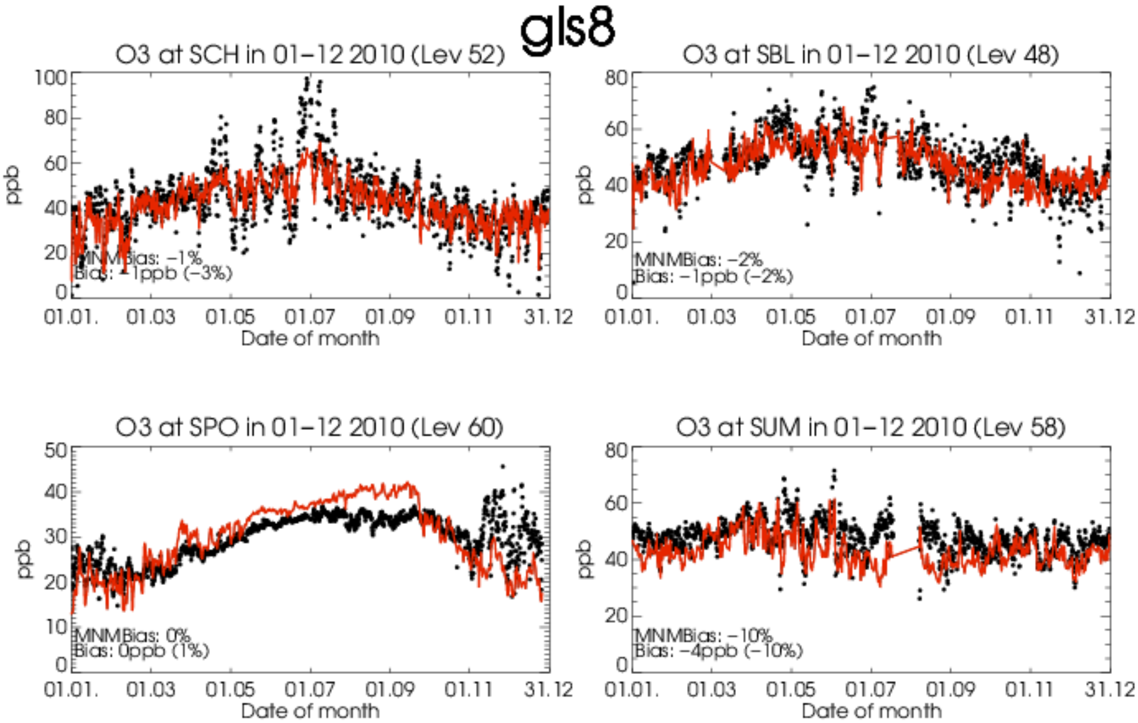
gls8
O3 at SCH in 01–12 2010 (Lev 52)
MNMBias: –1%
Bias: –1ppb (–3%)
O3 at SBL in 01–12 2010 (Lev 48)
MNMBias: –2%
Bias: –1ppb (–2%)
O3 at SPO in 01–12 2010 (Lev 60)
MNMBias: 0%
Bias: 0ppb (1%)
O3 at SUM in 01–12 2010 (Lev 58)
MNMBias: –10%
Bias: –4ppb (–10%)
ppb
Date of month
01.01. 01.03 01.05 01.07 01.09 01.11 31.12

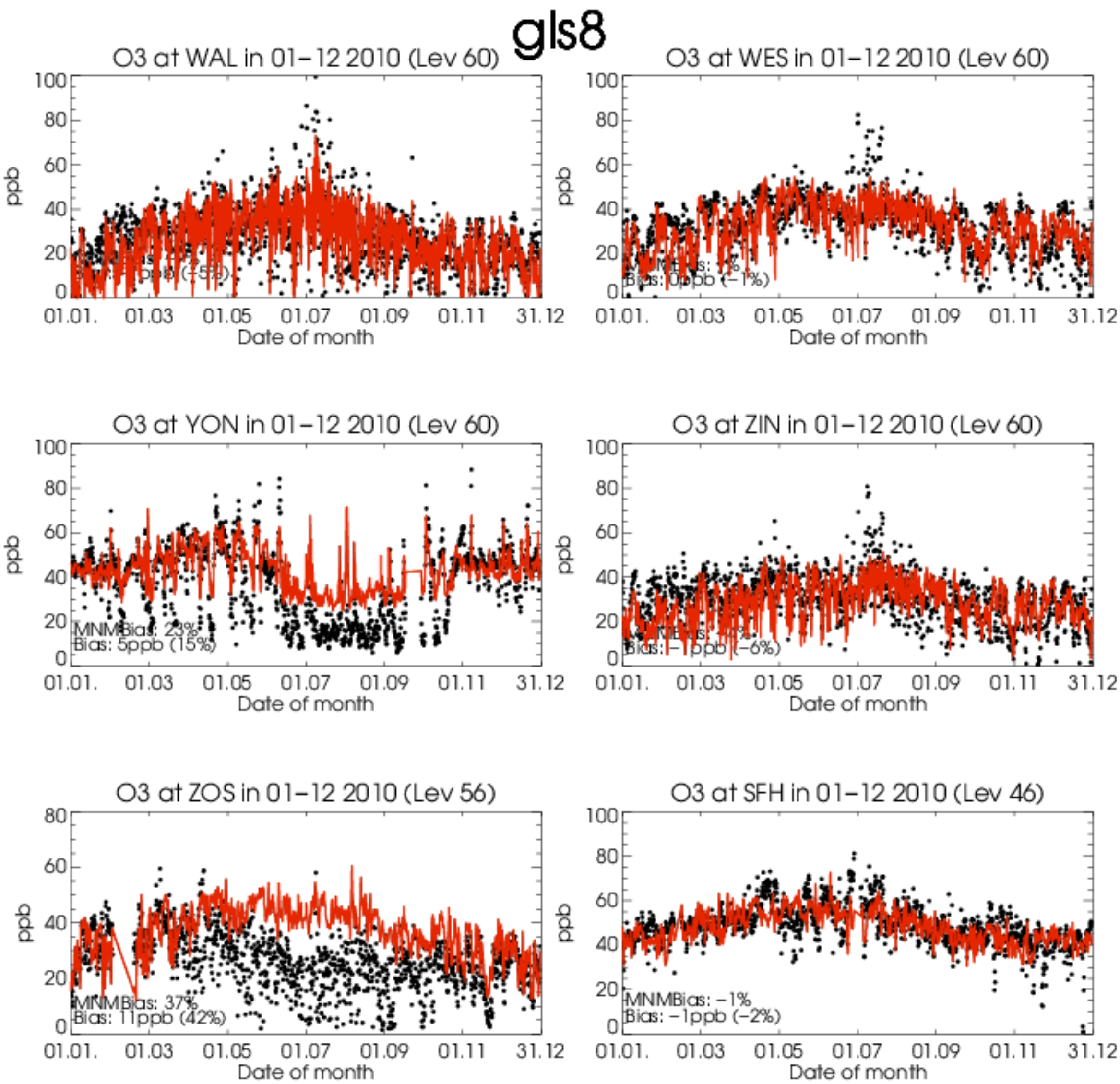

Fig. 2.2.7: Timeseries plots for O3 for GAW stations in the period 01-12 2010

2.2.3 Verification with European EMEP surface ozone observations

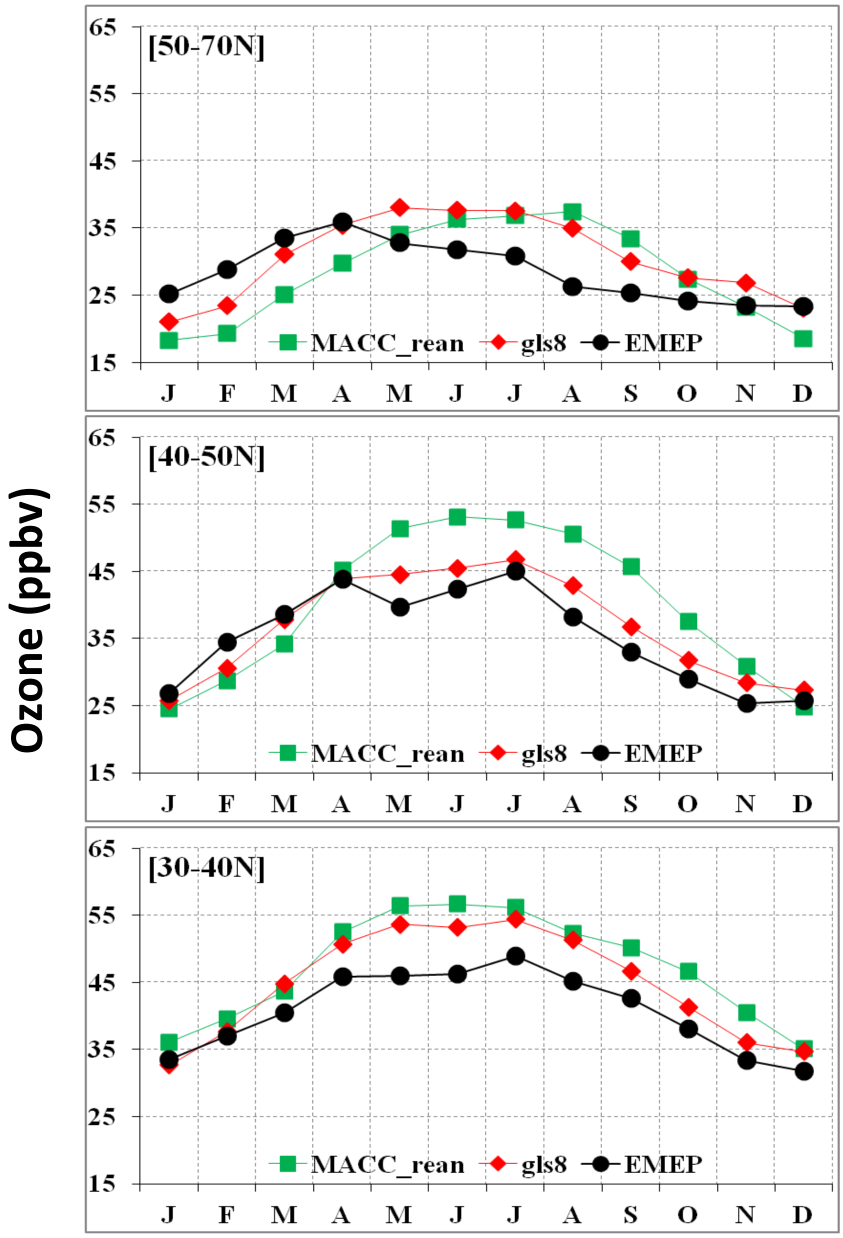

Figure 2.2.8. Mean monthly variability for the year 2010 of the new Reanalysis experiment gls8 (red robs) the MACC reanalysis (green squares), and the EMEP observations (black circles) over Northern Europe (1st row), Central Europe (2nd row), Southern Europe (3rd row)

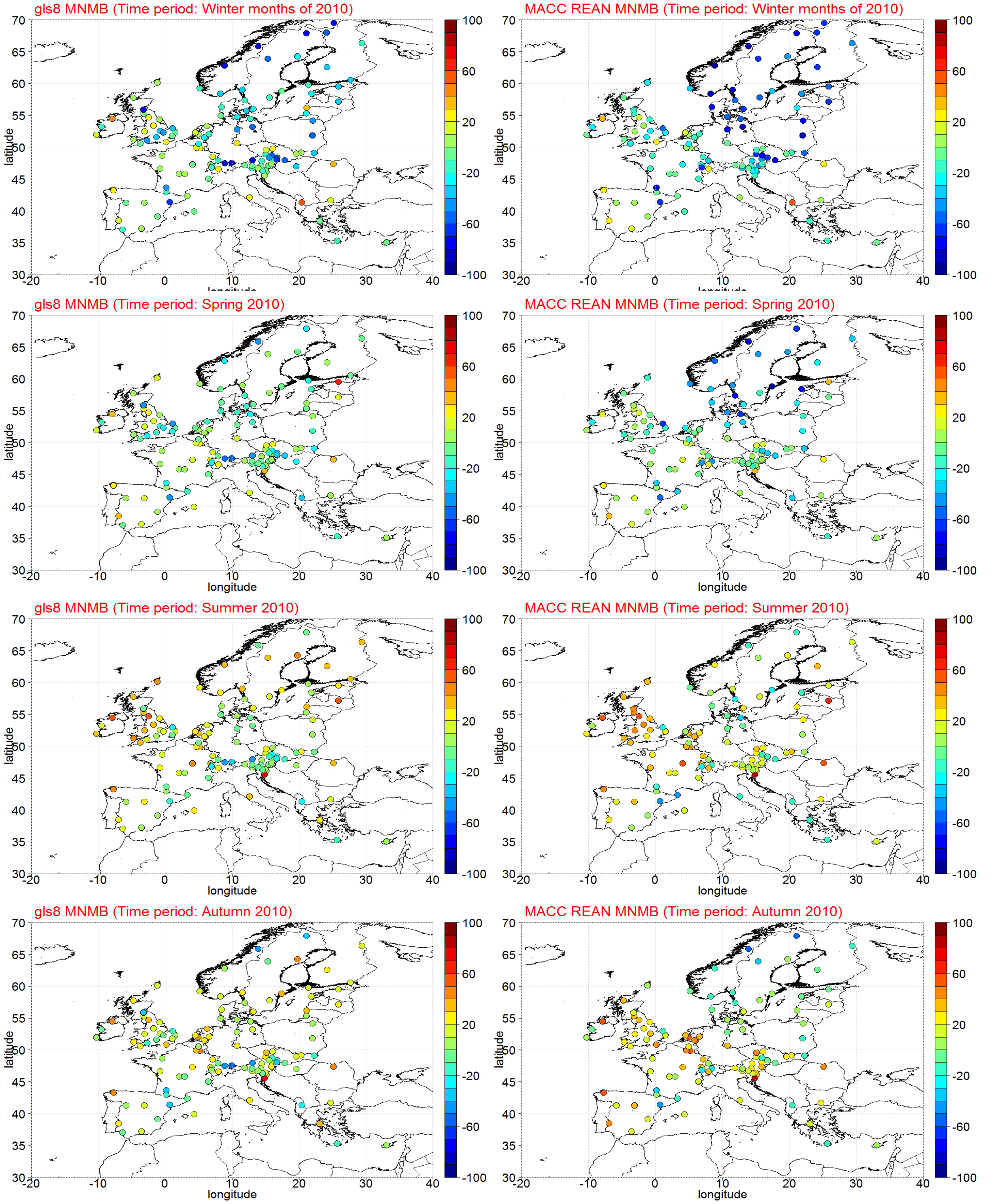

Figure 2.2.9. Modified Normalised Mean Biases (MNMBs) during Winter months of 2010 (1st row), Spring 2010 (2nd row), Summer 2010 (3rd row) and Autumn 2010 (4th row) for the new Reanalysis experiment gls8 (left) and the MACC reanalysis (rigth).

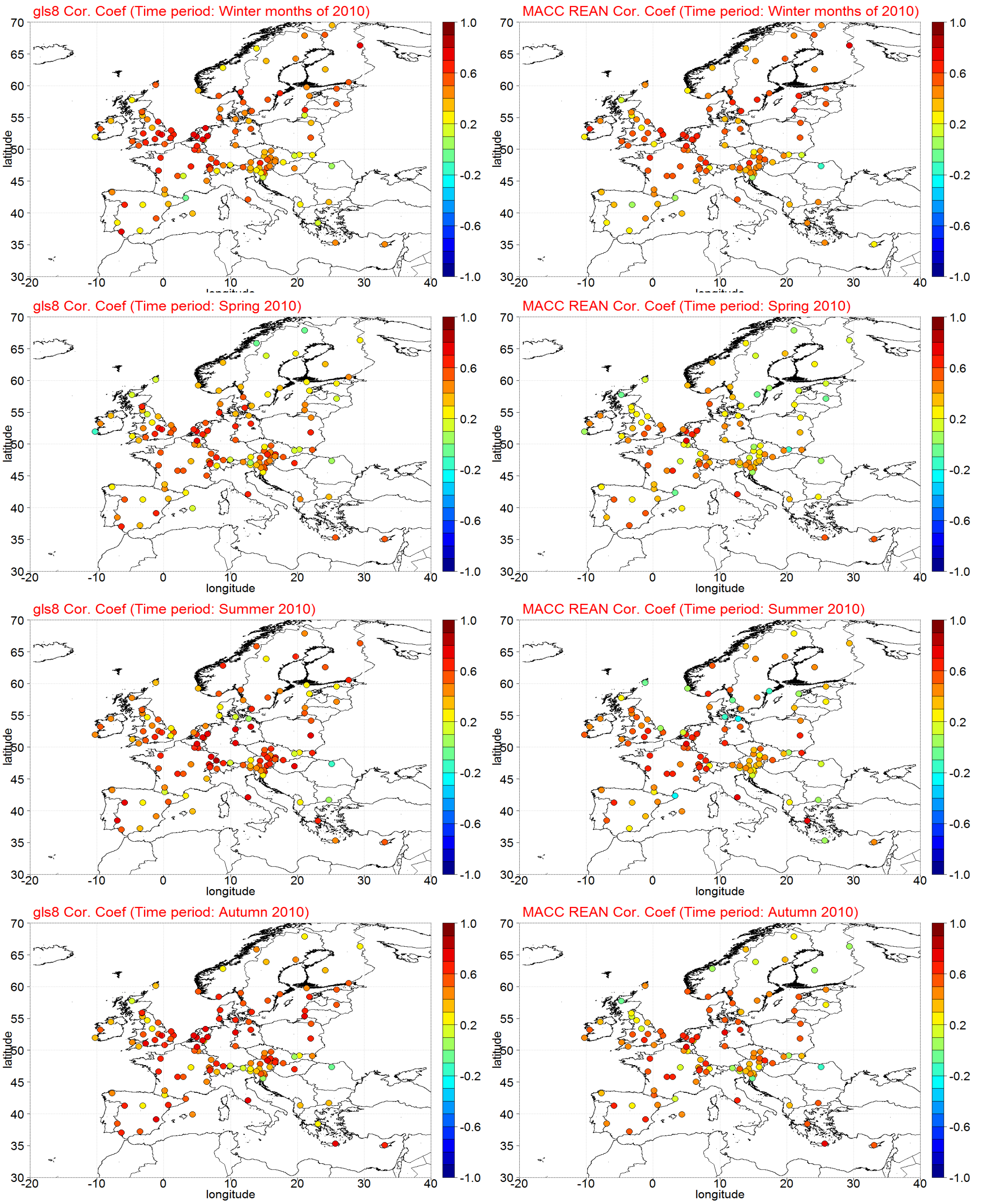

Figure 2.2.10. Correlation Coefficients (r) during Winter months of 2010 (1st row), Spring 2010 (2nd row), Summer 2010 (3rd row) and Autumn 2010 (4th row) between the new Reanalysis experiment gls8 and EMEP observations (left) and between the MACC reanalysis and EMEP observations (rigth).

2.2.4 Verification with IAGOS ozone observations

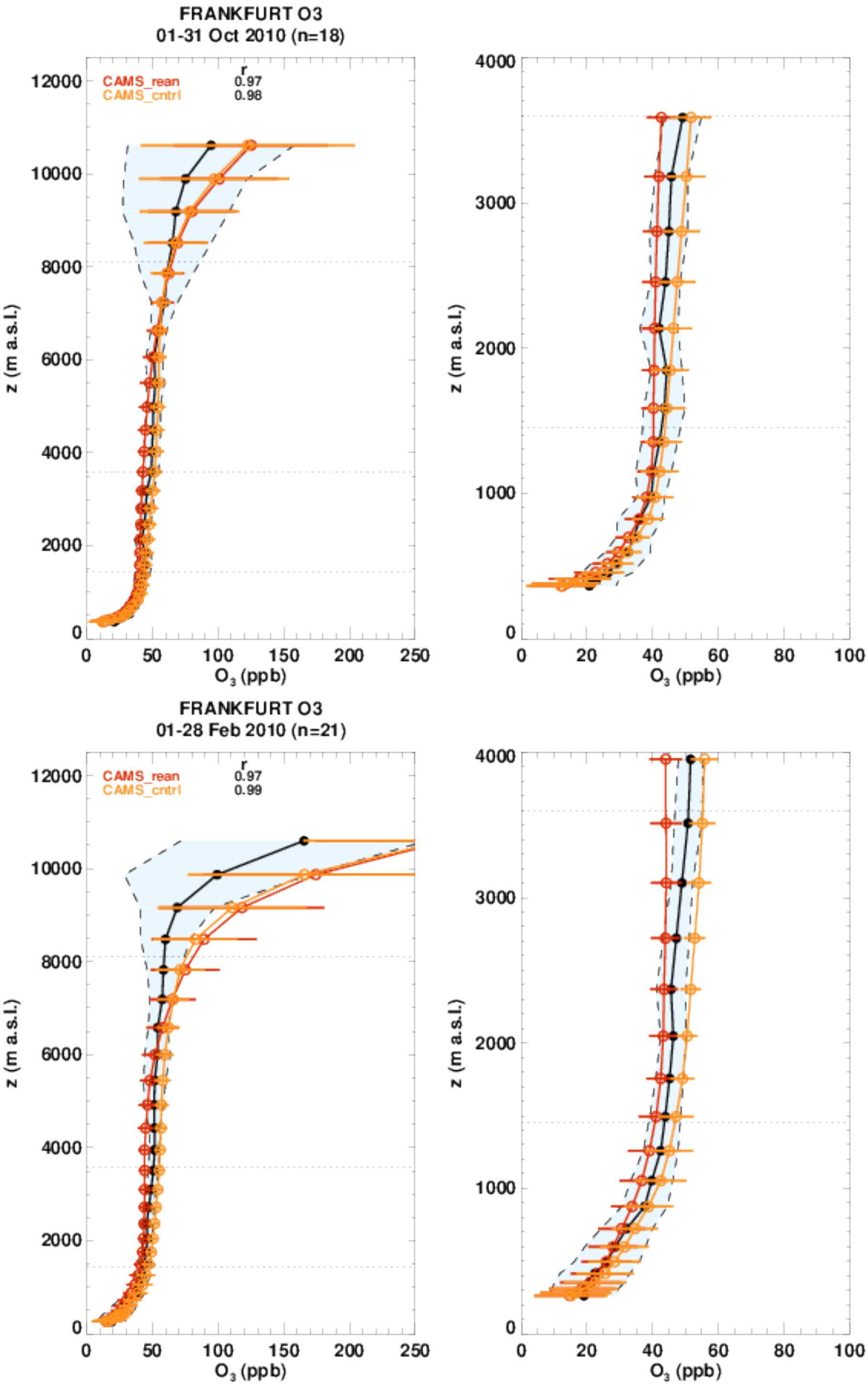

Figure 2.2.11: Monthly averaged ozone over Frankfurt for February and October 2010. The solid black line is the observations and the dashed black line shows the standard deviation of the observations.

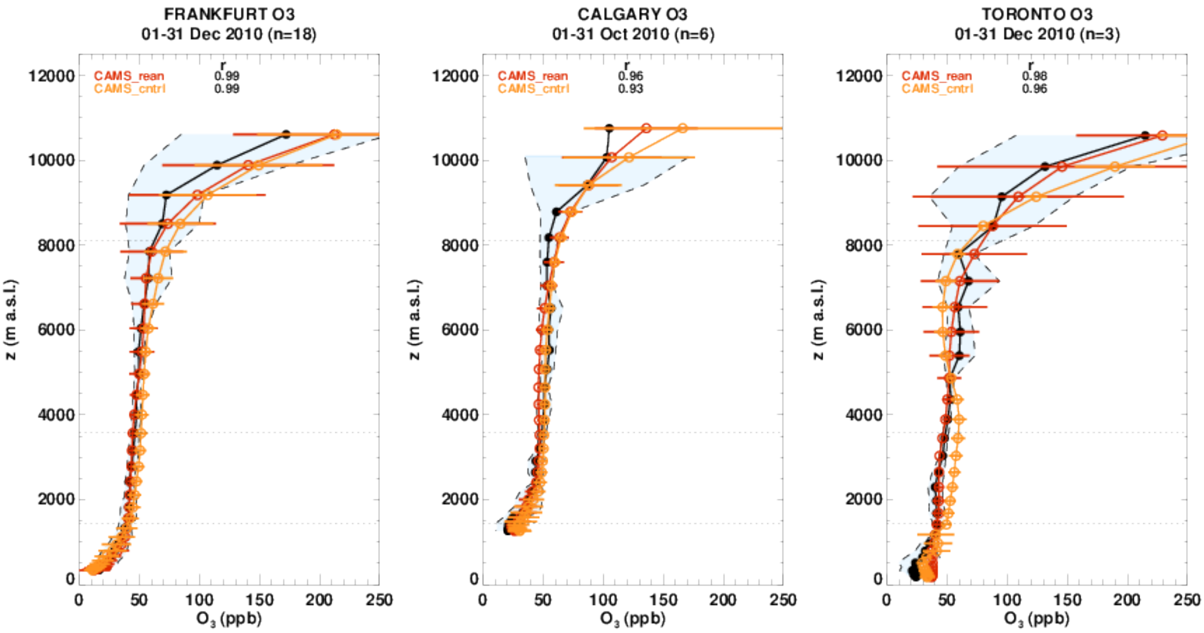

Figure 2.2.12: Monthly averaged ozone over Frankfurt for Frankfurt, Calgary and Toronto. The solid black line is the observations and the dashed black line shows the standard deviation of the observations.

2.2.5 Verification with ozone surface data in the Arctic

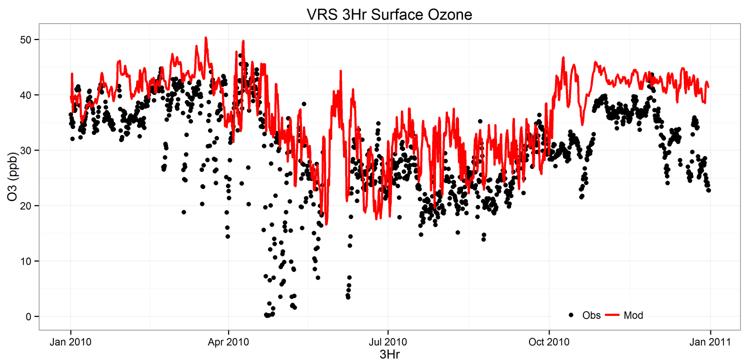

Fig. 2.2.13. Surface Ozone mixing ratios at the Arctic Villum Research Station, Station Nord, Greenland. MNMB = 21%, r = 0.61. The very low ozone values observed between February and May are attributed to halogen chemistry, which is not included in the CAMS model.

2.3 Carbon monoxide

2.3.1 Validation with Global Atmosphere Watch (GAW) Surface Observations

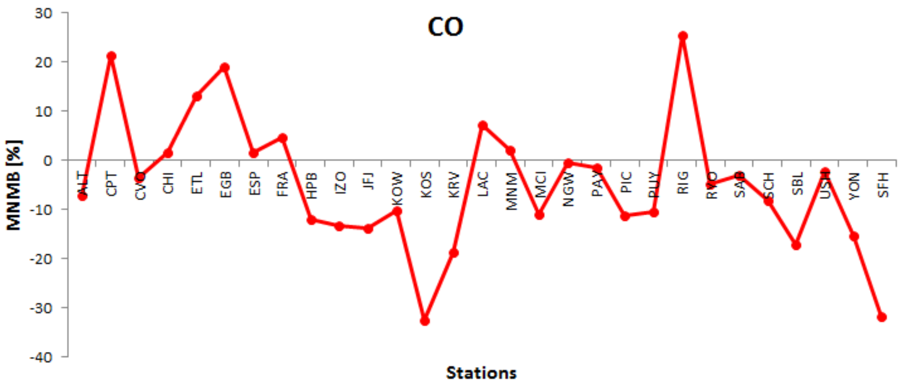

Fig. 2.3.1: MNMBs for CO for surface observations at GAW stations, averaged over 2010.

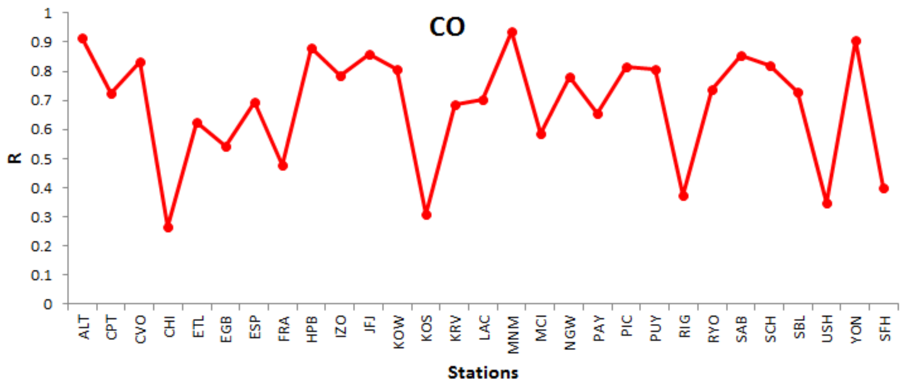

Fig. 2.3.2: Correlation corefficients R for CO for surface observations at GAW stations, averaged over 2010.

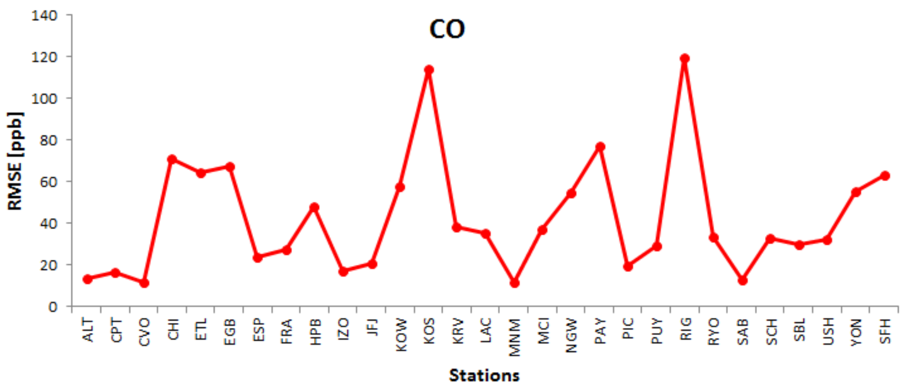

Fig. 2.3.3: RMSEs for CO for surface observations at GAW stations, averaged over 2010.

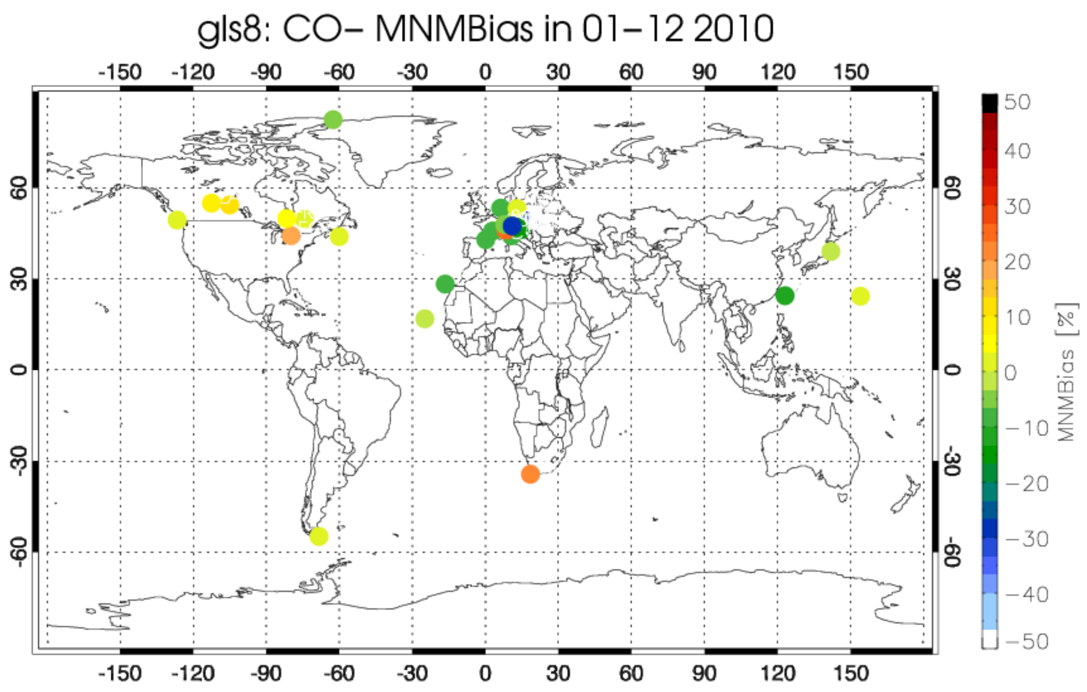

Fig. 2.3.4: Map of CO MNMBs at the GAW station locations over the time period January-December 2010.

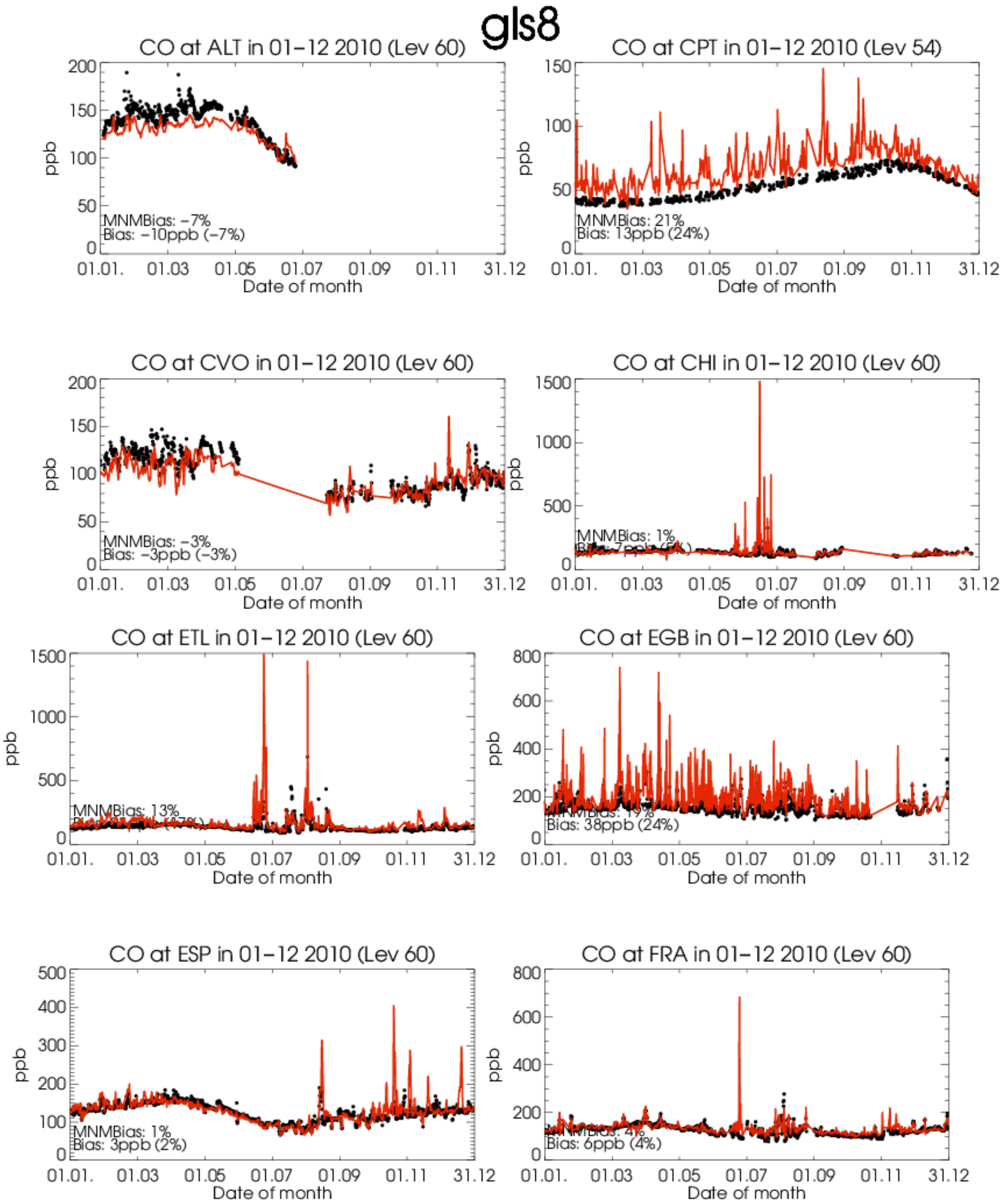
gls8
CO at ALT in 01–12 2010 (Lev 60)
MNMBias: –7%
Bias: –10ppb (–7%)
CO at CPT in 01–12 2010 (Lev 54)
MNMBias: 21%
Bias: 13ppb (24%)
CO at CVO in 01–12 2010 (Lev 60)
MNMBias: –3%
Bias: –3ppb (–3%)
CO at CHI in 01–12 2010 (Lev 60)
MNMBias: 1%
CO at ETL in 01–12 2010 (Lev 60)
MNMBias: 13%
CO at EGB in 01–12 2010 (Lev 60)
Bias: 38ppb (24%)
CO at ESP in 01–12 2010 (Lev 60)
MNMBias: 1%
Bias: 3ppb (2%)
CO at FRA in 01–12 2010 (Lev 60)
Bias: 6ppb (4%)
ppb
Date of month
01.01. 01.03 01.05 01.07 01.09 01.11 31.12

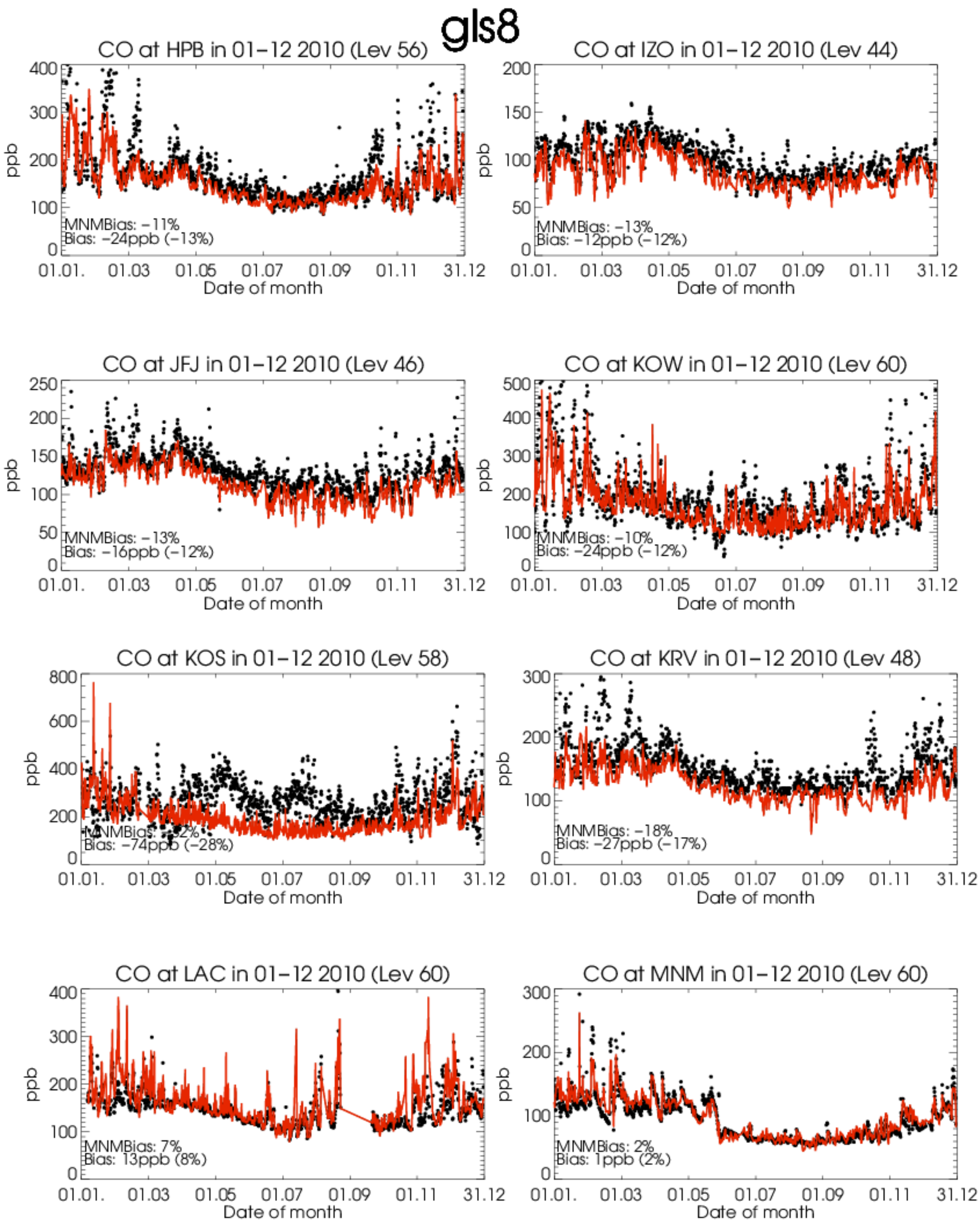
gls8
CO at HPB in 01–12 2010 (Lev 56)
MNMBias: –11%
Bias: –24ppb (–13%)
CO at IZO in 01–12 2010 (Lev 44)
MNMBias: –13%
Bias: –12ppb (–12%)
CO at JFJ in 01–12 2010 (Lev 46)
MNMBias: –13%
Bias: –16ppb (–12%)
CO at KOW in 01–12 2010 (Lev 60)
MNMBias: –10%
Bias: –24ppb (–12%)
CO at KOS in 01–12 2010 (Lev 58)
MNMBias: [illegible]
Bias: –74ppb (–28%)
CO at KRV in 01–12 2010 (Lev 48)
MNMBias: –18%
Bias: –27ppb (–17%)
CO at LAC in 01–12 2010 (Lev 60)
MNMBias: 7%
Bias: 13ppb (8%)
CO at MNM in 01–12 2010 (Lev 60)
MNMBias: 2%
Bias: 1ppb (2%)
ppb
Date of month
01.01. 01.03 01.05 01.07 01.09 01.11 31.12

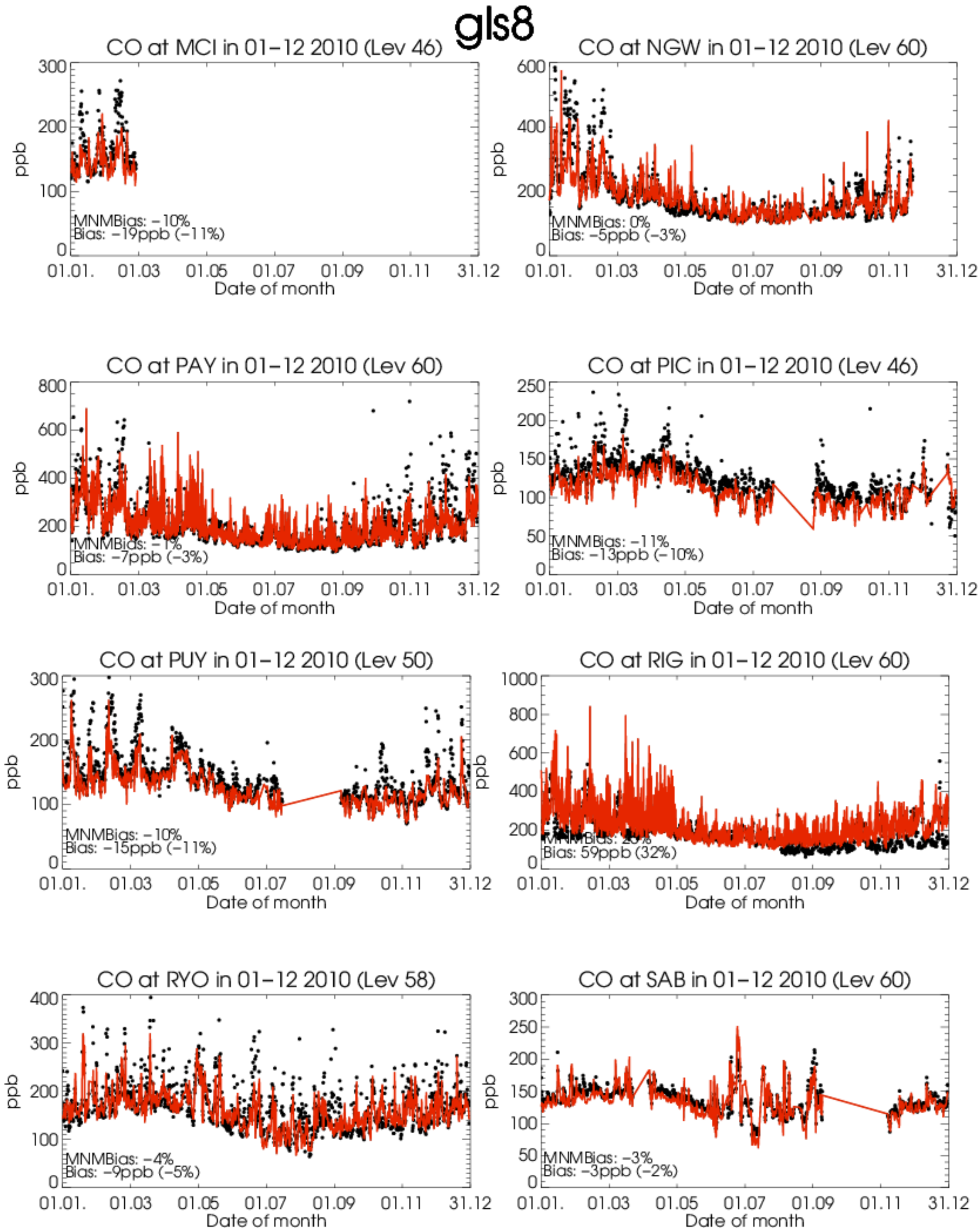
gls8
CO at MCI in 01–12 2010 (Lev 46)
MNMBias: –10%
Bias: –19ppb (–11%)
CO at NGW in 01–12 2010 (Lev 60)
MNMBias: 0%
Bias: -5ppb (-3%)
CO at PAY in 01–12 2010 (Lev 60)
MNMBias: –1%
Bias: -7ppb (-3%)
CO at PIC in 01–12 2010 (Lev 46)
MNMBias: –11%
Bias: –13ppb (–10%)
CO at PUY in 01–12 2010 (Lev 50)
MNMBias: –10%
Bias: –15ppb (–11%)
CO at RIG in 01–12 2010 (Lev 60)
Bias: 59ppb (32%)
CO at RYO in 01–12 2010 (Lev 58)
MNMBias: –4%
Bias: -9ppb (-5%)
CO at SAB in 01–12 2010 (Lev 60)
MNMBias: –3%
Bias: –3ppb (–2%)
ppb
Date of month
01.01. 01.03 01.05 01.07 01.09 01.11 31.12

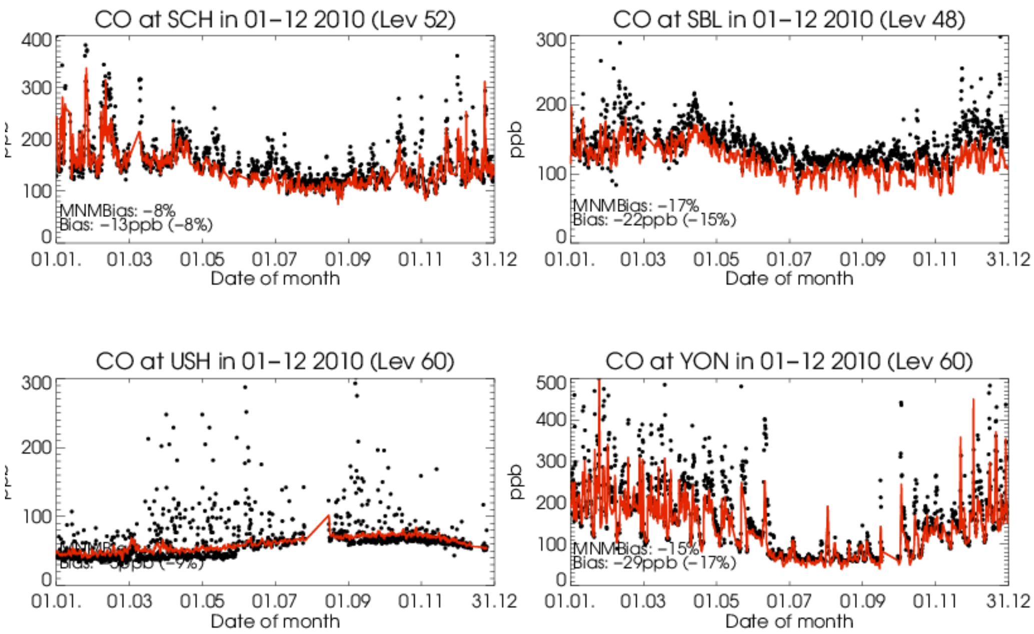

Fig. 2.3.5: Timeseries plots for CO for GAW stations in the period Jauary-December 2010.

2.3.2 IAGOS Aircraft observations

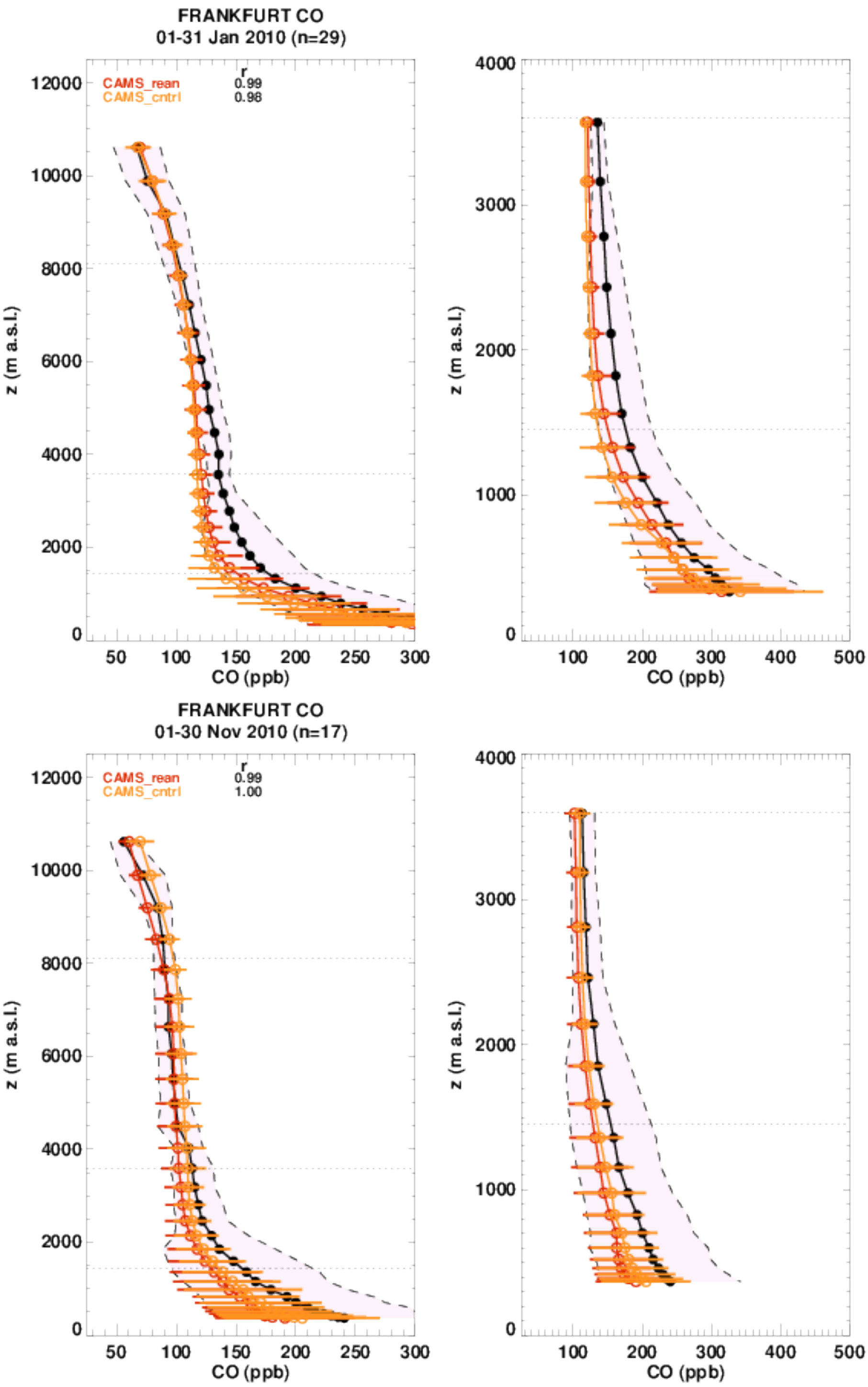

Figure 2.3.6 : Monthly averaged carbon monoxide over Frankfurt for January and November 2010. The solid black line is the observations and the dashed black line shows the standard deviation of the observations.

2.3.3 FTIR tropospheric CO observations

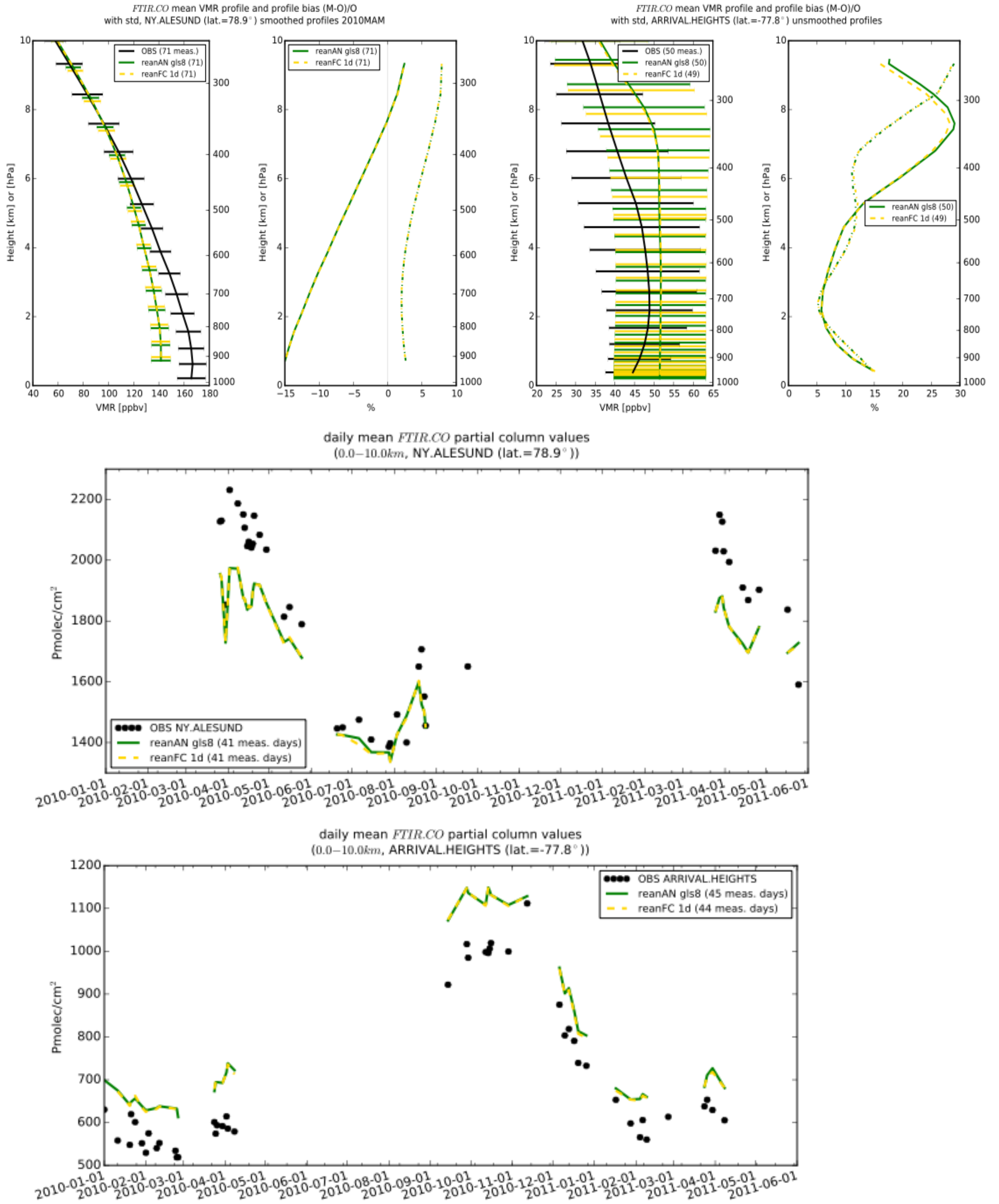

Figure 2.3.7. Comparison CO concentrations at two NDACC polar stations Ny Alesund and Arrival Heights. An underestimation is observed in the artic station, while an overestimation is seen at the Antarctic station.

Table 2.3.1. Seasonal relative mean bias (MB, %), standard deviation (STD, %) of the partial (upper stratospheric 0km – 10km) CO column for the considered period and number of observations used (NOBS), compared to NDACC microwave observations at all NDACC FTIR stations.
At northern latitude stations (Eureka, Kiruna, Thule, Ny Alesund, Zugspitze, St Petersburg, Bremen, Izana, Mauna Loa) a slight underestimation of REAN is observed (bias of 7%-9%, which is slightly higher than the measurement uncertainty of 7%) in the lower troposphere. In the southern hemisphere the difference lies within the measurements uncertainty range (Reunion, Lauder). For Reunion the osuite-AN underestimates with 6%, while rean-AN underestimates with 2%. For Lauder the osuite-AN underestimates with 2%, while for reanAN the bias is nearly vanishing. At Arrival Heights REAN strongly overestimates (>10%, FTIR measurements only during local spring/summer months). The converse is seen at Ny Alesund: a strong underestimation during local spring.

			DJF 2010			MAM 2010			JJA 2010			SON 2010			DJF 2011			MAM 2011		
		latitude	MB	stddev	nobs	MB	stddev	nobs	MB	stddev	nobs	MB	stddev	nobs	MB	stddev	nobs	MB	stddev	nobs
Eureka	AN	80.05	-5.08	2.13	7	-4.81	3.32	274	-3.13	5.06	138	-2.99	3.07	76	-3.38	1.74	5	-4.56	3.61	210
	FC 1d		-5.26	2.15	7	-4.89	3.34	274	-3.03	5.43	138	-3.21	3.09	76	-3.36	1.76	5	-4.63	3.53	210
Ny.Ale	AN	78.92				-8.86	2.12	71	-2.03	3.27	43	-5.79	0.21	5				-7.94	5.50	33
	FC 1d					-8.84	2.10	71	-2.25	3.25	43	-5.09	0.14	5				-8.05	5.40	33
Thule	AN	76.52				-6.85	2.04	144	-7.18	5.44	61	-7.07	2.99	4				-4.39	5.99	105
	FC 1d					-6.91	2.05	144	-7.26	5.60	61	-7.44	2.89	4				-4.58	5.74	105
Kiruna	AN	67.84	-16.31	4.01	4	-9.42	2.14	33	-8.27	2.40	18	-7.83	3.60	33	-8.66	2.25	31	-8.17	2.50	78
	FC 1d		-15.90	4.12	4	-9.27	2.01	33	-8.44	2.36	18	-7.97	3.54	33	-8.81	2.29	31	-8.25	2.51	78
St.Pet	AN	59.88	-1.48	0.96	10	-6.55	5.28	140	-5.04	4.45	113	-3.20	3.89	11	3.65	3.82	3	-4.41	3.19	189
	FC 1d		-0.88	1.27	10	-7.81	4.47	140	-6.66	4.32	113	-4.18	3.28	11	3.51	3.82	3	-4.74	2.60	189
Zugspi	AN	47.42	-4.97	4.18	197	-4.68	3.29	358	-6.42	5.47	293	-9.45	5.17	541	-5.93	3.27	385	-4.32	3.93	498
	FC 1d		-4.35	4.34	197	-4.78	3.27	358	-6.96	5.63	293	-8.21	3.66	541	-5.10	3.04	385	-4.75	3.63	498
Jungfr	AN	46.55	-4.77	2.40	30	-4.56	4.16	68	-9.12	4.92	163	-8.69	4.80	86	-7.63	5.01	53	-5.93	4.72	97
	FC 1d		-4.19	2.75	30	-4.68	4.55	68	-9.52	4.59	163	-8.26	4.91	86	-6.26	3.96	53	-6.10	4.55	97
Toront	AN	43.60	2.01	18.46	11	1.86	7.05	122	-2.93	7.91	73	-0.52	7.98	51	0.72	13.57	25	-0.70	7.72	33
	FC 1d		2.52	18.00	11	0.89	6.95	122	-2.84	7.43	73	0.00	7.86	51	0.48	13.87	25	-0.69	6.99	33
Izana	AN	28.30				-7.26	2.58	30	-7.93	5.71	102	-10.25	3.79	41	-8.08	2.59	46	-8.36	3.38	24
	FC 1d					-7.29	2.47	30	-7.60	5.90	102	-9.36	4.25	41	-8.99	3.63	46	-7.66	3.40	24
Mauna.	AN	19.54	-10.89	4.81	36	-16.12	0.00	1												
	FC 1d		-11.78	5.10	36	-16.24	0.00	1												
La.Reu	AN	-20.90	-0.77	11.58	26	-2.77	4.26	16	-1.65	4.37	209	-8.74	5.12	74	-9.72	5.67	42	0.28	7.11	182
	FC 1d		-0.53	12.49	26	-2.73	3.02	16	-1.28	4.08	209	-8.26	5.62	74	-9.55	5.11	42	0.50	6.68	182
Wollon	AN	-34.41	6.58	22.72	255	5.00	16.89	601	4.22	14.46	463	1.56	10.45	450	7.14	15.07	331	8.69	11.42	430
	FC 1d		4.20	19.93	255	5.43	16.93	601	4.17	14.28	463	1.13	10.34	450	6.31	14.57	331	8.78	11.41	430
Lauder	AN	-45.04	-5.29	4.49	17	0.30	5.71	29	3.35	3.50	16	-0.49	5.90	29	-3.43	5.02	22	0.45	8.99	26
	FC 1d		-4.03	5.87	17	1.34	5.56	29	3.33	4.45	16	0.04	5.64	29	-1.65	4.53	22	2.56	7.64	26
Arriva	AN	-77.82	15.27	4.76	14	18.92	4.41	8				11.89	4.00	10	9.96	3.67	14	10.98	3.24	4
	FC 1d		15.49	4.48	13	18.90	3.90	8				11.87	4.04	10	9.37	3.75	14	10.53	2.85	4

TCCON CO observations

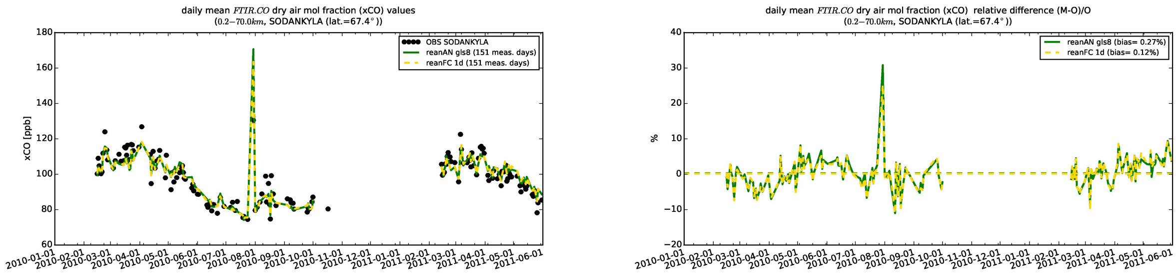

Fig. 2.3.8: TCCON-model CO comparison at the Arctic site Sodankylä (67.4 °N). The modeled CO agrees relatively well with the measurements. The spike in July 2010 is seen in the model as well as in the measurements.

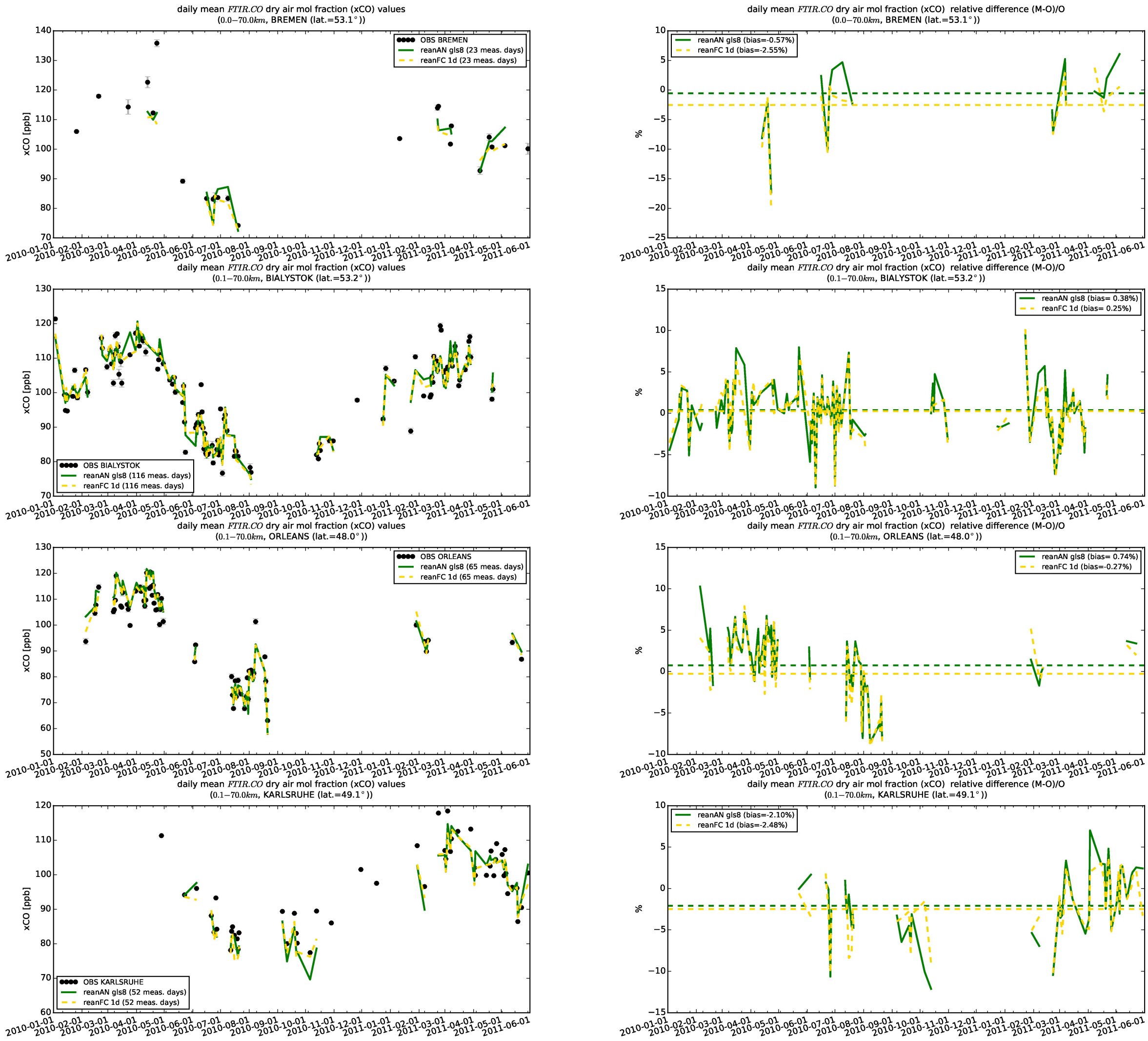

Fig. 2.3.9: TCCON-model CO comparison for four European mid-latitude sites. The seasonality is well represented by the models.

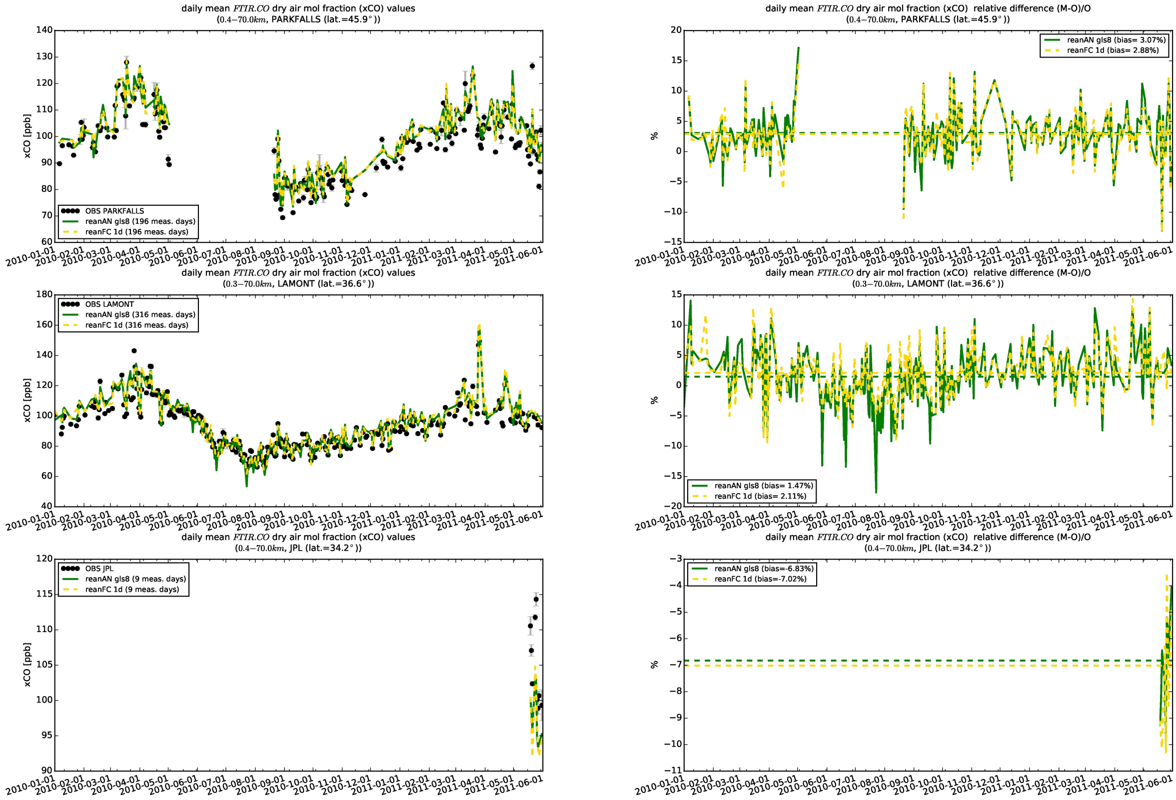

Fig. 2.3.10: TCCON-model CO comparison for three US-American TCCON sites. The models agree well with the measurements.

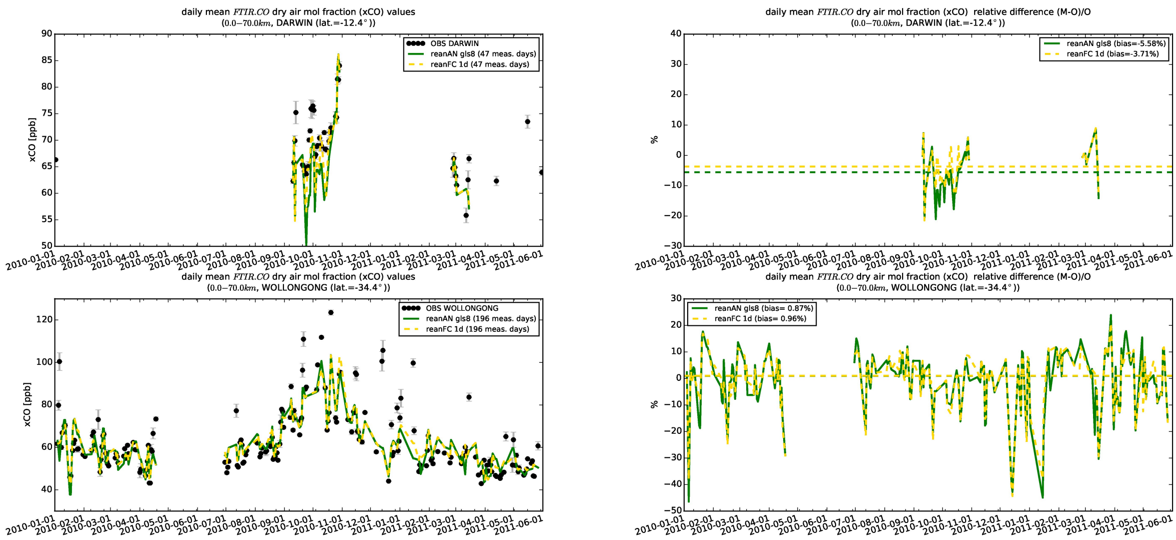

Fig. 2.3.11: TCCON-model CO comparison for the two Australian sites Darwin (12.4°S) and Wollongong (34.4°S). At Wollongong the measured CO shows individual values which differ from the seasonal pattern and are not represented by the model.

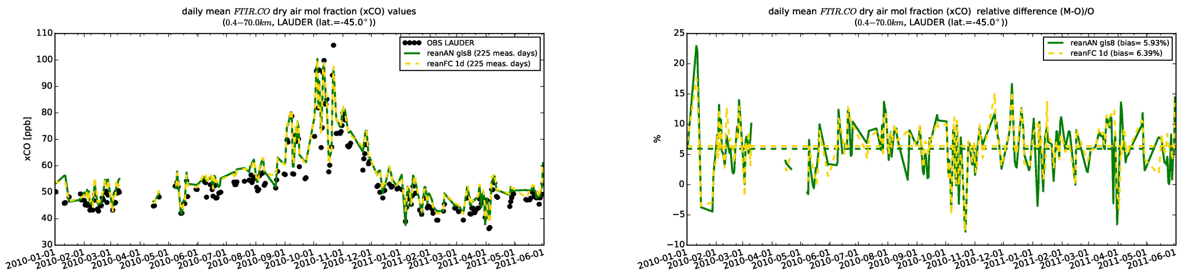

Fig. 2.3.12: TCCON-model CO comparison for Lauder, New Zealand (45°S). The model agrees reasonably well with the measurements.

2.3.4 MOPITT and IASI tropospheric CO observations

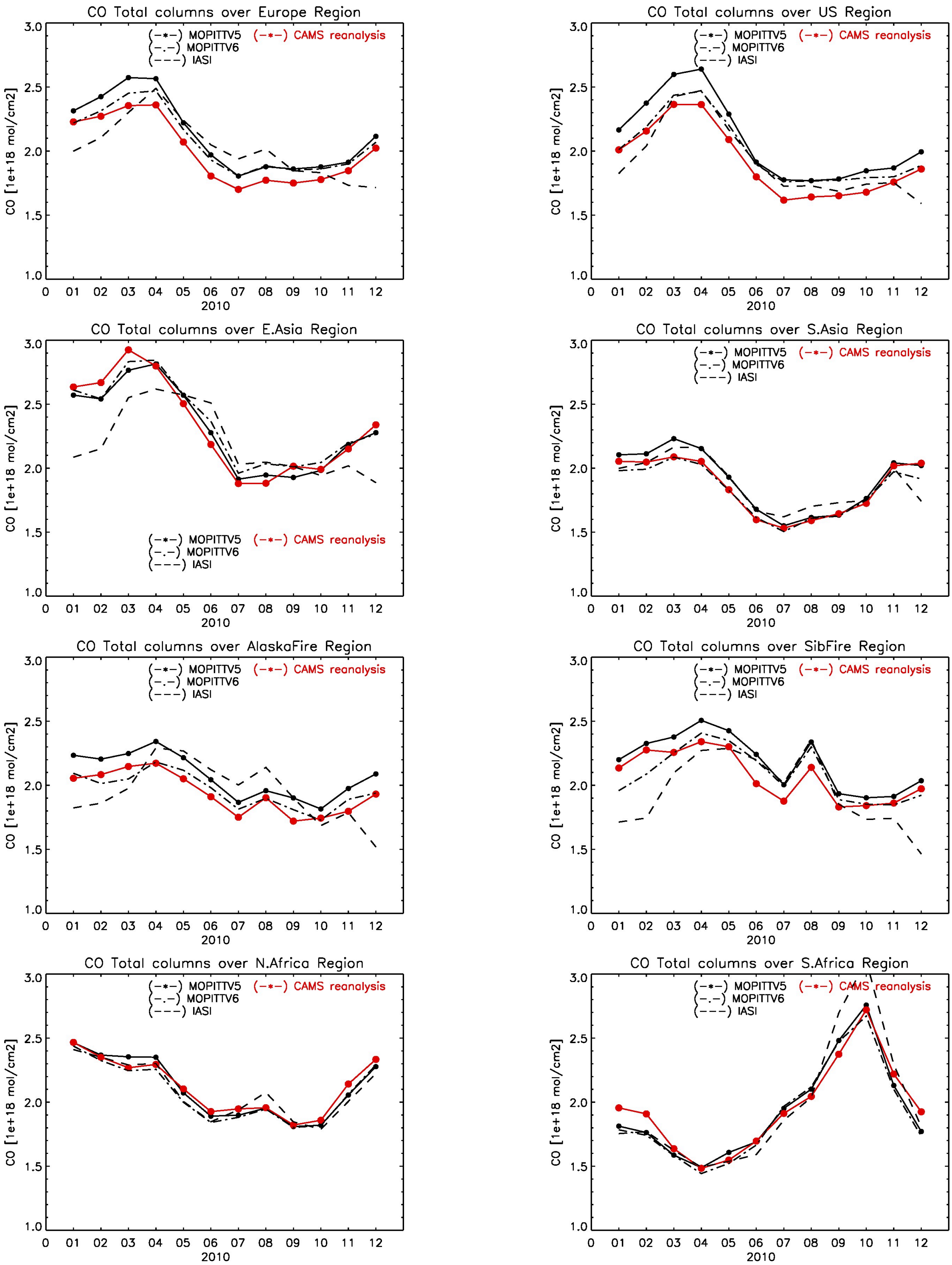

Fig.2.3.8. CO total columns for satellite retrievals (black) MOPITT V5 and V6, IASI and 2010 reanalysis data (red) over selected regions for 2010.

2.4 Nitrogen dioxide

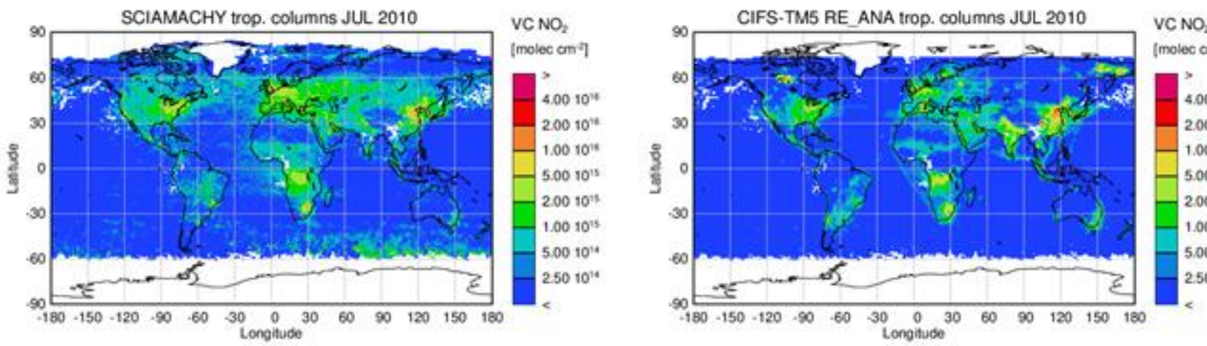

Figure 2.4.1. SCIAMACHY tropospheric NO2 column for July 2010 (left) compared to the reanalysis (right). Tropospheric NO2 has known problems (too large values for biomass burning in boreal forests, too high shipping signals). Apart from that it is OK and comparable to MACC reanalysis.

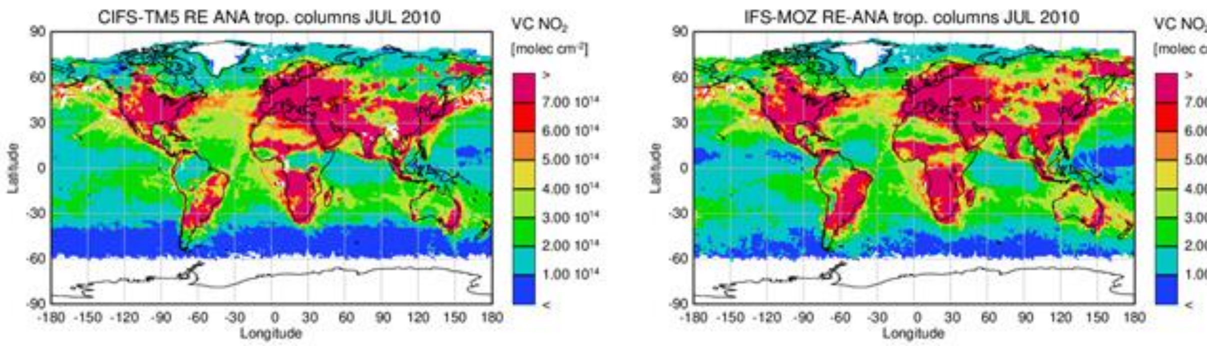

Figure 2.4.2. Comparison of the CAMS reanalysis (left) and the MACC reanalysis based on the coupled Mozart-IFS system (right). Tropospheric NO2 shows unusually low values in some areas of the tropics over the continents (Central Africa, Northern South America), lower than in MACC reanalysis and lower than in SCIAMACHY.

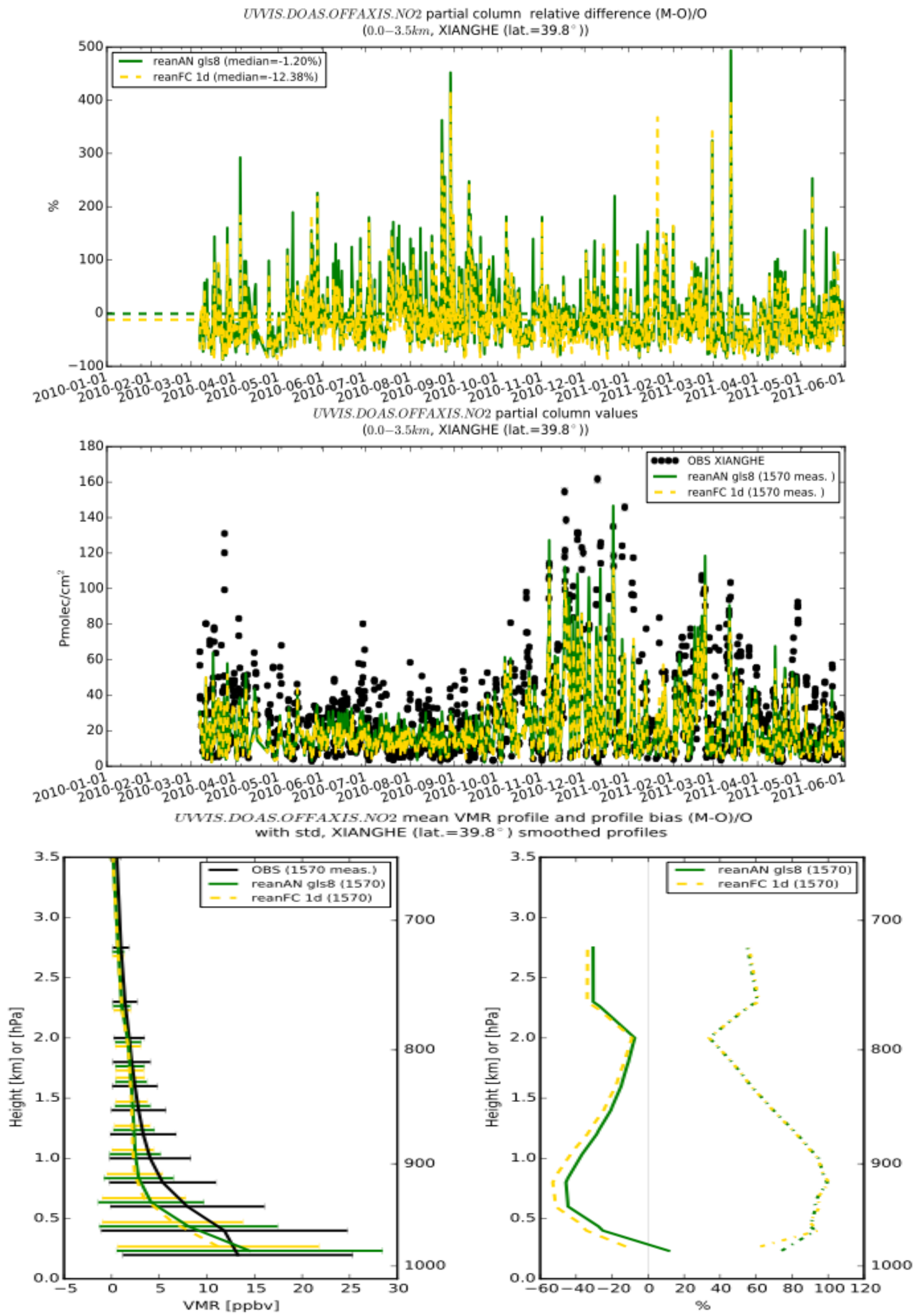

Figure 2.4.3. Tropospheric NO2 evaluated with MAX-DOAS against the high polluted area of Xianghe, Beijing.Comparison of partial column 0-3.5km (left) and averaged profile difference (right). The high pollution events are not well captured, while background values are OK. Relative mean bias indicates that the analysis performs somewhat better than the forecast.

2.5 Formaldehyde (HCHO)

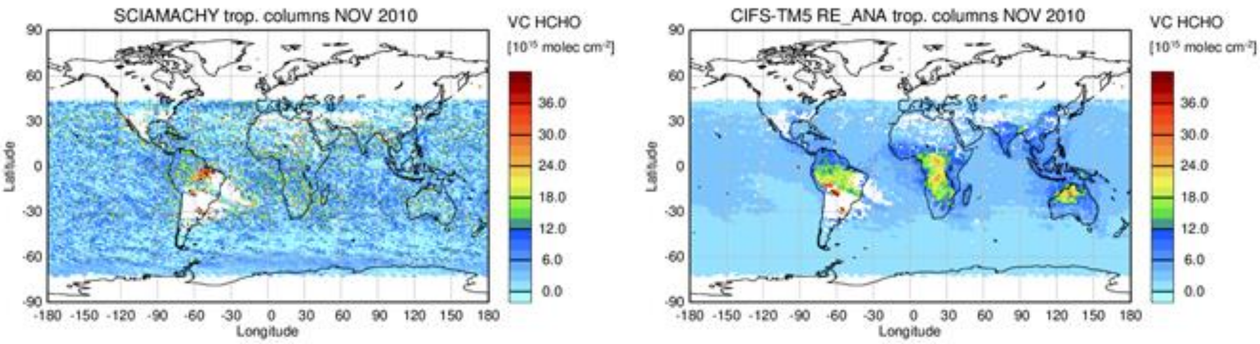

Figure 2.5.1. SCIAMACHY HCHO columns for November 2010 (left) compared to the reanalysis (right). Tropospheric HCHO appears generally too high, in particular in September, October, November over Africa and Australia. The agreement with the satellite data was much better with MACC reanalysis.

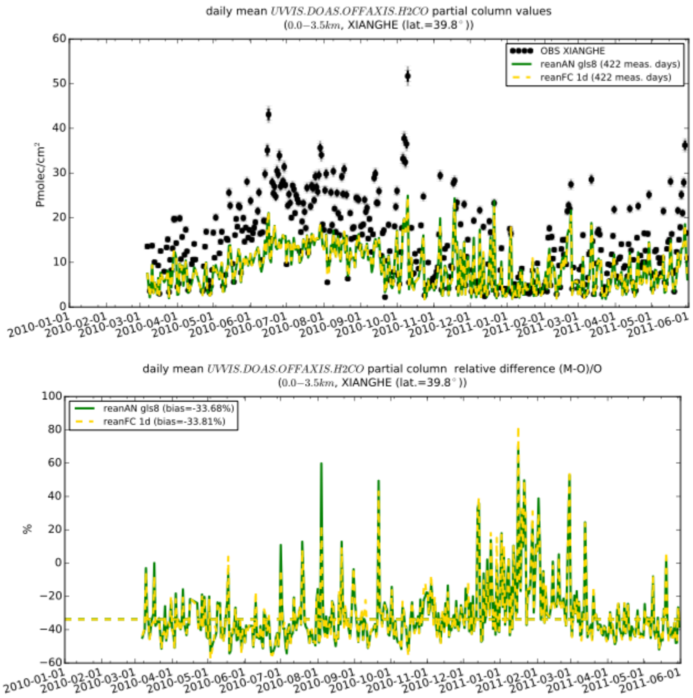

Figure 2.5.2. Tropospheric H2CO evaluated with UV-Vis DOAS against the high polluted area of Xianghe, Beijing. Comparisonare made of partial columns between 0-3.5km. Note that the smoothed model columns may deviate from the actual model columns due to introduction of the UVVIS apriori data. Background values are well captured, high pollution events are underestimated.

2.6 Stratospheric ozone

2.6.1 Ozone sonde results

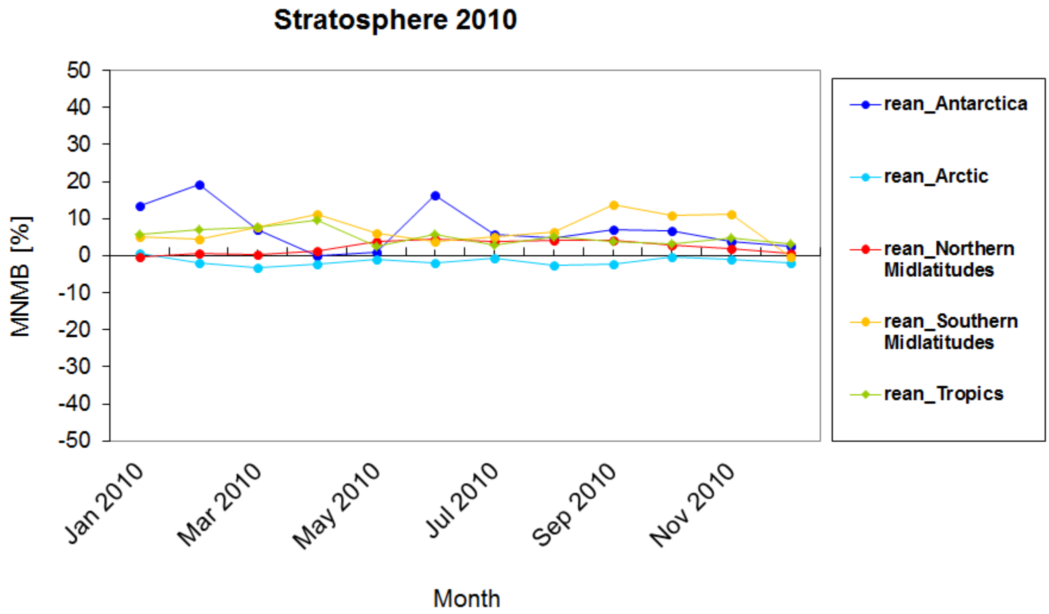

Fig. 2.6.1: MNMBs (reanalysis minus ozone sonde) for all 5 regions in the stratosphere (between 90 and 10 hPa, and between 60 and 10 hPa in the Tropics).

2.6.2 Comparison with satellite observations

O3 against MLS_v4: 03-10hPa from 20100101 to 20110630

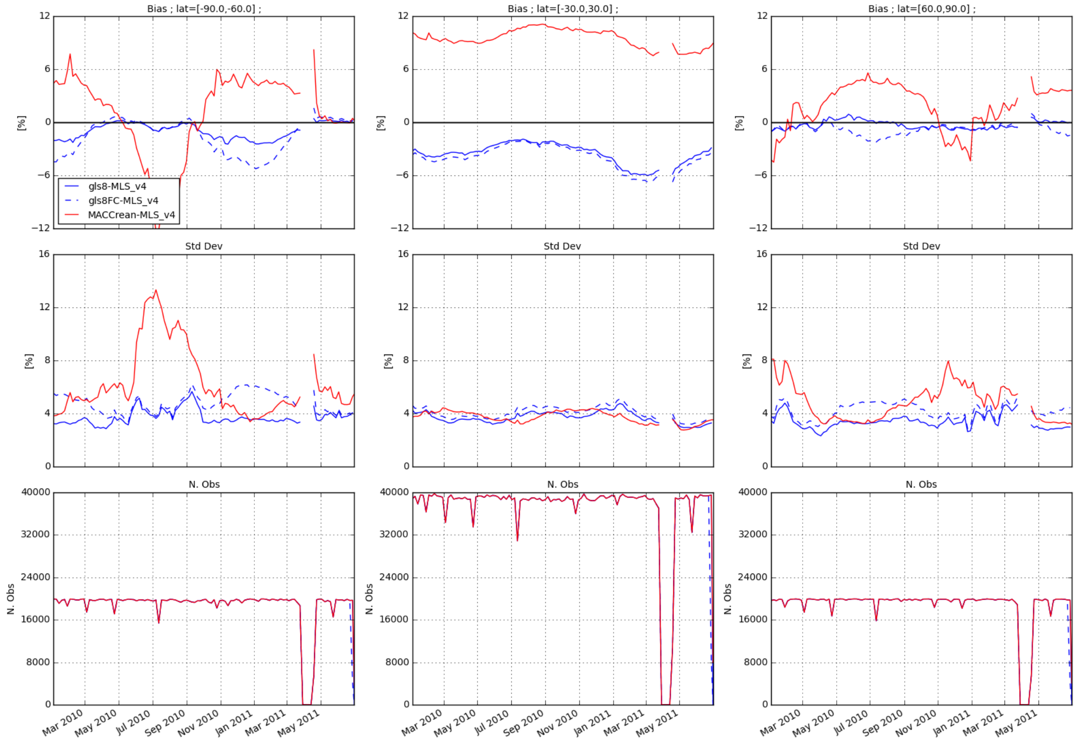

O3 against MLS_v4: 30-70hPa from 20100101 to 20110630

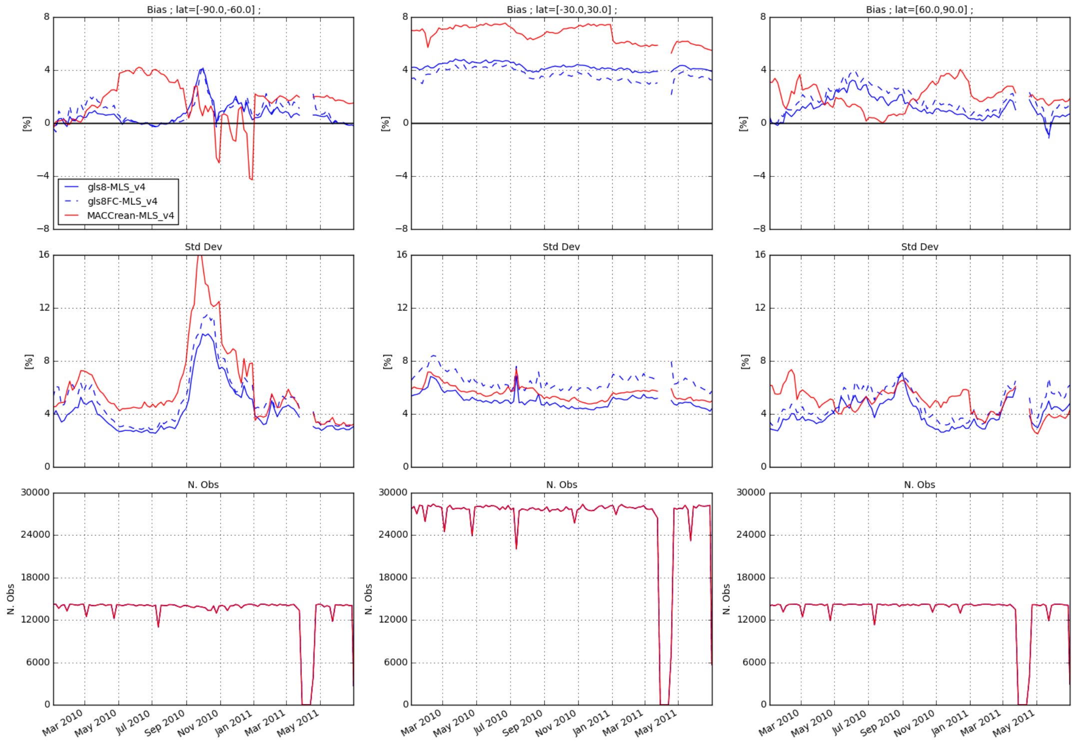

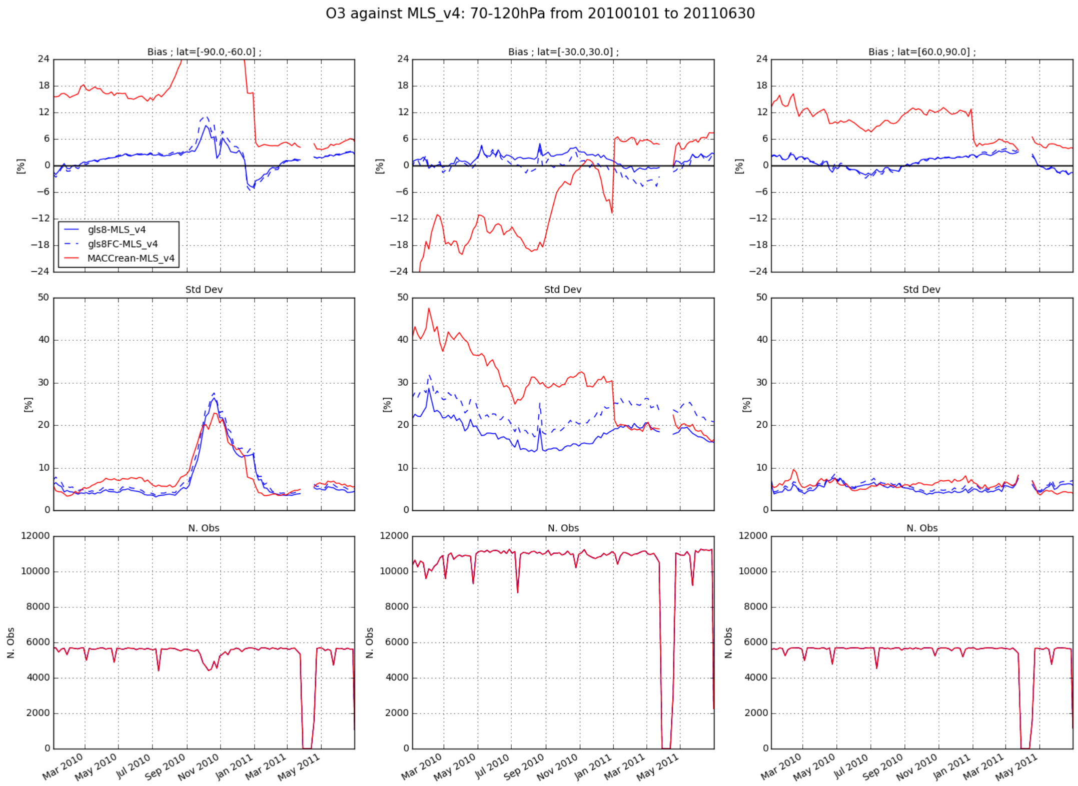

Fig. 2.6.2 Comparisons of stratospheric ozone against MLS v4, for 3-10 hPa (first set of panels), 30-70 hPa (second set) and 70-120 hpa (last set). Each set contains results for Antarctica (left), tropics (middle) and Arctic (right). Shown are the bias (top row), standard deviation (middle) and number of observations (bottom). Agreement with observations is generally much better than in the MACC reanalysis for ozone in polar regions and in tropical region for higher stratosphere (03-10hPa), middle stratosphere (30-70hPa) and lower stratosphere (70-120hPa). For the considered period, the MACC reanalysis assimilated AURA MLS V02 NRT, while gls8 assimilates a more recent version of AURA MLS, which explains this behavior.

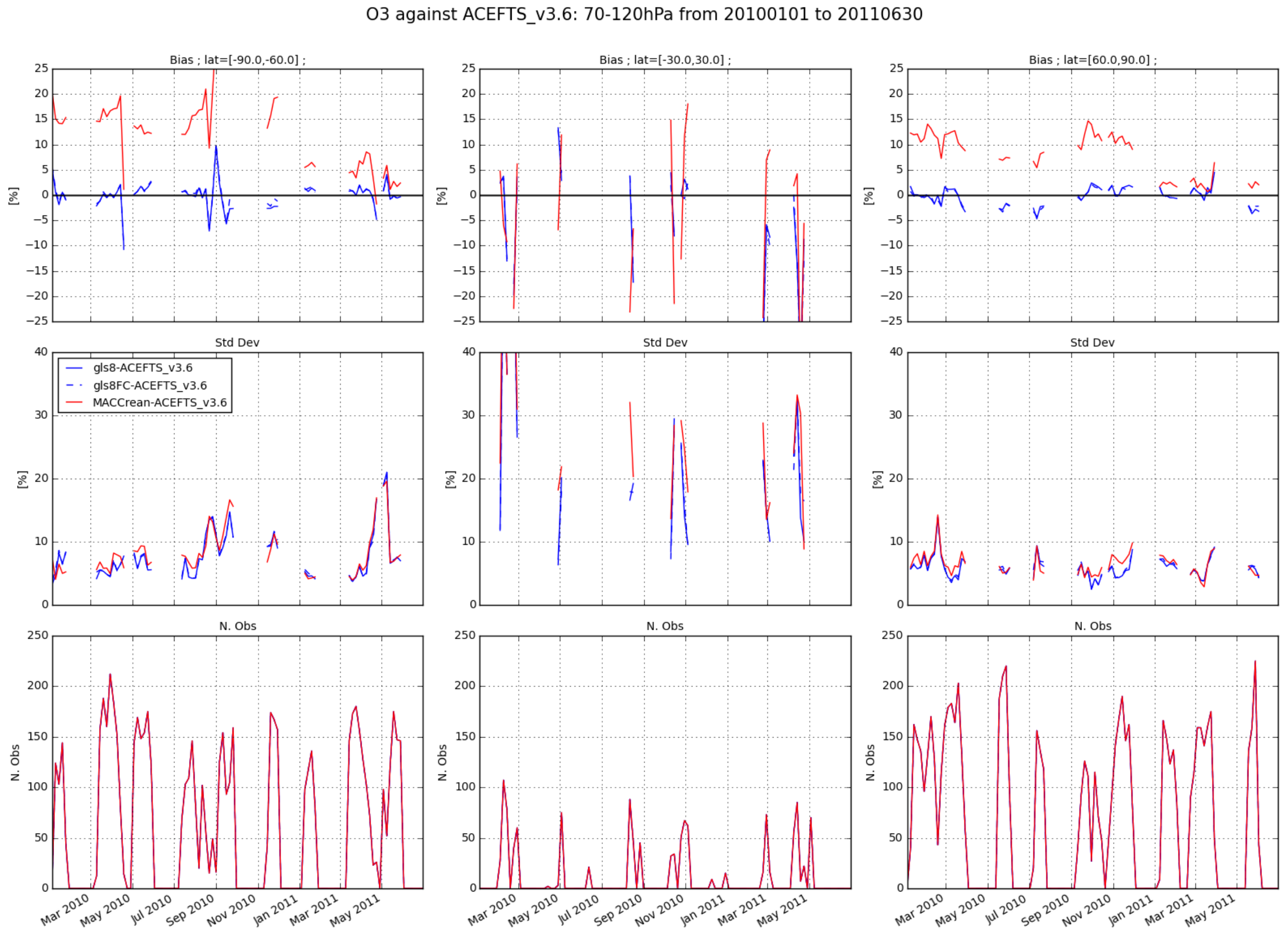

Fig. 2.6.3 Comparisons of stratospheric ozone against ACEFTS, for the pressure range 70-120 hpa. Blue lines: gls8; red line: MACC reanalysis. Each set contains results for Antarctica (left), tropics (middle) and Arctic (right). Shown are the bias (top row), standard deviation (middle) and number of observations (bottom). The number of valid profiles from ACEFTS is much more limited and varies in time. The data are too sparse in the tropical regions to draw a conclusion, but a quick look at the time-series of the bias wrt ACEFTS in the polar regions of the lower stratosphere show clearly an improvement.

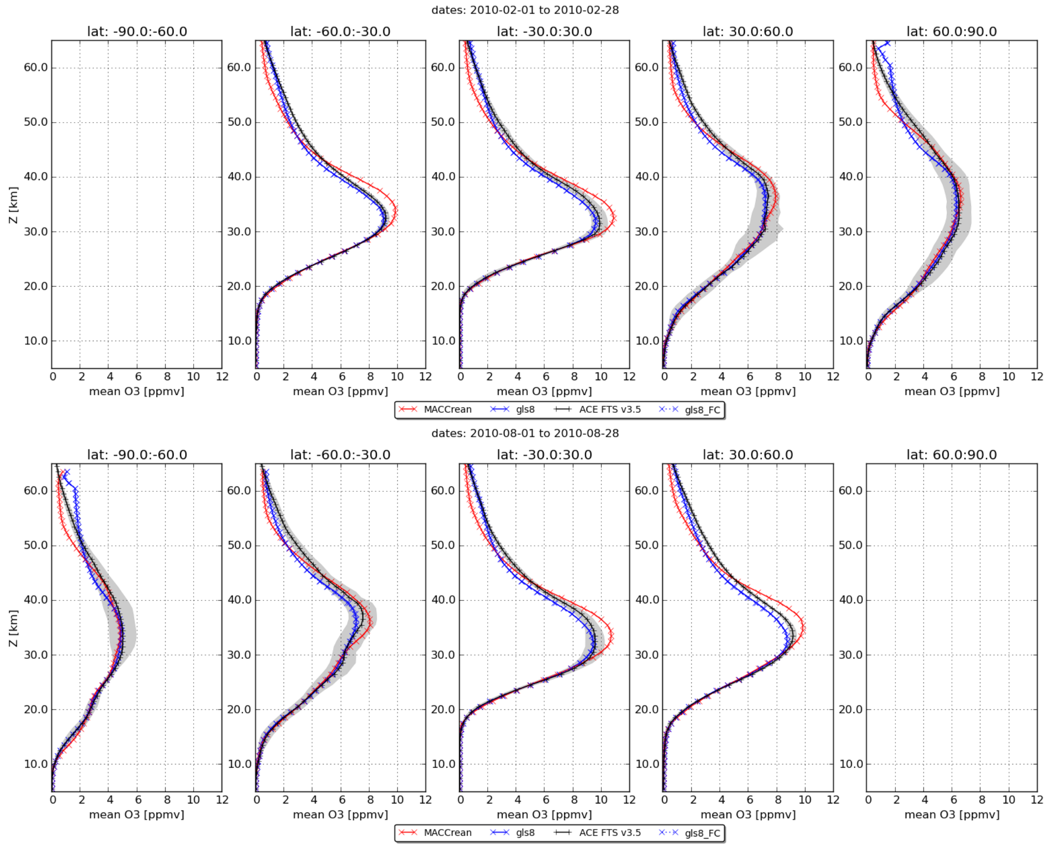

Fig. 2.6.4. Comparisons of stratospheric ozone profiles against ACE FTS v3.5, for February 2010 (top row) and August 2010 (bottom row). Blue line: gls8; red line: MACC reanalysis. Each set contains results for Antarctica (left), tropics (middle) and Arctic (right). Shown are the bias (top row), standard deviation (middle) and number of observations (bottom). The shape of the profiles (in volume mixing ratio) has improved in comparison with the MACC reanalysis, where a positive bias was clearly visible between 30km and 40km. However there seems to be an anomaly in gls8 in the higher stratosphere above 55km where a positive bias develops at the end of the polar summer.

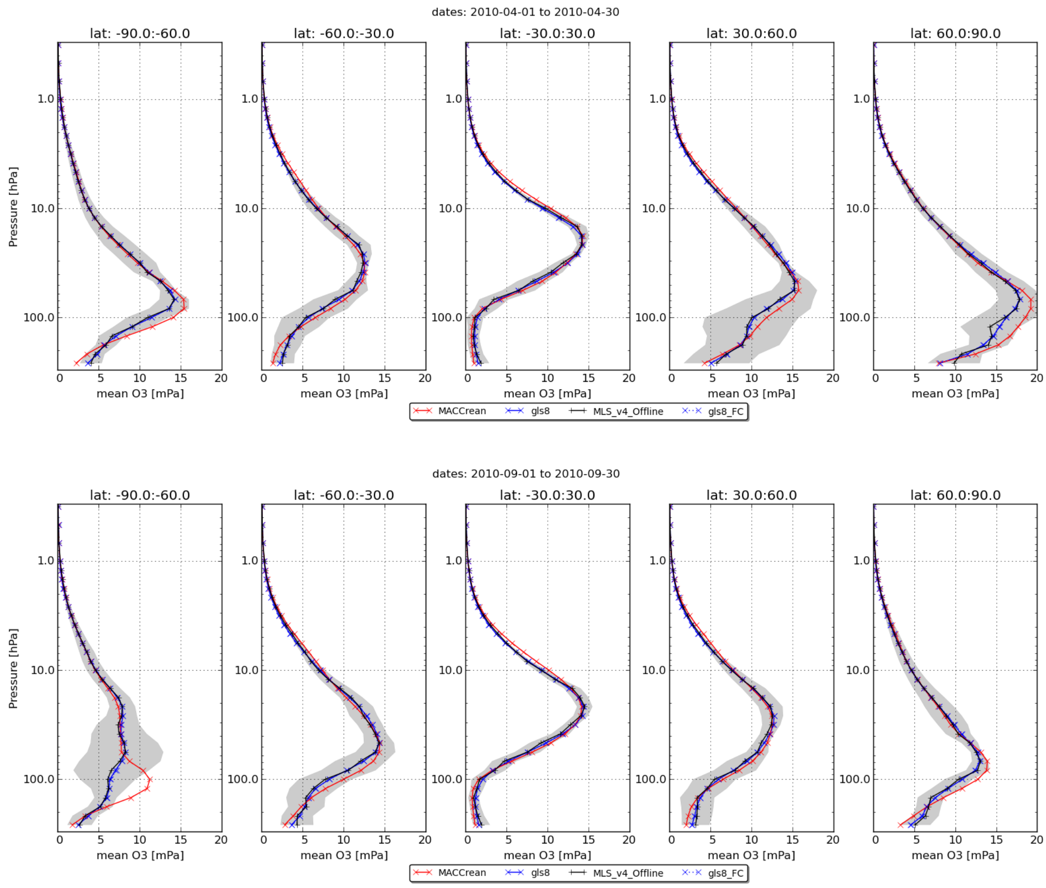

Fig. 2.6.5 Comparisons of stratospheric ozone profiles against MLS v4 offline (black line), for April 2010 (top row) and September 2010 (bottom row). Blue line: gls8; red line: MACC reanalysis. Each set contains results for Antarctica (left), tropics (middle) and Arctic (right). Shown are the bias (top row), standard deviation (middle) and number of observations (bottom). Because of the assimilation of AURA MLS, the shape of the gls8 profiles are much closer to the observations; the deviations which were visible in the lower part of the profiles (in partial pressure) of the MACC reanalysis have been corrected in gls8.

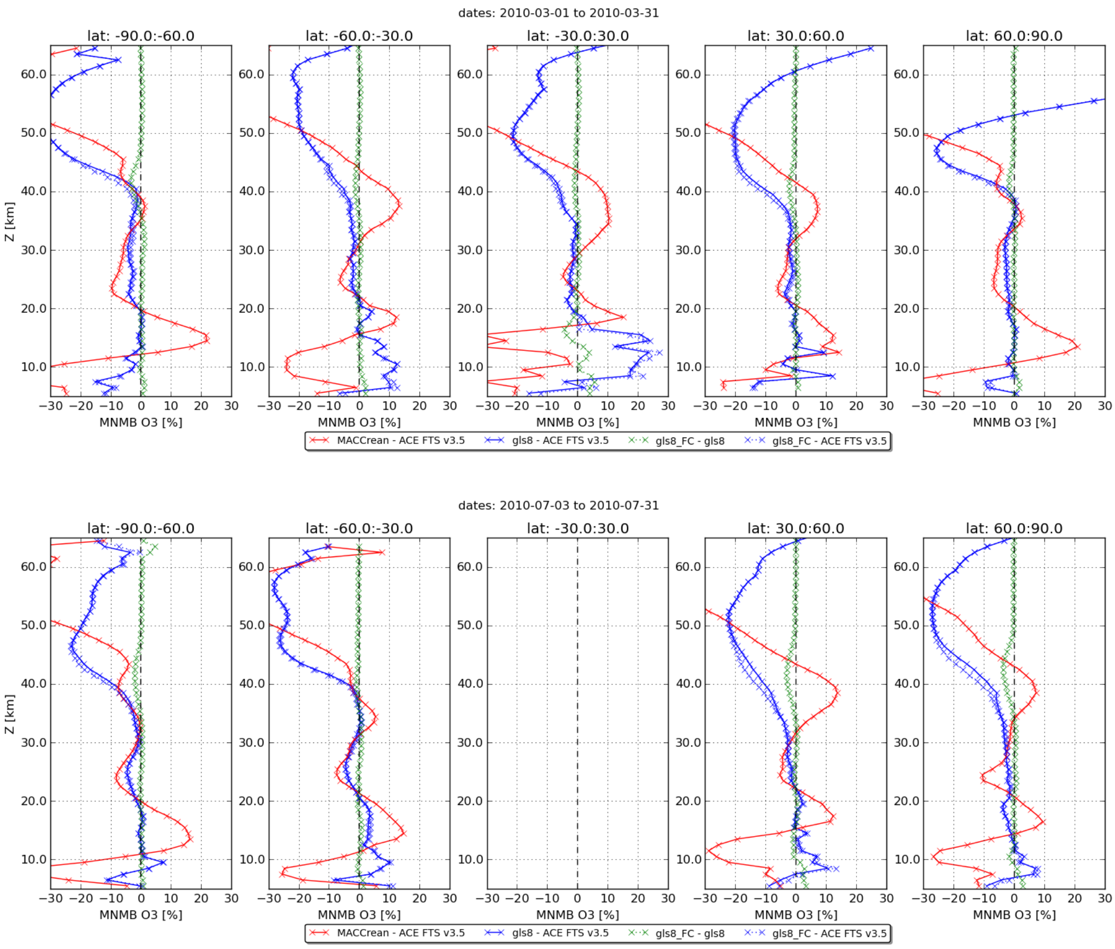

Fig. 2.6.6. Relative comparisons of stratospheric ozone profiles against ACE FTS v3.5), for March 2010 (top row) and July 2010 (bottom row). Blue line: gls8; red line: MACC reanalysis. Each set contains results for Antarctica (left), tropics (middle) and Arctic (right). Shown are the bias (top row), standard deviation (middle) and number of observations (bottom). Green line: gls8 forecast minus analysis. A closer look at the MNMB against ACEFTS shows that the gls8 profiles are more regularly close to ACEFTS observations up to 40km. Between 40km and 50km approximately, the 0-day forecasts (0h to 24h) of gls8 present a slight negative bias wrt the analysis, especially at the polar regions.

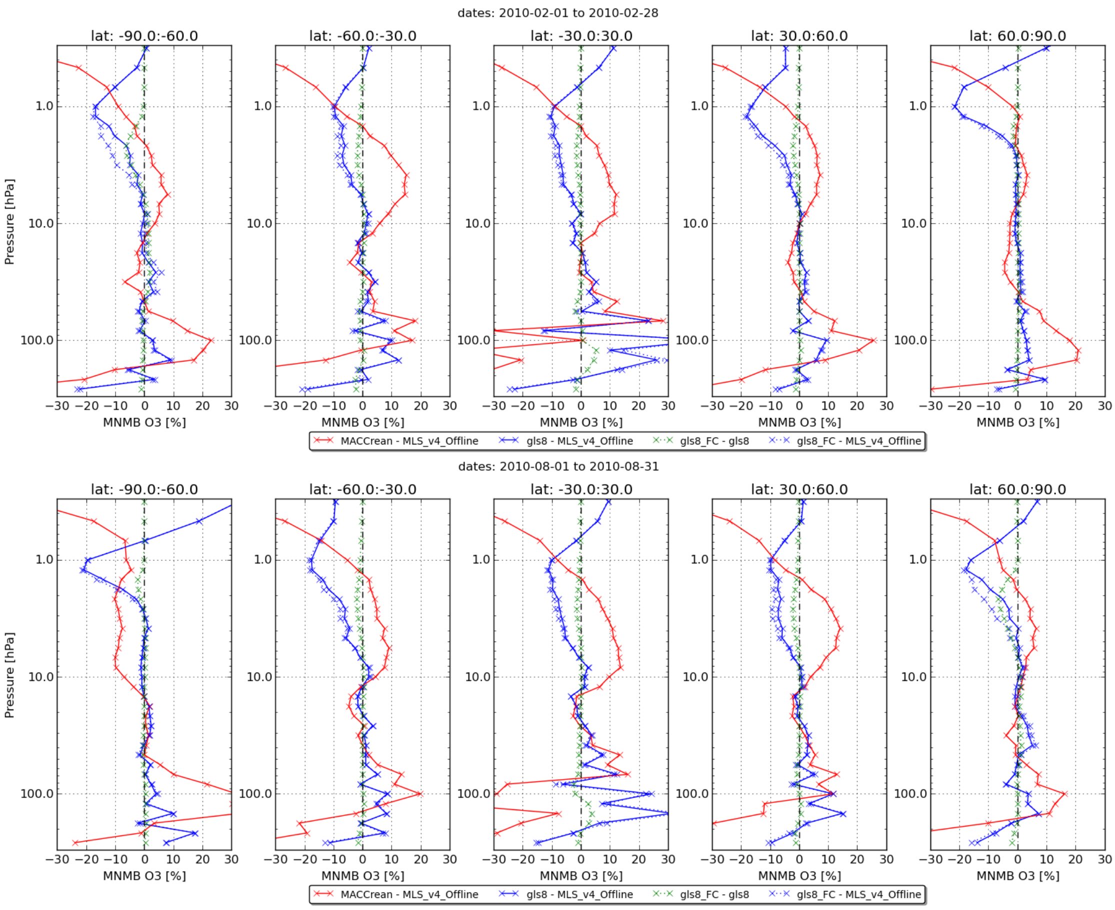

Fig. 2.6.7. Relative comparisons of stratospheric ozone profiles against MLS v4 offline, for February 2010 (top row) and August 2010 (bottom row). Blue line: gls8; red line: MACC reanalysis. Each set contains results for Antarctica (left), tropics (middle) and Arctic (right). Shown are the bias (top row), standard deviation (middle) and number of observations (bottom). Green line: gls8 forecast minus analysis. A closer look at the MNMB against AURA MLS shows that the gls8 profiles are more regularly close to AURA MLS observations up to 3hPa. Between 4hPa and 1hPa approximately, the 0-day forecasts (0h to 24h) of gls8 present a slight negative bias wrt the analysis, especially at the polar regions.

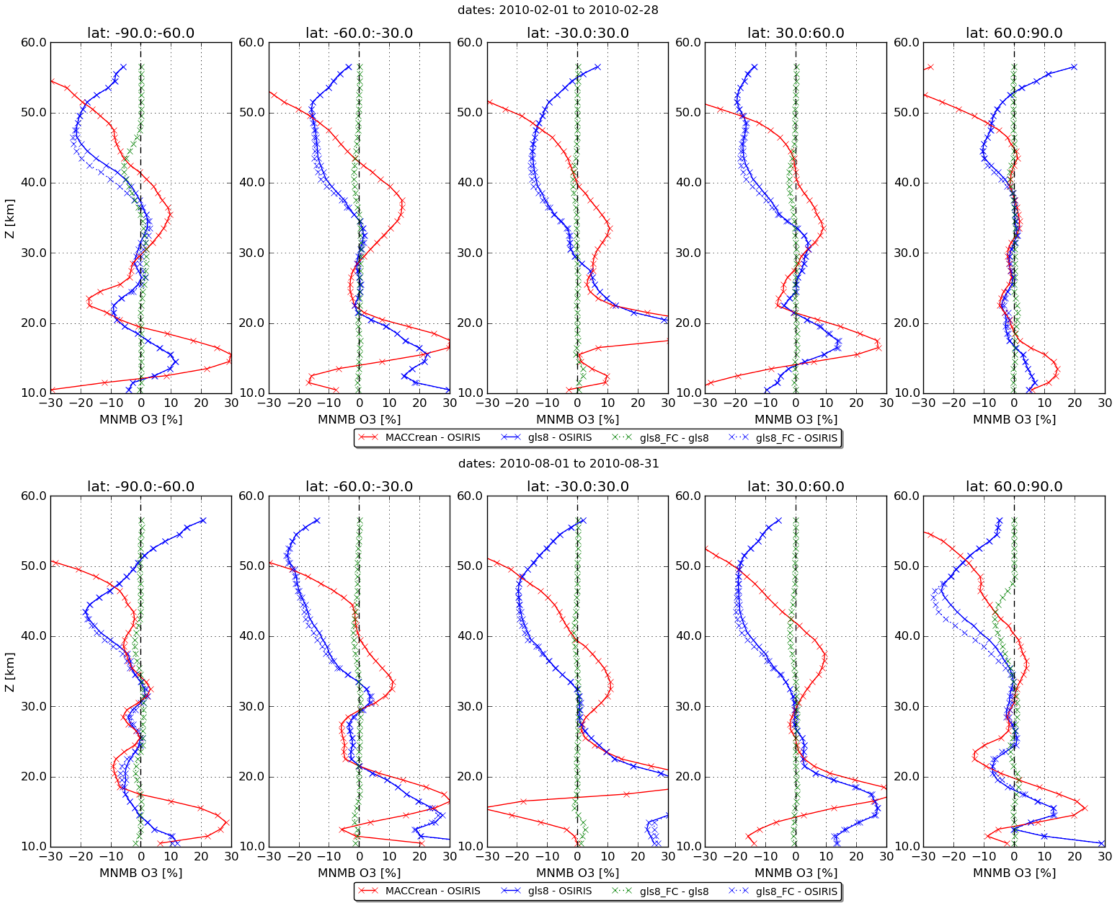

Fig. 2.6.8. Relative comparisons of stratospheric ozone profiles against OSIRIS, for February 2010 (top row) and August 2010 (bottom row). Blue line: gls8; red line: MACC reanalysis. Each set contains results for Antarctica (left), tropics (middle) and Arctic (right). Shown are the bias (top row), standard deviation (middle) and number of observations (bottom). Green line: gls8 forecast minus analysis. As an independent source of observations, the MNMB wrt OSIRIS confirms that the bias is always negative between 35km and 55 km approximately, while under 25km the profile of the MNMB is more irregular, depend on the season and varies according to the source of satellite observation used.

2.6.3 Comparison with NDACC observations

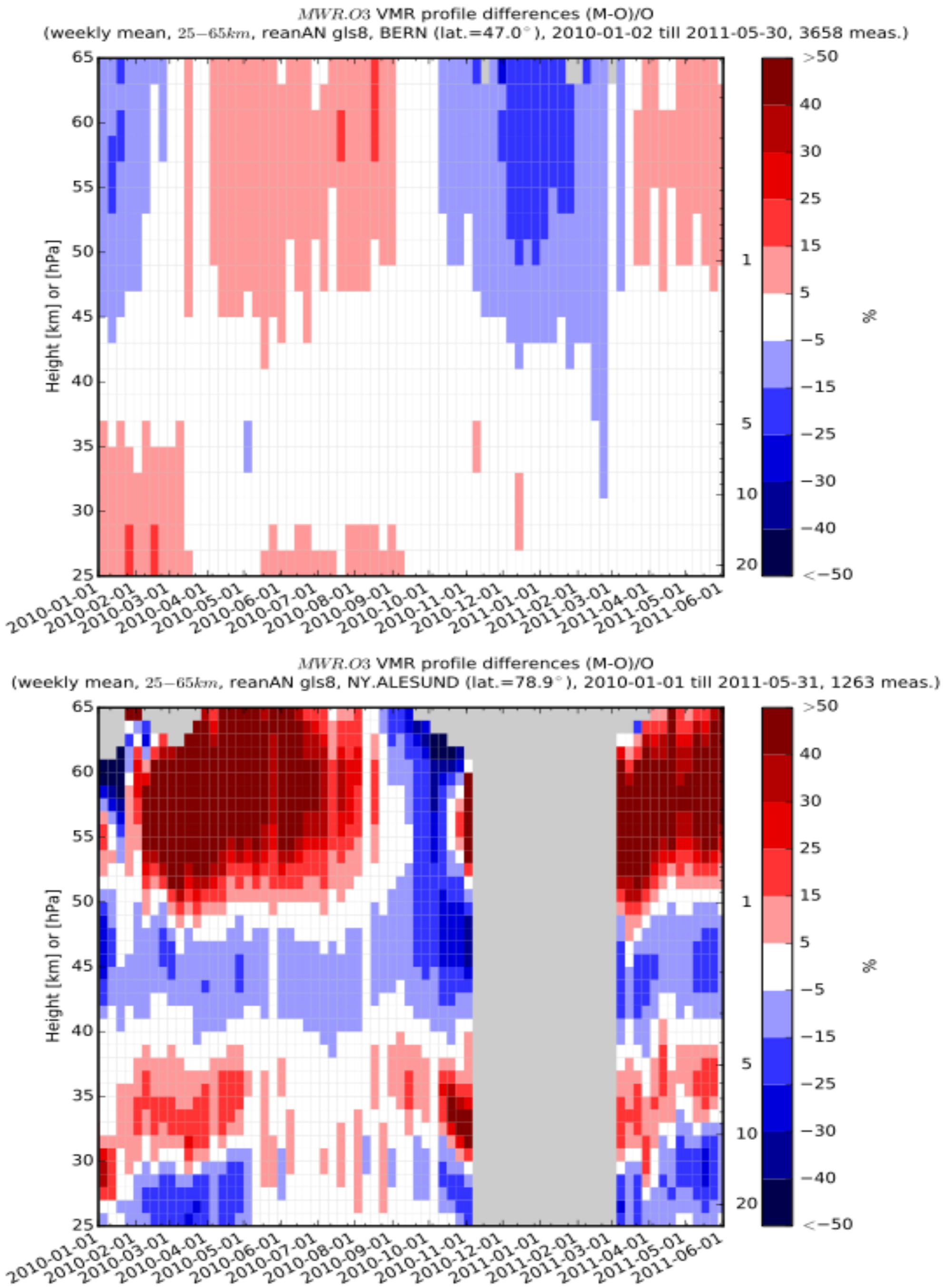

Figure 2.6.9. Comparison of the weekly mean profile bias between the O_3 mixing ratios of gls8 and the NDACC station at Ny Alesund (bottom) and Bern (top). The model performs well in stratosphere between 20-40km (=within MWR and LIDAR uncertainty ranges ~7%). Mesospheric ozone is overestimated during spring/summer, underestimated during autumn/winter.

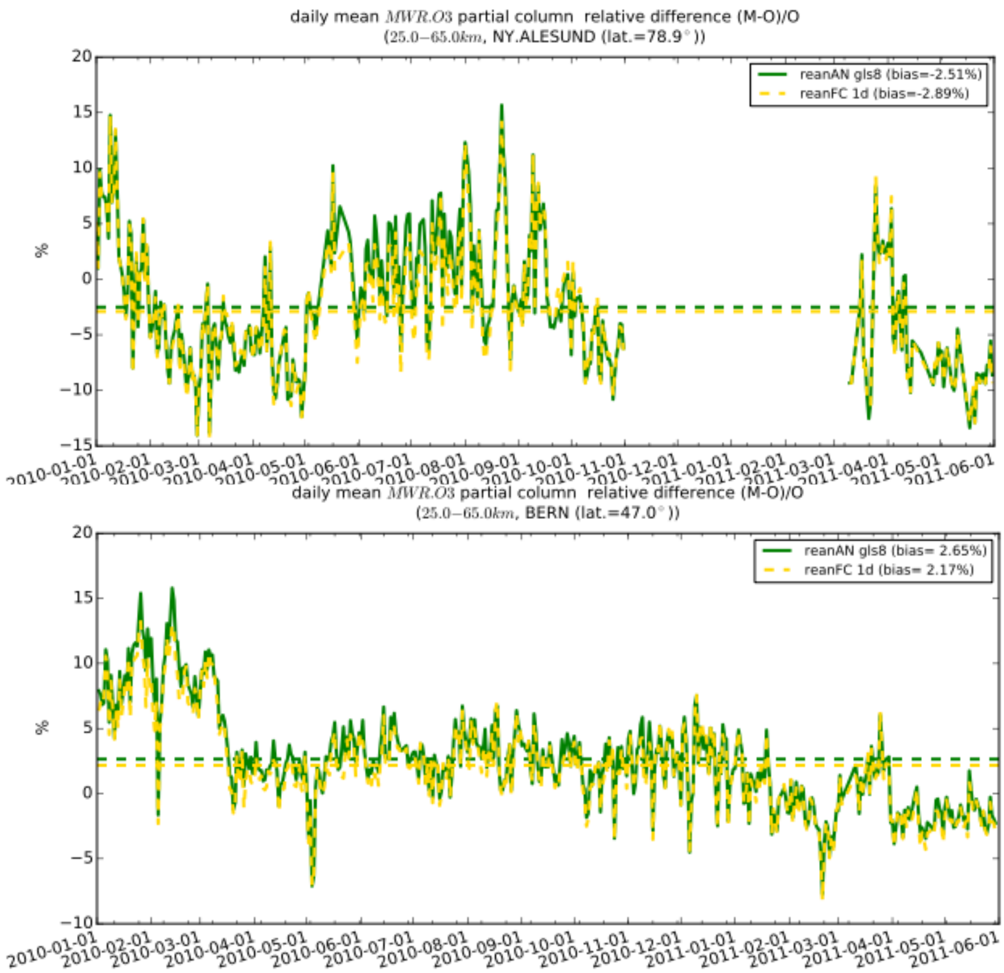

Figure 2.6.10. Comparison of the daily mean O_3 partial column bias between 25km and 60km for NDACC station at Ny Alesund (top) and Bern (bottom). The osuiteAN bias in 2015-2016 at NY ALESUND was 7% on the partial column between 25 and 65km, while for REAN this bias is <3%. At NyAlesund the mesospheric overestimation by the osuite reaches values >40% for the profile concentrations. REAN stratospheric profile bias at Bern is below <5% .

2.7 Stratospheric NO2

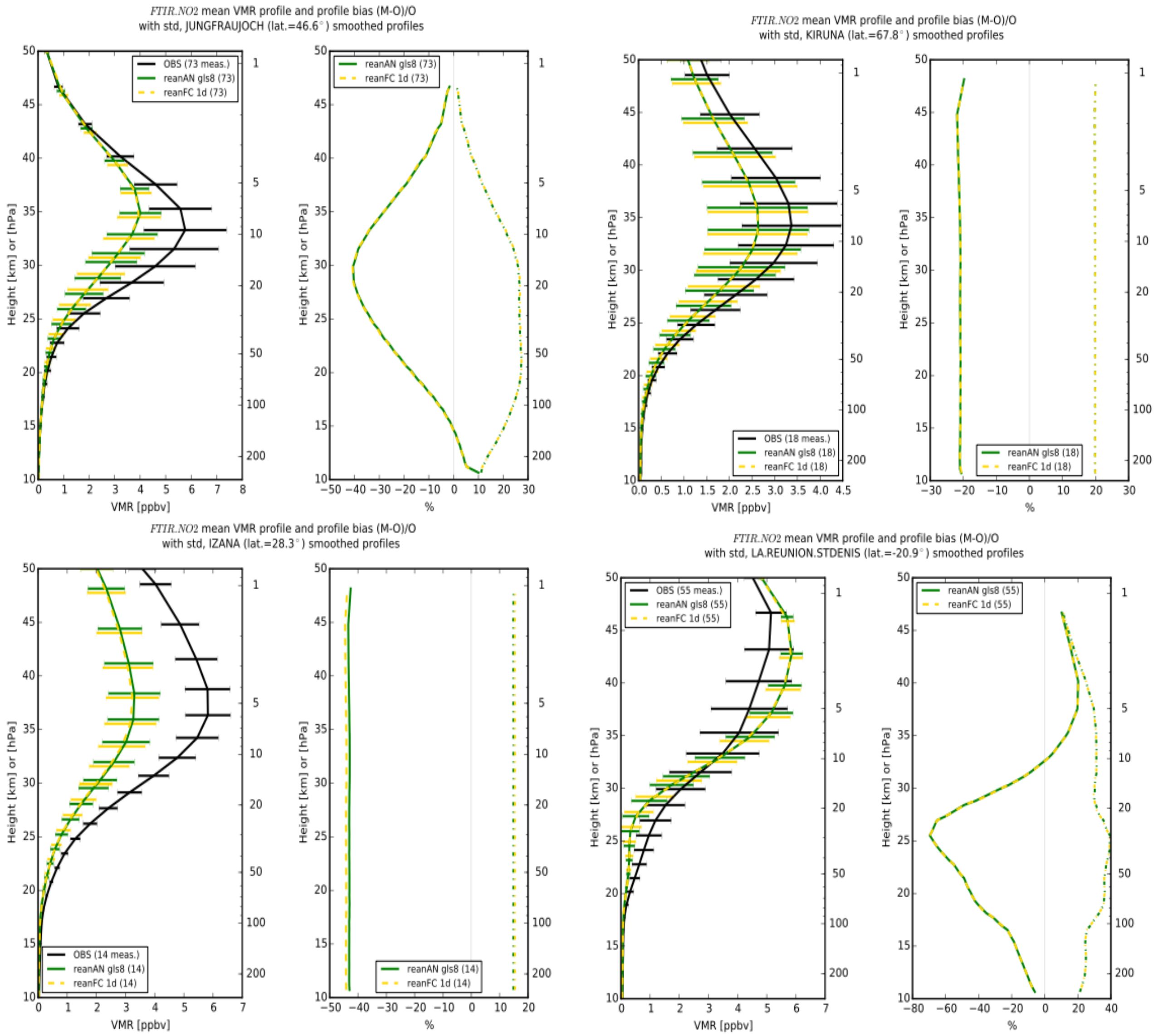

Figure 2.7.1. Comparison of the profile bias between the NO_2 mixing ratios for rean AN vs FC at Izana, Kiruna, Reunion and Jungfraujoch-.The profiles reperesent averaged profiles for 2010-mid 2011. The highest sensitivity to NO_2 of the FTIR measurement is located at ±25km. Large biases are as expected, because the C-IFS configuration does not include a description of stratospheric chemistry.

2.8 Greenhouse gases (CO_2 and CH_4)

2.8.1 ICOS surface data

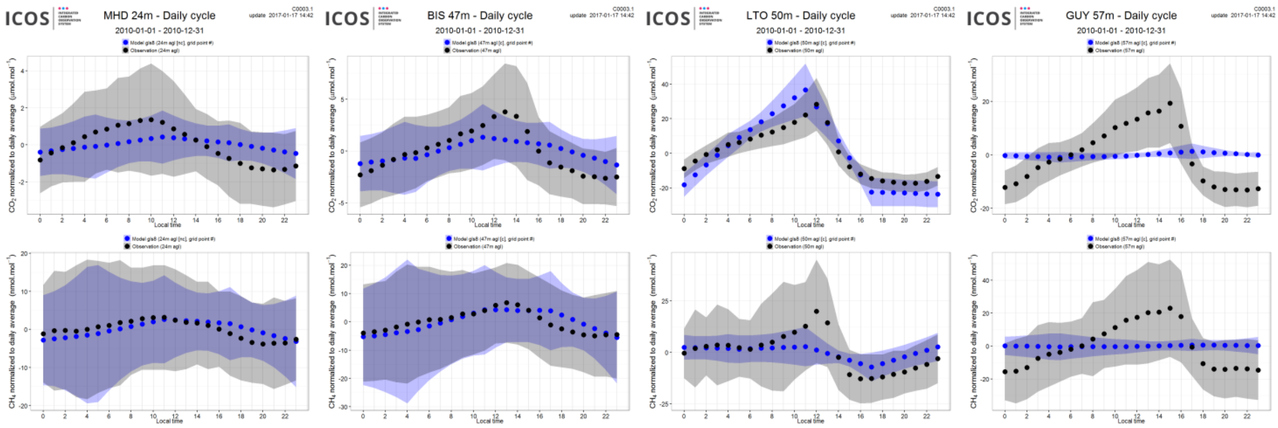

Fig. 2.8.1. Comparison of the mean CO_2 (above) and CH_4 (below) diurnal cycles at four surface sites. The model (gls8, blue) underestimates the CO_2 diurnal cycle at the two coastal stations (MHD, BIS), whereas the CH_4 cycles are well represented. At Lamto station (Ivory Coast) the CO_2 signal is pretty well simulated, but the model does not reproduce the CH_4 maximum observed at noon. The model fails to reproduce the strong diurnal cycles observed at Guyaflux.

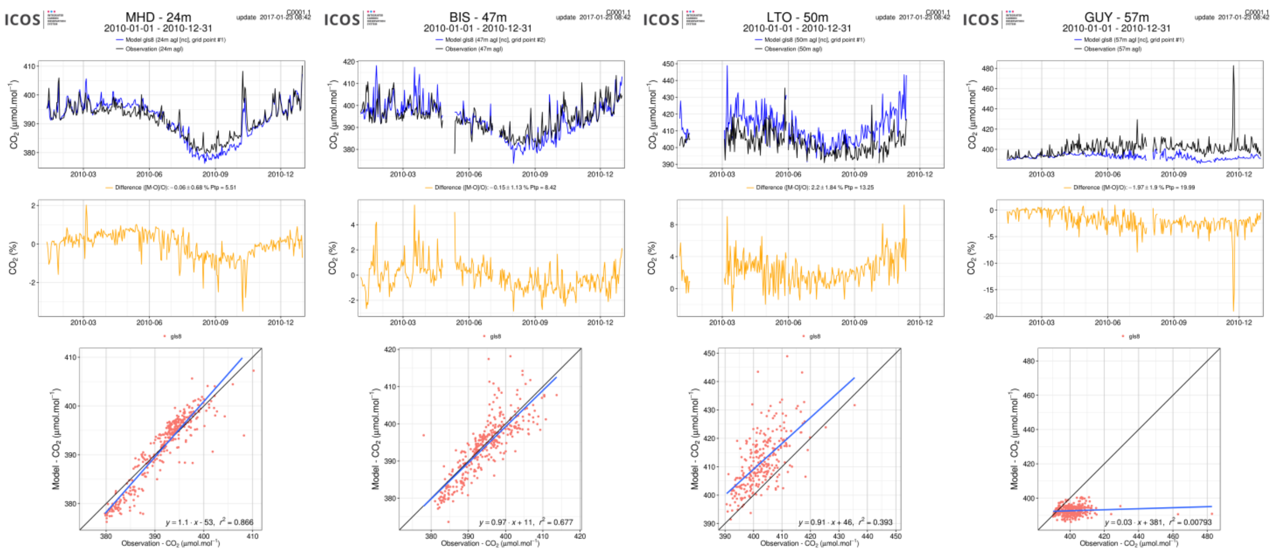

Fig. 2.8.2. Comparison of the CO_2 daily averages. At the two European stations the model captures relatively well the phase of seasonal and synoptic events. The model overestimates the amplitude of the seasonal cycle by about 1% with higher concentrations in the end of winter and too low in the end of summer. In the tropics, the model systematically overestimates CO_2 concentrations at Lamto by 1 to 5%. This is the revers situation in the Guyaflux station where the model underestimates the concentrations, and fails to represent the synoptic variability.

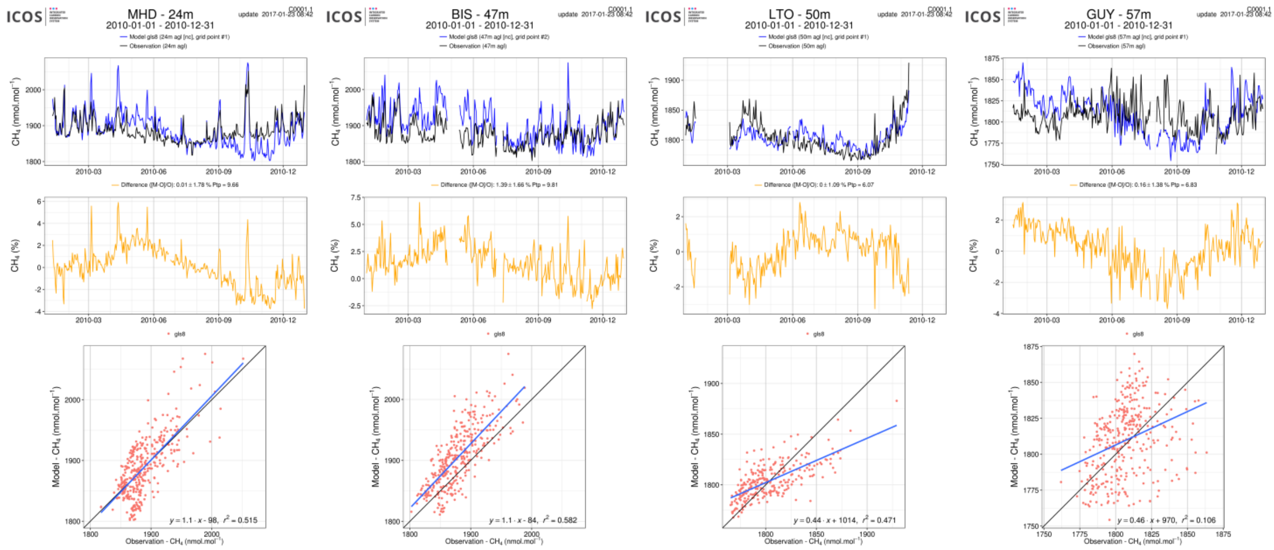

Fig. 2.8.3. Comparison of the CH_4 daily averages. The phasing of the synoptic events is generally well simulated at the two European sites. At the seasonal scale the model switches from simulating too high CH_4 concentrations in spring (up to +3%) to too low concentrations in fall (down to -3%). At Lamto the model underestimates the synoptic scale variability, but properly simulates the seasonal increase occurring in November 2010. This signal, called Harmattan, corresponds to the detection of the biomass burning period in West Africa.

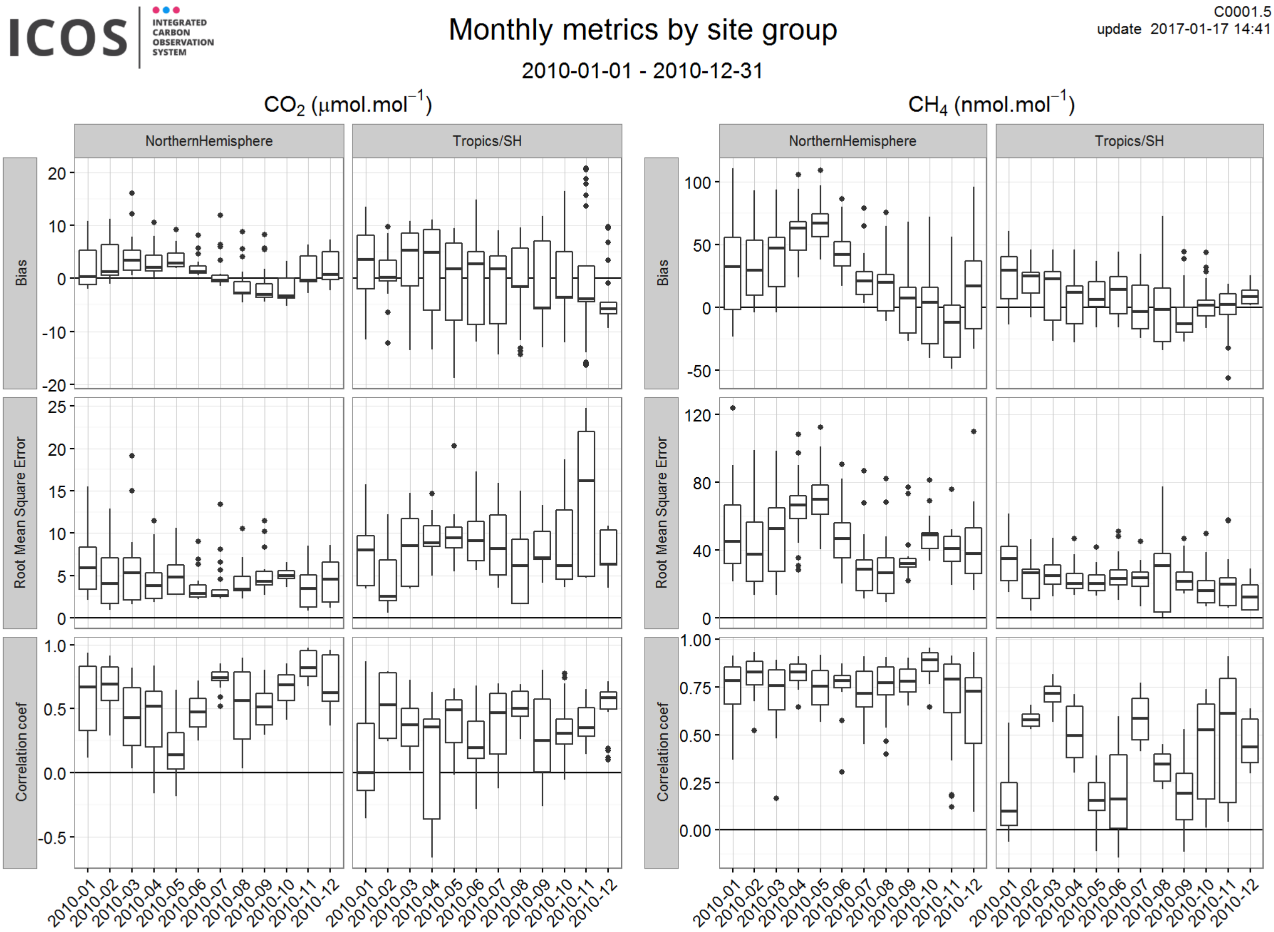

Fig. 2.8.4. Monthly means metrics (bias, RMS and correlation coefficient) of CO_2 (left) and CH_4 (right) simulations for the Europeans sites (MHD, BIS) and tropical sites (LTO, GUY). For the European stations the bias presents similar seasonal features for both CO_2 and CH_4: too high concentrations in spring, too low in fall. The correlation coefficients remain constant for CH_4 (~0.8), but for CO_2 it decreases from 0.7 in winter to 0.4 in summer when the biosphere induce more synoptic scale variability. At tropical sites, the coefficients correlations are generally lower than 0.5.

2.8.2 TCCON CO2 total columns

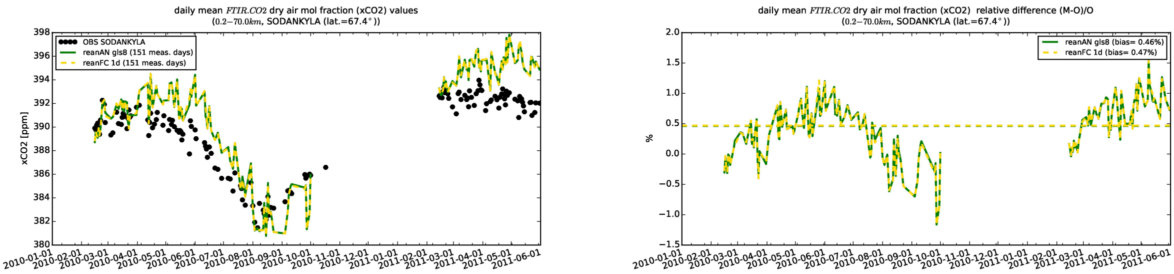

Fig. 2.8.5: TCCON-model CO_2 comparison at the Arctic site Sodankylä (67.4 °N). The discrepancies between model and measurement are up to 1%. The highest discrepancies occur during the onset of the growing season.

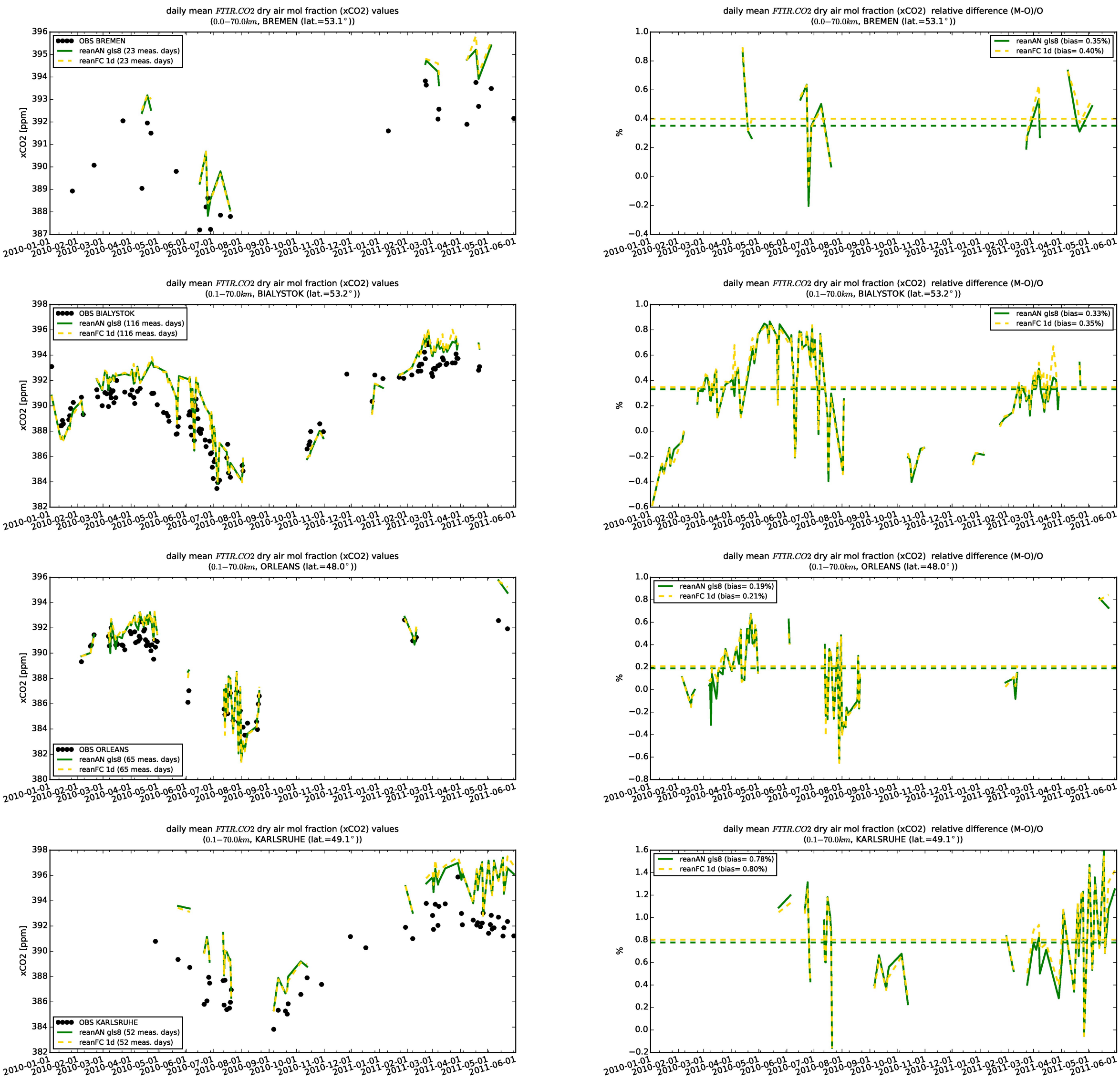

Fig. 2.8.6: TCCON-model CO_2 comparison for four European mid-latitude sites. The highest overestimation by the models occur during the onset of the growing season. The model simulations show short term variations, which are not seen in the measurements.

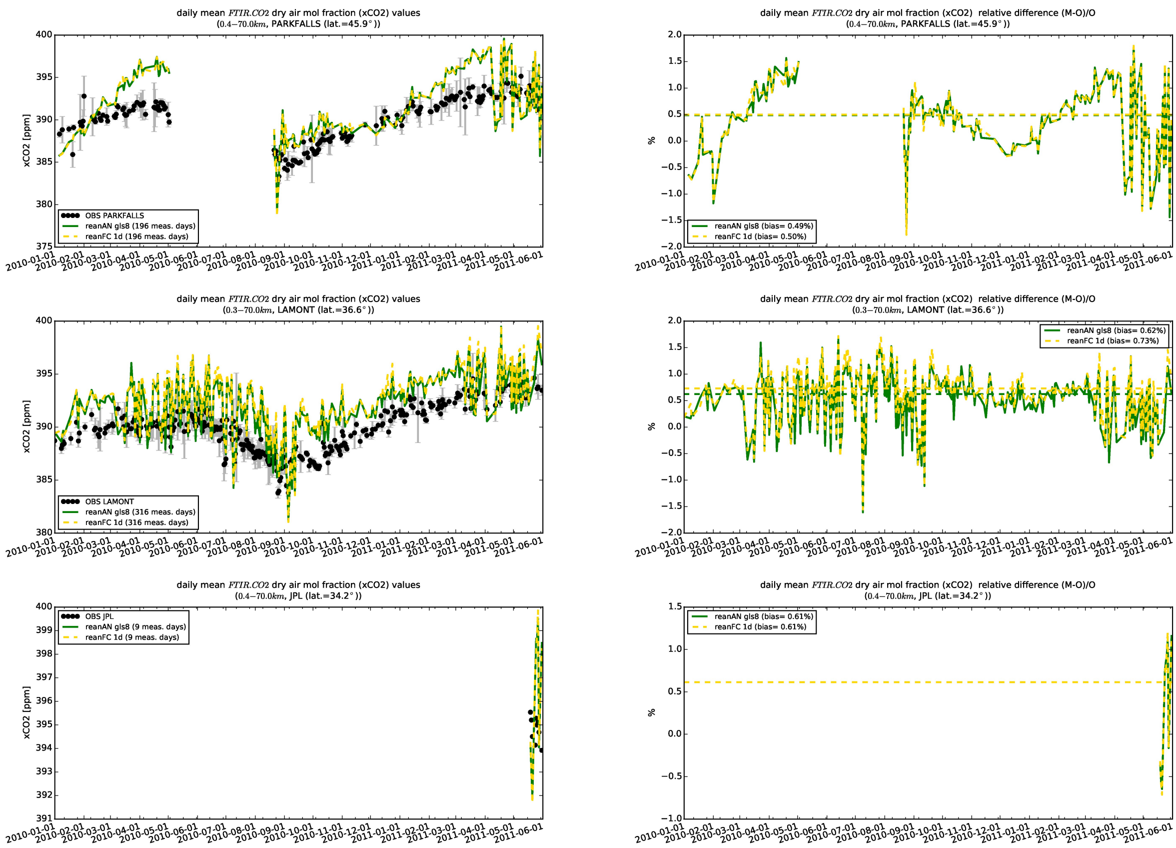

Fig. 2.8.7: TCCON-model CO_2 comparison for three US-American TCCON sites. As expected the discrepancies are similar to the ones observed at European mid-latitude sites. The unreasonable high short-term variation in the model data are also clearly seen for the US sites.

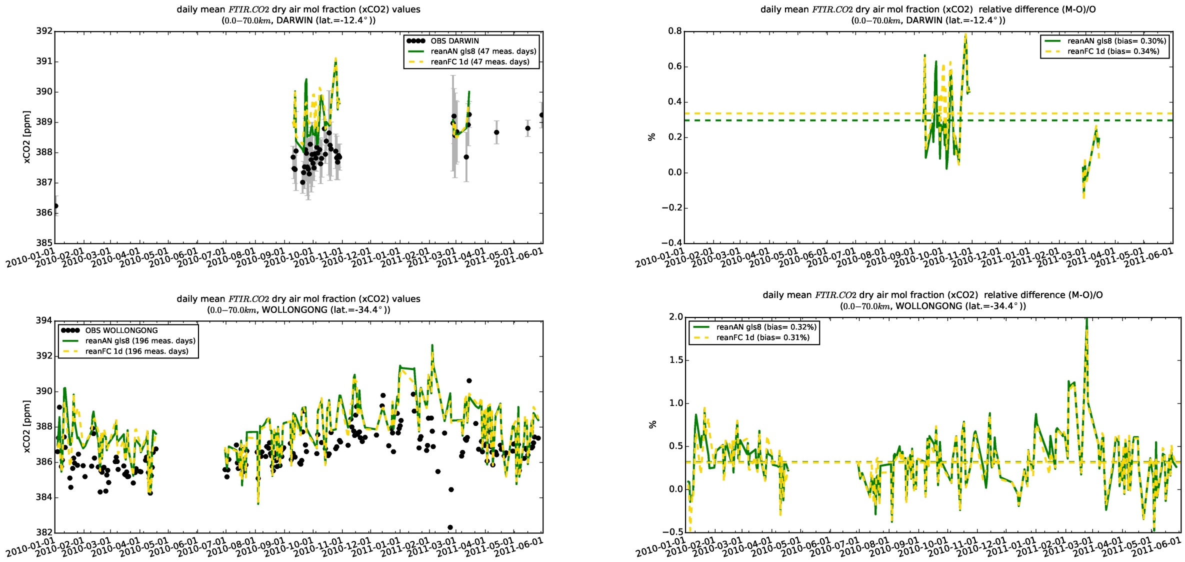

Fig. 2.8.8: TCCON-model CO_2 comparison for the two Australian sites Darwin (12.4°S) and Wollongong (34.4°S). At both sites the models overestimates the CO_2. The too high short-term variability in the model simulations is also present at these sites.

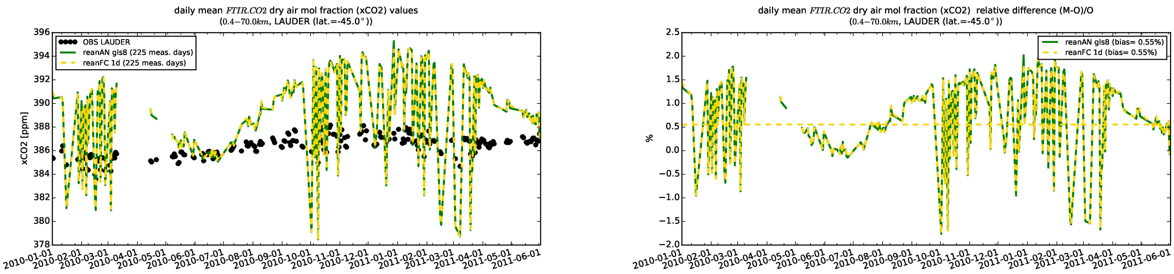

Fig. 2.8.9: TCCON-model CO_2 comparison for Lauder, New Zealand (45°S). The models strongly overestimates the CO_2 for most of the year. In addition it shows very strong unreasonable short-term variations of up to 3%.

2.8.3 TCCON CH4 total columns

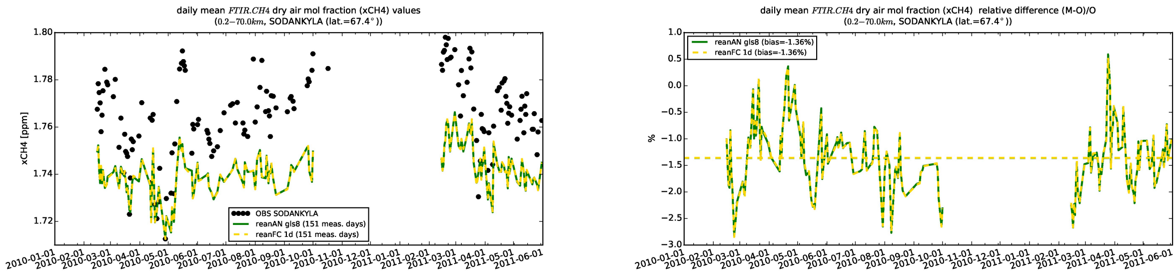

Fig. 2.8.10: TCCON-model CH_4 comparison at the Arctic site Sodankylä (67.4 °N). The modeled CH_4 significantly lower than the measured CH_4, in some cases more than 2.5%.

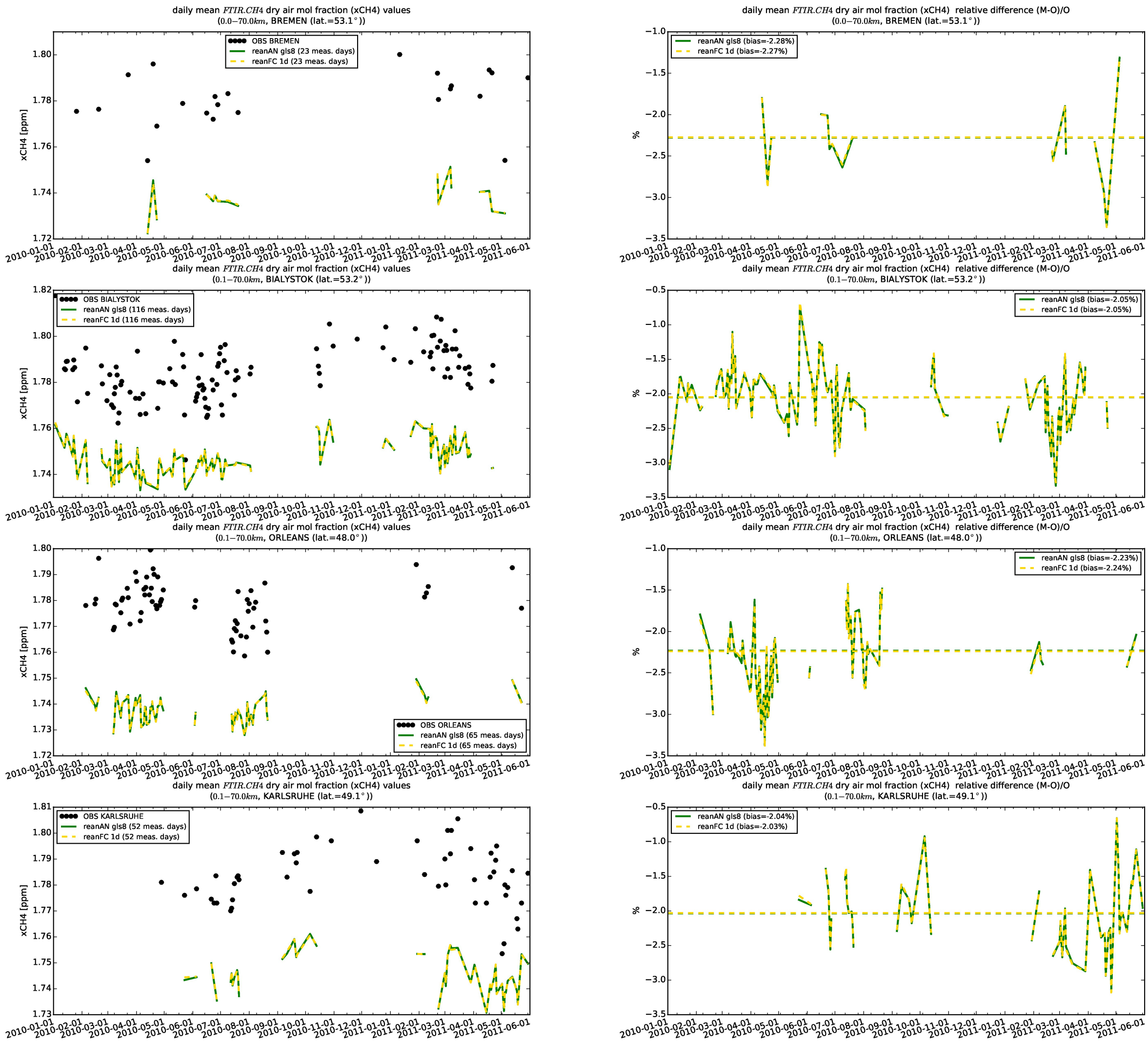

Fig. 2.8.11: TCCON-model CH_4 comparison for four European mid-latitude sites. At all sites the models underestimate the measurements by about 2-2.5% on average.

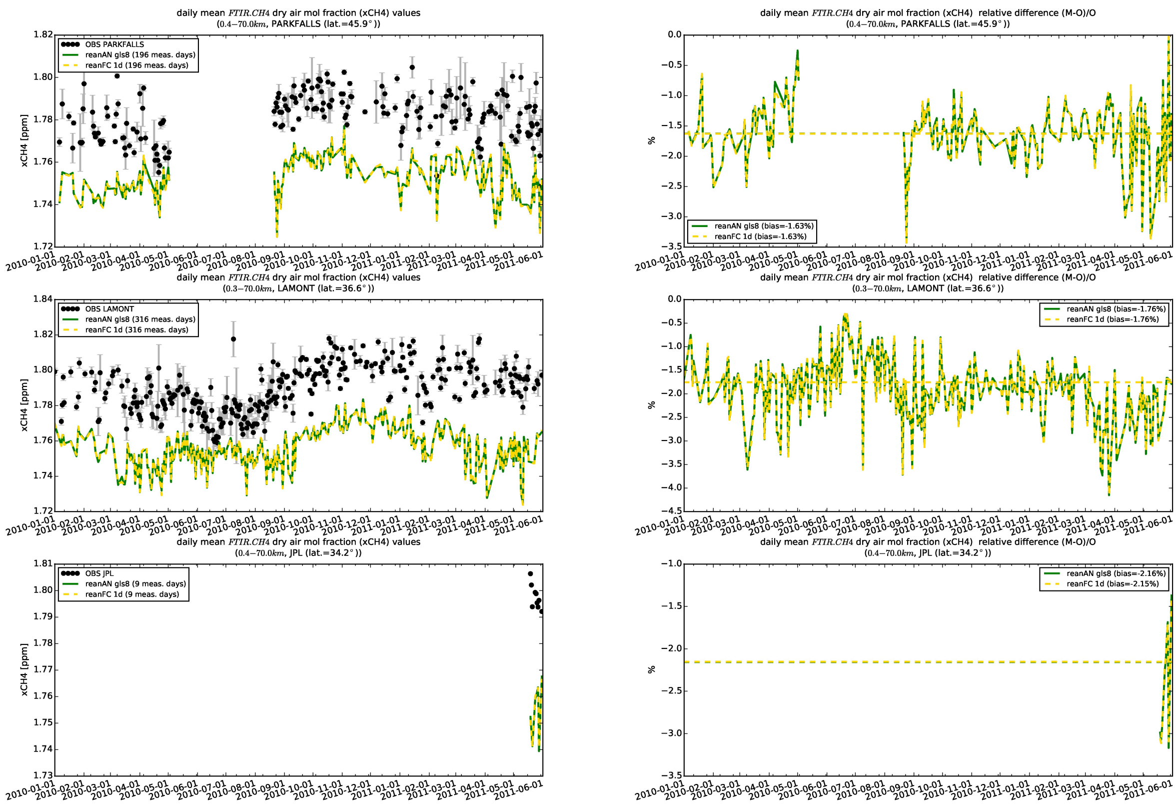

Fig. 2.8.12: TCCON-model CH_4 comparison for three US-American TCCON sites. Similar to the European mid-latitude sites the models underestimate the CH_4 by 2-2.5%.

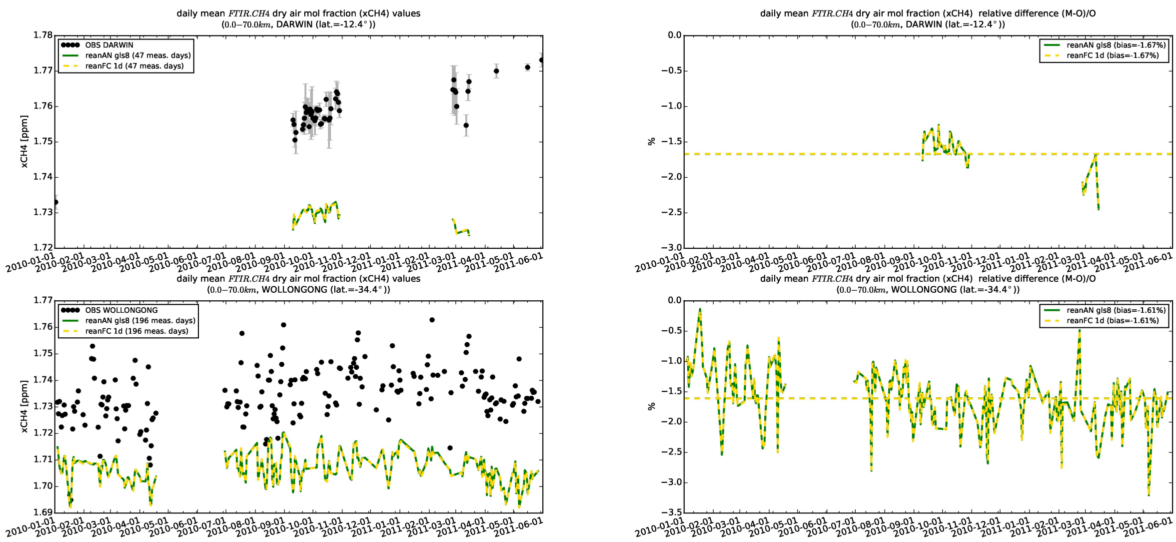

Fig. 2.8.13: TCCON-model CH_4 comparison for the two Australian sites Darwin (12.4°S) and Wollongong (34.4°S). The models underestimate the measured CH4 by 1.5-2%.

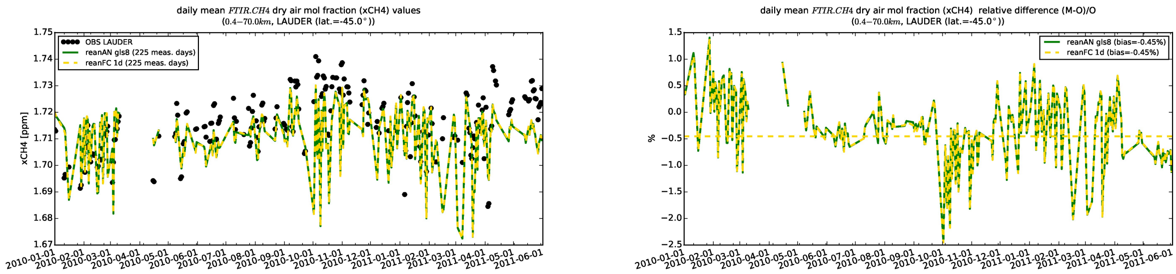

Fig. 2.8.14: TCCON-model CH_4 comparison for Lauder, New Zealand (45°S). The model data agrees better with the measurements compared to the other sites. However, discrepancies of up to 2% are observed, which is high for CH_4.

3. References

Eskes, H., Huijnen, V., Arola, A., Benedictow, A., Blechschmidt, A.-M., Botek, E., Boucher, O., Bouarar, I., Chabrillat, S., Cuevas, E., Engelen, R., Flentje, H., Gaudel, A., Griesfeller, J., Jones, L., Kapsomenakis, J., Katragkou, E., Kinne, S., Langerock, B., Razinger, M., Richter, A., Schultz, M., Schulz, M., Sudarchikova, N., Thouret, V., Vrekoussis, M., Wagner, A., and Zerefos, C.: Validation of reactive gases and aerosols in the MACC global analysis and forecast system, Geosci. Model Dev., 8, 3523-3543, doi:10.5194/gmd-8-3523-2015, 2015.

Eskes, H.J., V. Huijnen, S, Basart, A. Benedictow, A.-M. Blechschmidt, S. Chabrillat, H. Clark, Y. Christophe, E. Cuevas, H. Flentje, K. M. Hansen, J. Kapsomenakis, B. Langerock, M. Ramonet, A. Richter, M. Schulz, A. Wagner, T. Warneke, C. Zerefos: Observations characterisation and validation methods document. Copernicus Atmosphere Monitoring Service (CAMS) report, CAMS84_2015SC1_D84.8.1_2016Q2_201603, March 2016. Available from: http://atmosphere.copernicus.eu/user-support/validation/verification-global-services

Flemming, J., Huijnen, V., Arteta, J., Bechtold, P., Beljaars, A., Blechschmidt, A.-M., Diamantakis, M., Engelen, R. J., Gaudel, A., Inness, A., Jones, L., Josse, B., Katragkou, E., Marecal, V., Peuch, V.-H., Richter, A., Schultz, M. G., Stein, O., and Tsikerdekis, A.: Tropospheric chemistry in the Integrated Forecasting System of ECMWF, Geosci. Model Dev., 8, 975-1003, doi:10.5194/gmd-8-975-2015, 2015.

Huijnen, V., H.J. Eskes, A. Wagner, M. Schulz, Y. Christophe, M. Ramonet, S. Basart, A. Benedictow, A.-M. Blechschmidt, S. Chabrillat, H. Clark, E. Cuevas, H. Flentje, K.M. Hansen, U. Im, J. Kapsomenakis, B. Langerock, A. Richter, N. Sudarchikova, V. Thouret, T. Warneke, C. Zerefos, Validation report of the CAMS near-real-time global atmospheric composition service. System evolution and performance statistics; Status up to 1 June 2016, Copernicus Atmosphere Monitoring Service (CAMS) report, CAMS84_2015SC1_D.84.1.4_2016Q3_201609, September 2016.

Inness, A., Blechschmidt, A.-M., Bouarar, I., Chabrillat, S., Crepulja, M., Engelen, R. J., Eskes, H., Flemming, J., Gaudel, A., Hendrick, F., Huijnen, V., Jones, L., Kapsomenakis, J., Katragkou, E., Keppens, A., Langerock, B., de Mazière, M., Melas, D., Parrington, M., Peuch, V. H., Razinger, M., Richter, A., Schultz, M. G., Suttie, M., Thouret, V., Vrekoussis, M., Wagner, A., and Zerefos, C.: Data assimilation of satellite-retrieved ozone, carbon monoxide and nitrogen dioxide with ECMWF's Composition-IFS, Atmos. Chem. Phys., 15, 5275-5303, doi:10.5194/acp-15-5275-2015, 2015.

ECMWF - Shinfield Park, Reading RG2 9AX, UK

Contact: info@copernicus-atmosphere.eu